INTEGRATED MAGNETIC AND OPTICAL NANOTECHNOLOGY FOR EARLY CANCER DETECTION AND MONITORING

A Dissertation
Presented to
The Academic Faculty

by

Tushar R. Sathe

In Partial Fulfillment
of the Requirements for the Degree
Doctor of Philosophy in the
School of Biomedical Engineering

Georgia Institute of Technology
December, 2007

INTEGRATED MAGNETIC AND OPTICAL NANOTECHNOLOGY

FOR EARLY CANCER DETECTION AND MONITORING

Approved by:

Dr. Shuming Nie, Advisor
School of Biomedical Engineering
Georgia Institute of Technology

Dr. Niren Murthy
School of Biomedical Engineering
Georgia Institute of Technology

Dr. Joseph Le Doux
School of Biomedical Engineering
Georgia Institute of Technology

Dr. Z.L. Wang
School of Material Science and Engineering
Georgia Institute of Technology

Dr. Roberd Bostick
School of Public Health
Emory University

Date Approved: Sept. 21, 2007

To Mamma, Papa, Daddu, and Mukta

ACKNOWLEDGEMENTS

First and foremost, this dissertation would not have been possible without the constant support of my mentor and advisor Shuming Nie. In research and in life, one tends to take certain things for granted until they find themselves in moments of difficulty or crisis. Shuming does an excellent job of keeping his students motivated and I am indebted to him for giving me the opportunity to interact and work with him. From him I learned that with a little sprinkling of luck and lots of hard work and determination, it is possible to achieve anything in life. However, with success comes failure and each failure makes a person more determined to succeed. I'm always reminded of a line from Kipling "*If you can meet with Triumph and Disaster and treat those two impostors just the same; Yours is the Earth and everything that's in it, and--which is more--you'll be a Man, my son!*"

I am also lucky to have interacted with gifted, talented and smart people in my lab. The great rapport I had with them and their encouragement, advice and willingness to always lend a helping hand made it fun to be in lab. In particular, I would like to thank my collaborators Amit Agrawal, Yun Xing, Brad Kairdolf and Matt Rhyner. Collaborations can sometimes be difficult to manage, but working with them made my life easier. Since we have so many lab members I cannot begin to individually thank all of them, but I will always cherish your friendship. Dr. Amit Agrawal and I not only share a few publications, but also a great friendship. I will remember the guitar-sessions and the impromptu cooking. Andrew Smith is a brilliant man who has the potential to do great things. I will miss our chats that ranged from guitar riffs to nanoparticle synthesis. Dominic "Dominator" Ansari was my "cubicle-mate" and taught me to take a chill pill and not worry too much all the time. It was a pleasure to interact with the rookies, Chris, Mike,

Anthony, Ali Saheb, and Kate Lee and learn some new techniques or procedures that I had no idea about. Gloria Kim was our group events coordinator and she helped lab members bond together by organizing outdoor activities. The post-docs, past and present, including Gang Ruan, Ximei Qian, Jun, Xiaohu Gao, Yun Xing, Aaron Mohs, Jian Liu and Debatosh were always there to lend a ear or provide advice. Gang in particular helped me discover my strengths and weaknesses and was a good person to hang out with over a game of soccer, or a beer at a restaurant. Ximei was always there to motivate me and provide positive feedback. Thanks are also due to Michelle Bluman for her help with expediting orders.

I would also like to thank Dr. Jaswant Chaddha, his wife Pamela and nurse Cawana who provided blood samples for my studies. Their enthusiasm and excitement to work with our group was simply amazing. During the final stages of my doctoral studies I found a great friend and source of inspiration in Priyanka. She helped me when the going got tough and I thank her for her endless support, and for her ability to provide a sense of calm during the last few hectic months.

Finally, I would like to thank my family for always believing in my abilities. I had a dream of accomplishing something big and my parents sacrificed a lot to provide me an excellent education, unconditional love and support. I also thank them for giving me a caring elder brother Mihir. When I first came to the US, I was fortunate to have Mihir show me the ropes and make my transition to the US a very smooth one. Mihir and his wife Mukta have always looked out for me and I am deeply indebted to them for their love, and constant support.

TABLE OF CONTENTS

LIST OF TABLES

LIST OF FIGURES

LIST OF SYMBOLS AND ABBREVIATIONS

k_B	Boltzmann constant ($1.3806503 \times 10^{-23}\ m^2\ kg\ s^{-2}\ K^{-1}$)
K	Particle anisotropy constant
V	Particle volume
T	Temperature
F_m	Magnetic force
M	magnetic dipole
B	Magnetic Induction
M	Magnetization
X	Magnetic susceptibility
H	Magnetic field strength
μ_0	permeability of vacuum
Δv	difference in velocity
R	Particle radius
°C	degree celsius
APC	allophycocyanin
BP	Band Pass
BSA	Bovine Serum Albumin
CCD	Charge-Coupled Device
CD	Cluster of Differentiation
CdSe	Cadmium Selenide
CTC	Circulating Tumor Cell
DAPI	4',6-diamidino-2-phenylindole
DCC	Dicyclohexylcarbodiimide
DM	Dichroic Mirror

DNA	Deoxyribonucleic acid
EDC	1-ethyl-3-(3-dimethylaminopropyl) carbodiimide
EDTA	ethylenediamine tetraacetic acid
ELISA	Enzyme Linked Immunosorbent Assay
EMT	Epithelial-Mesenchymal Transition
EpCAM	Epithelial Cell Adhesion Molecule
ER	Estrogen Receptor
FACS	Fluorescence Activated Cell Sorting
FAST	Fiber Array Scanning Technology
Fe_3O_4	Iron (II,III) Oxide (Magnetite)
FISH	Fluorescence In Situ Hybridization
HER2	Human Epidermal growth factor Receptor 2
ICP-MS	Inductively Coupled Plasma – Mass Spectroscopy
IDL	Interactive Data Language
IgG	Immunoglobulin G
IHC	Immunohistochemistry
IR	Infrared
LNP	Luminescent Nanoparticles
LP	Long Pass
M	Molar
MALDI-TOF	Matrix-Assisted Laser Desorption/Ionization – Time of Flight
MMP	Magnetic Microparticle
MNC	Mononuclear cell
MRI	Magnetic Resonance Imaging
MW	Molecular Weight
NaCl	Sodium Chloride

NCI	National Cancer Institute
NdFeB	Neodymium-Iron-Boron
NHS	N-hydroxysuccinimide
OSHA	Occupational Safety and Health Administration
PCR	Polymerase Chain Reaction
PAA	Poly(acrylic acid)
PBMC	Peripheral Blood Mononuclear Cells
PBS	Phosphate Buffered Saline
PE	Phycoerythrin
PEG	Poly(ethylene glycol)
PEO	Poly (ethylene oxide)
PET	Positron Emission Tomography
PMAO	Poly (maleic anhydride alt-1-octadecene)
PMMA	Polymethyl methacrylate
PMT	Photomultiplier Tube
PR	Progesterone Receptor
QD	Quantum Dot
QD-COOH	Carboxylated Quantum Dot
QD-OH	Hydroxyl modified Quantum Dot
RBC	Red Blood Cell
RT-PCR	Real-Time Polymerase Chain Reaction
SDS	Sodium dodecyl sulfate
SNR	Signal to Noise Ratio
TBE	Tris-Borate-EDTA Buffer
TDA	Tetradecylamine
TEM	Transmission electron microscopy

TMR	Tetramethyl rhodamine
TNF	Tumor Necrosis Factor
TOPO	Trioctylphosphine oxide
UV	Ultraviolet
WBC	White Blood Cell
ZnS	Zinc Sulfide

SUMMARY

Despite significant developments in imaging modalities and therapeutics, mortality rates of cancer remain unchanged. It is known that detection and treatment of the disease before it has spread to other organs improves patient survival considerably. Nanometer-sized materials have unique optoelectronic and magnetic properties not available from their bulk phase. Since they are in the same mesoscopic size regime as biological molecules, they can be used to target and quantify individual molecules in a cell or in solution. In particular, semiconductor quantum dots (QD) are a new class of fluorophores that are bright, photostable, and can be simultaneously excited to emit different wavelengths of light. Magnetic iron oxide nanoparticles are another class of unique nanomaterials that exhibit superparamagnetism and are strongly magnetized only in the presence of a magnetic field. Early detection requires greater detection sensitivity, therefore there is a need for technologies that will not only permit detection of cancer but will allow the disease to be monitored through the expression of molecular markers. There is great potential for nanotechnology to meet this need, and if successful, it can make a significant impact on the cancer diagnostic landscape.

In this dissertation, we describe the integration of semiconductor QDs and magnetic iron oxide nanoparticles and potential applications for (i) early detection of cancer biomarkers through routine screening, and (ii) disease monitoring through the capture and analysis of rare circulating tumor cells. First, we describe the development of integrated magneto-optical beads that can be optically encoded and magnetically separable for isolating low concentration of multiple biomolecules from solution. Iron oxide nanocrystals provide superparamagnetic properties for bead separation and target enrichment, but also attenuate the QD fluorescence intensity. Nonetheless, we have

prepared and characterized highly uniform dual-functions beads with three ratiometric signatures. Second, we demonstrate improved detection sensitivity by combining immunomagnetic beads and highly luminescent nanoparticles in a sandwich assay. Through the enrichment of protein from solution using magnetic beads and increased specificity from the dual-selectivity of the assay, we demonstrate detection sensitivity 100-1000 times greater than solid-phase immunoassays.

Next, we describe integration of magnetic and QD nanotechnology for the selective capture and molecular profiling of rare cells. We demonstrate the ability to spectroscopically determine relative molecular levels of markers to distinguish invasive cells from epithelial tumor cells. We also show breast cancer profiling that can enable one to determine most effective therapy.

During the isolation of tumor cells from whole blood, we encountered non-specific binding of magnetic nanoparticles to leukocytes present in blood. Therefore, we studied nanoparticle-cell interactions using QDs to determine a solution to this problem. This was done by comparing QD association with cells as a function of surface coatings. Not surprisingly, we observed that anionic nanoparticles with carboxylic acid groups (-COOH) strongly associated with leukocytes, but interestingly this association was cell specific. In the presence of plasma, they were uptaken by monocytes, whereas they were found in the perinuclear region of neutrophils (granulocytes) when plasma proteins were absent. Hydroxyl-modified QDs (QD-OH) were also compared with PEGylated micelle encapsulated QDs and showed little association with any leukocytes. From this study, we were able to conclude that by modulating the surface charge of nanoparticles, non-specific associations with cells can be controlled. Apart from improving magnetic nanoparticle coatings for more specific cell capture, this work also opens interesting questions about the immunological properties of nanoparticles in whole blood.

CHAPTER 1

INTRODUCTION

1.1 Motivation

Metastatic cancer results when the disease spreads from a primary tumor site to vital organs and is responsible for most cancer deaths. Despite significant investment in developing novel cancer treatments, improvement in patient outcome remains modest. Most of this investment, both private and public, is directed towards improving current treatments and developing new ones against aggressive forms of cancer [1]. Given the incremental gains seen in therapeutics for advanced disease, it is unlikely that a “golden bullet” that will drastically reduce cancer mortality will materialize soon. Although the mapping of the human genome and developments in nano-scale polymeric drug delivery vehicles has opened new possibilities for targeted molecular therapeutics, its impact on the lives of cancer patients will not be known for the next 10 years. It is well known that detecting cancer at its earliest, most treatable stage gives patients the greatest chance of survival and so there should be a concerted effort in developing reliable early detection strategies for all types of cancer [2, 3]. According to latest estimates provided by the American Cancer Society, 560,000 Americans are expected to die of cancer in 2007, which is equivalent to 4 jumbo jet crashes every day (1,500 deaths/day) [4]. Cancer is the second most common cause of death in the US after heart disease and accounts for 1 of every 4 deaths. Developing early detection technology and routine diagnostic assays to monitor treatment of currently used chemotherapies can reduce this mortality rate, as was the case for cervical cancer after the Pap smear test. Therefore, the potential impact of combining effective detection with therapeutics when the disease is confined to one organ is significant [1].

Research into tumor biology has revealed that cancer is a heterogeneous disease. Even within a single tumor, cells can show markedly different behaviors and can lead to varying prognoses. Long gone is the idea of cancer being a disease that is unique to tumor location. We now know that cancer is a collection of diseases that are going through several steps necessary to exhibit invasiveness. Tumor heterogeneity can be acute to the extent that neighboring cells in a tumor may appear morphologically distinct and not share the same genetic makeup[5]. This genetic instability together with the stochastic process in which cells transition from normal to highly invasive and immortal cells makes cancer detection an arduous task.

This molecular nature of cancer can be utilized to obtain real-time information of the state of the disease. The genes and proteins associated with tumor phenotypes represent biomarkers that provide correlation with cancer type, stage, and location[6]. The discovery of more than one biomarker implicated in cancer of a specific organ has led to development of multiplexed microarray technology to detect several biomarkers in one step[7-9]. As research in systems biology reveals the molecular pathways of the disease, quantitative data on the levels of these biomarker panels can provide us with useful information about the behavior and progression of the tumor. In turn, this will allow for personalized therapy and monitoring of patient response so that cancer can be tackled more effectively on an individual basis.

Compared to invasive procedures like needle biopsies, blood represents a relatively non-invasive source of information about the well being of the human body. With the advent of serum proteomics and the presence of elevated levels of cancer-associated proteins in the blood of cancer patients, it will be possible to monitor these biomarkers on a routine basis and optimize treatment [10]. In this dissertation, we have made an attempt to address these requirements by combining two types of nanotechnologies that have the potential to impact the diagnostic landscape.

1.2 Scope and Organization

Detecting tumor-associated molecules and cells at the earliest disease stage will probably involve ultrasensitive detection technology since tumor cell and tumor-associated molecule concentration in blood are likely to be very low. Further, the presence of a complex blood environment and non-tumor interfering factors make it more important to selectively isolate the targets. A technology that will permit enrichment of these molecules/cells from large sample volumes and permit their ultrasensitive detection will address this need.

Nanoparticles possess distinct optical, electronic and magnetic properties that are not available in the bulk phase [11]. Advances in nanoparticle synthesis have opened up a plethora of biomedical applications [12-18]. Additionally, the similarity in size between nanoparticles and biological molecules like DNA and proteins permits individual molecules to be probed. The size of nanoparticles also opens up interesting questions about their behavior and interactions with living systems. *In the context of this dissertation, the hypothesis for a majority of this work is that although optical and magnetic nanoparticles can singularly offer the ability to improve on current detection technology, the integration of these two may enhance the overall detection sensitivity while providing quantitative information of targeted molecules*.

This dissertation has been organized into 7 chapters. Chapter 2 provides a brief background about optical and magnetic nanotechnologies, and their combination. This chapter also provides the reader with a brief explanation of tumor metastasis, and nanoparticle-blood interactions. In Chapters 3 & 4 we discuss the development and applications of microbeads for early detection assays. In particular, Chapter 3 describes development of dual-function beads by embedding iron oxide nanoparticles and semiconductor quantum dots (QD) so that they can be optically encoded (for multiplexed analysis) and magnetically separable. Chapter 4 discusses the development of a

magnetic bead-based sandwich assay that utilizes luminescent nanoparticles (QDs and dye-doped nanoparticles) for ultrasensitive detection of biomolecules (protein and DNA) in solution. In chapters 5, we describe a method to quantify multiple biomolecules from circulating tumor cells by first enriching them with magnetic nanoparticles and profiling tumor biomarkers on the cell. During the course of this study, we encountered an issue of non-specific binding of nanoparticles to blood cells. Therefore, we have tried to understand these interactions in Chapter 6 by using QDs. Finally, in chapter 9, we provide a brief summary of the work included in this dissertation and discuss future directions that did not fall within the scope of this work.

1.3 References

[1] Etzioni R, Urban N, Ramsey S, McIntosh M, Schwartz S, Reid B, Radich J, Anderson G and Hartwell L, The case for early detection. *Nat Rev Cancer* **3**:243-252 (2003).

[2] Fujiwara K, Fujimoto N, Tabata M, Nishii K, Matsuo K, Hotta K, Kozuki T, Aoe M, Kiura K, Ueoka H and Tanimoto M, Identification of epigenetic aberrant promoter methylation in serum DNA is useful for early detection of lung cancer. *Clin Cancer Res* **11**:1219-1225 (2005).

[3] Garnick MB, Prostate cancer: screening, diagnosis, and management. *Ann Intern Med* **118**:804-818 (1993).

[4] Cancer Facts & Figures, American Cancer Society. American Cancer Society, Atlanta, GA (2007).

[5] Fialkow PJ, Clonal Origin of Human Tumors. *Biochimica Et Biophysica Acta* **458**:283-321 (1976).

[6] Sidransky D, Emerging molecular markers of cancer. *Nat Rev Cancer* **2**:210-219 (2002).

[7] Simon R, Diagnostic and prognostic prediction using gene expression profiles in high-dimensional microarray data. *Br J Cancer* **89**:1599-1604 (2003).

[8] Sommer A and Haendler B, Androgen receptor and prostate cancer: molecular aspects and gene expression profiling. *Curr Opin Drug Discov Devel* **6**:702-711 (2003).

[9] Yanagisawa K, Xu BJ, Carbone DP and Caprioli RM, Molecular fingerprinting in human lung cancer. *Clin Lung Cancer* **5**:113-118 (2003).

[10] Rai AJ and Chan DW, Cancer proteomics: Serum diagnostics for tumor marker discovery. *Ann N Y Acad Sci* **1022**:286-294 (2004).

[11] Smith A and Nie S, Chemical analysis and cellular imaging with quantum dots. *ANALYST* **129**:672-677 (2004).

[12] Agrawal A, Sathe T and Nie S, Nanoparticle Probes for Ultrasensitive Biomolecular Detection and Imaging, in In Press, ed by Xu XN. Wiley Interscience (2006).

[13] Chan WC, Maxwell DJ, Gao X, Bailey RE, Han M and Nie S, Luminescent quantum dots for multiplexed biological detection and imaging. *Curr Opin Biotechnol* **13**:40-46 (2002).

[14] Nam JM, Thaxton CS and Mirkin CA, Nanoparticle-based bio-bar codes for the ultrasensitive detection of proteins. *Science* **301**:1884-1886 (2003).

[15] Penn SG, He L and Natan MJ, Nanoparticles for bioanalysis. *Curr Opin Chem Biol* **7**:609-615 (2003).

[16] Rosi NL and Mirkin CA, Nanostructures in biodiagnostics. *Chem Rev* **105**:1547-1562 (2005).

[17] Zhao X, Tapec-Dytioco R and Tan W, Ultrasensitive DNA detection using highly fluorescent bioconjugated nanoparticles. *J Am Chem Soc* **125**:11474-11475 (2003).

[18] Alivisatos P, The use of nanocrystals in biological detection. *Nat Biotechnol* **22**:47-52 (2004).

CHAPTER 2

BACKGROUND

In the past, designing multi-functional nanoparticles has been hindered by the inability to synthesize monodisperse nanoparticles and precisely tune their optoelectronic and magnetic properties. Both semiconductor quantum dots and iron oxide magnetic nanoparticles possess unique properties that are unavailable in their bulk phases [1, 2] and each of these technologies has made a significant contribution to cancer detection [3-5], and even therapy [6-8]. In this chapter, we provide a brief overview of QDs, magnetic nanoparticles, and a review of current technologies incorporating both. Next, we provide the reader with a brief introduction to cancer metastasis, circulating tumor cell detection, and the major components of blood that can interact with nanoparticles.

2.1 Magnetic iron oxide nanoparticles

The history of magnetism in civilization is ancient. More fascinating is the millennia old application of magnetite powder in medicine; the first medical use was reported in 10^{th} century Egypt [9]. In recent times, the physics of magnetic nanoparticles has revealed interesting and unique properties that have opened up a diverse range of applications. Magnetic iron oxide nanoparticles with diameters less than 25 nm represent a new class of nanomaterials that possess properties that are not found in bulk iron oxide. These properties are directly dependent on size as magnetization and relaxation depend on particle volume (Equation 1).

$$\tau = \tau_o \exp(KV/k_BT) \qquad (1)$$

where K is the particle anisotropy constant, V is the particle volume, k is Boltzmann's constant and T is temperature[10]. Therefore, as size (volume) is reduced, KV will eventually overcome thermal energy (k_BT) causing magnetic moment of the particles to fluctuate. At a certain size (typically 25 nm for magnetite), the particle is said to superparamagnetic. As a result, the magnetic moment fluctuates rapidly in a random direction leaving a net moment of zero[11]. Such particles can then be strongly magnetized under external magnetic field yet exhibit now magnetic remnance when the field is removed.

For biomedical applications, the size limit for superparamagnetism is advantageous because it matches the size regime of most biomolecules such as proteins (5-50 nm) and is 1000-fold smaller than mammalian cells [11]. Together with their capability to be manipulated with external permanent magnets, they have been used in a plethora of applications such as bioseparation [12-17], biomolecule tagging and detection [18, 19], magnetic hyperthermia [20, 21] (destruction of targeted cells through heat generation in particles), in vivo cell tracking [22-24], MRI contrast enhancement and drug delivery [6, 25, 26].

In particular, bioseparation applications are quite important because of the need to separate out low quantities of biological entities/targets from a large sample volume. Most often, these biological entities are in a complex environment containing millions of native molecules. Currently, detection of cancer-associated biomarkers and rare cells that are found in low amounts from bodily fluids is either laborious, time consuming or technically challenging. By attaching targeting moieties to magnetic nanoparticles, several groups have demonstrated enrichment of proteins [27-29], bacteria [30, 31] and cells [32, 33] with high degree of efficiency.

When magnetic nanoparticles are placed in the presence of a homogeneous magnetic field, they experience a magnetic force that pulls them towards the magnet. This magnetic force can be described as follows. When a magnetic nanoparticle is dispersed in a diamagnetic medium like water, the force can be described by equation (2):

$$F_m = (m \cdot \nabla)B \quad (2)$$

Where, m is the magnetic dipole and B is the magnetic induction. In water, the total moment on the nanoparticle can be written as $m = V_m M$, where V_m is the particle volume and M is its magnetization, which in turn is given by $M = \Delta\chi H$, where $\Delta\chi$ is the particle's magnetic susceptibility and H is the magnetic field strength [34]. Also, for conditions where nanoparticles are in dilute water solution, $B = \mu_0 H$. When we put these relations together we get,

$$F_m = V_m \Delta\chi \nabla(1/2 * B \cdot H) \quad (3)$$

When magnetic nanoparticles, tagged to a cell or molecules of interest, experience a magnetic force, they have to overcome hydrodynamic drag force and gravitational force. For small particles, gravitational force is negligible due to the low mass. Also, buoyancy force can affect motion due to the magnetic field but is also negligible in this case. Therefore, magnetic force has to overcome drag to enable particle to be pulled towards the magnet. This drag force can be described by equation 4, which is in fact the Stokes' equation:

$$F_d = 6\pi\eta R_m \Delta v \quad (4)$$

Where η is the viscosity of medium, R_m is the particle radius and Δv is the relative velocity of the tagged cells (magnetic sedimentation velocity). If we equate (3) and (4), we get

$$\Delta v = \frac{R_m^2 \Delta \chi}{9 \mu_0 \eta} \nabla (B^2) \quad (5)$$

Equation (5) can now be used to determine magnetic sedimentation velocity of nanoparticles as a function of size. Everything else remaining constant, the time required for magnetic nanoparticles to be sedimented completely (pulled towards magnet) is inversely proportional to the square of the radius. Larger microbeads, which are composed of thousands of magnetic nanoparticles enclosed in a polymer matrix can be sedimented in seconds, whereas individual magnetic nanoparticles will take hours. Depending on the application and the size of the target, nanoparticles or beads may be used. For example, in this dissertation, we have used nanoparticles to capture cells (Chapter 5) since the specific binding of several thousand nanoparticles on the cell surface results in quick sedimentation. However, for isolating biomolecules such as DNA and protein, we have used microbeads (Chapter 4) due to the inability to bind many nanoparticles to each molecule.

Synthesis of magnetic nanoparticles

Influenced by progress made in the synthesis of other nanocrystals, such as quantum dots, magnetic nanoparticle synthesis has improved tremendously. In general, the two most common synthesis procedures involve decomposition of organometallic precursors, and the coprecipitation of iron salts in emulsions. When organometallic precursors are heated at high temperatures in the presence of organic surface coordinating ligands, it is possible to obtain iron oxide nanoparticles with tight size control (5-10% standard deviation in diameter)[35]. Hyeon et al. demonstrated synthesis of iron nanoparticles by the decomposition of iron pentacarbonyl[36]. Similarly, Sun et al. were able to produce magnetite nanoparticles of various sizes (2-16 nm) through a one-step, highly robust procedure involving the reduction of iron (III) acetylacetonate in the

presence of oleylamine and oleic acid[37]. The resulting nanoparticles are stable, soluble in non-polar solvents and are resistant to oxidation. The size distribution and particle uniformity is evident from TEM images taken when dispersed in a non-polar solvent.

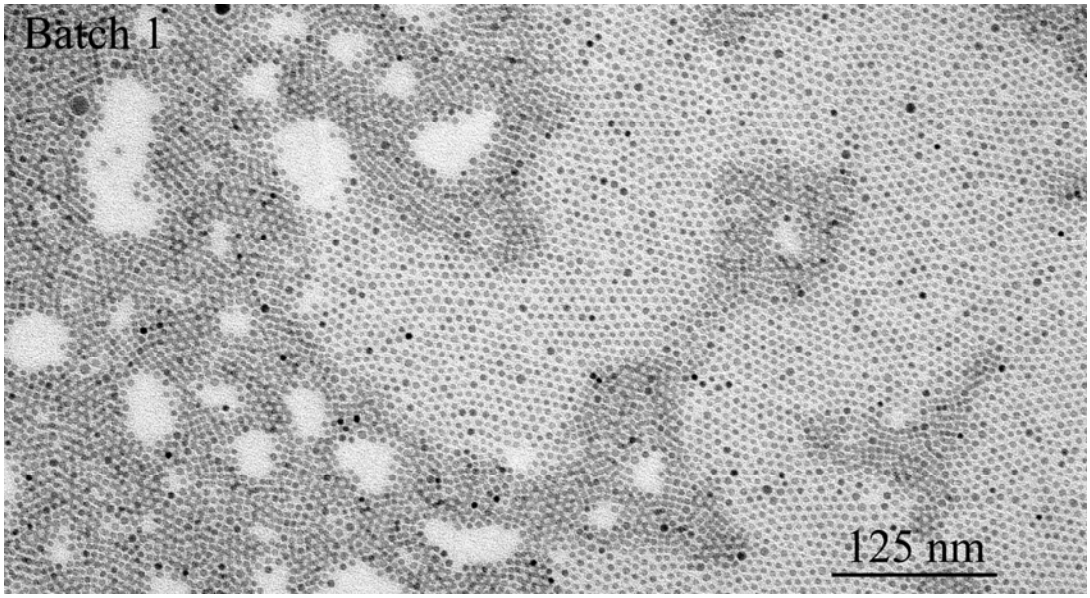

Figure 2.1 Transmission electron micrograph of iron oxide nanoparticles. These nanoparticles were produced by $Fe(acac)_3$ decomposition in organic solvents.

The nanoparticles produced by the above methods are coated with organic surface ligands due to association between the metal atoms, alkyl-amines (oleylamine) and alkyl-carboxylates (oleic acid) presents in the reaction solution. As a result they are only soluble in organic solvents[11]. For biomedical applications, they must be phase transferred into the aqueous phase using polymer coatings or ligand substitution procedures.

2.2 Semiconductor Quantum Dots

Quantum dots (QD) are semiconductor inorganic nanocrystals that exhibit size-tunable fluorescent properties. Recently they have garnered attention in the biomedical

science arena due to their superior photoluminescent characteristics compared to traditionally used organic fluorophores [1]. Although organic dye molecules are widely used in biological detection assays due to their availability, QDs are emerging as a comparable class of fluorophores[1]. Commonly available QDs that are used in biology are composed of CdSe nanocrystals capped with a thin layer of ZnS [38-40]. CdSe is typically used as the core because its band-gap energy spans the the visible region (400-800 nm) of the electromagnetic spectrum.

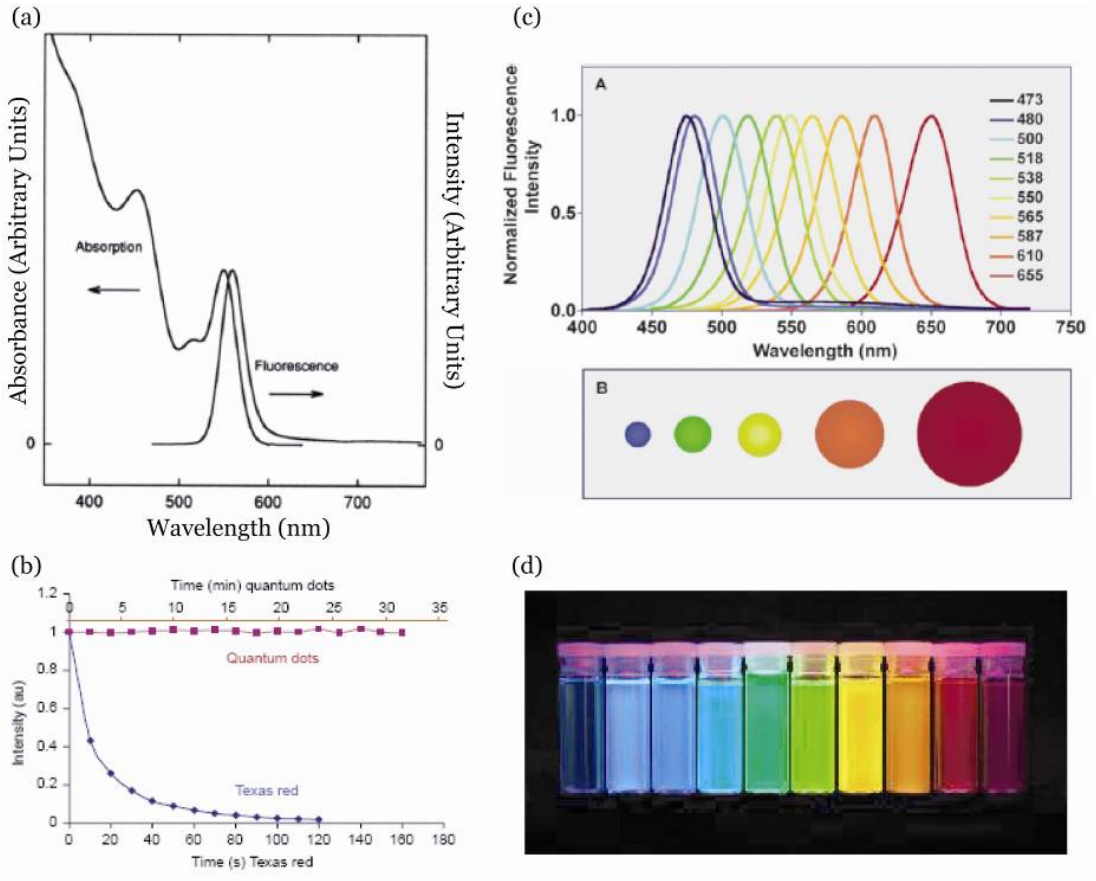

Figure 2.2: Photoluminescent properties of QDs. Compared to organic dyes, QDs have (A) Broad absorption band and a narrow symmetric excitation peak [41]. (B) Exceptional photostability [42] (C) Size-tunable emission [1], (D) Multiple color emission from single excitation source [43].

For most commercially available QDs, the emission wavelength is dependent on the physical size of the dots. In some cases emission can also be tuned by changing the composition of QDs. Therefore, it is possible to obtain a range of colors ranging from blue to red (**Figure 2.2**). QDs are superior to organic dyes in many ways. First, they are resistant to photobleaching and can be imaged for an extended period (up to several hours) making it useful for applications involving prolonged exposure to an excitation source[42, 44, 45]. Second, a single UV light source can excite QDs that emit different wavelengths of light. This is an important property as it allows for multiplexing and optical encoding[46]. Third, QDs have a broad excitation cross-section and a large Stoke's shift which allows for high Signal-to-Noise Ratio (SNR) and reduced cross-talk between fluorophores. Lastly, QDs have a large excitation coefficient (in the order of 100-1000 times more than fluorescent dyes) and as a result they are very bright [42, 47].

2.3 Bead-based assays

The growing popularity of bead-based assays in biology is due to several factors. Although microarray technology and other solid-phase detection technologies have successfully been employed for high-throughput multiplexed analysis, they suffer from detection sensitivity limits due to fixed surface area [48]. Bead assays are essentially a miniaturization of microarrays since each bead can be uniquely encoded for multiple targets [49, 50]. Unlike solid-phase biochips and microarrays, microbeads (micron-sized spherical particles) are easy to manipulate and provide much faster reaction kinetics due to their suspension in homogeneous solution and the associated advantages in diffusion rates. In addition, microbeads have large surface areas and can be used to enrich target molecules and to increase the dynamic range of target detection. The material of the bead serves as a host to molecules and nanoparticles at very high densities, which enhances their individual properties considerably. Recently, optically encoded beads

have been developed for commercial flow cytometry based application. A popular example is the Luminex bead product [49, 51], which incorporates two dyes in varying ratios to produce 100 spectrally distinct microspheres. Similarly, QDs have been successfully incorporated producing intensely bright microbeads[43, 52-54].

2.4 Magneto-optical nanotechnology

Exploration of potential applications of magneto-optical composite material has only recently been investigated. The primary motivation for research in this area is to combine the functionalities offered by each type of nanomaterial to address biomedical needs. In the case of magneto-optical technology, the goal is to obtain composite materials that can retain the nano-scale properties that each individual nanoparticle would otherwise have. There are many exciting applications for these materials in the biomedical sciences. For example, by correlating the deep imaging capabilities of magnetic resonance imaging (MRI) with ultrasensitive optical imaging, a surgeon could visually identify tiny tumors or other small lesions during an operation and remove the diseased cells and tissue completely [4]. Medical imaging modalities such as MRI and PET can identify diseases non-invasively, but they do not provide a visual guide during surgery. The development of magnetic-QD hetero-dimer probes could solve this problem [55, 56]. Synthesis of composite materials at the nanometer [55, 57-65] and micrometer [66-68] scale has been demonstrated by various researchers. In some cases the goal has been to create nanoprobes that can emit a fluorescent signal and behave as a contrast agent for MRI applications. In other cases, the goal has been to create materials that can be magnetically manipulated yet exhibit favorable optical properties [66, 69-71]. For example, Su et al. described an elegant method to use immunomagnetic nanoparticles to capture *E.Coli* bacteria and detect them with great accuracy using QD [31].

2.5 Circulating Tumor Cells

Tumor metastasis involves a series of discrete steps that result in the dissemination of tumor cells to distant sites through the blood (**Figure 2.3**)[72]. First, the tumor cells must invade the tissue surrounding the tumor so as to obtain access to the blood vessels and lymphatic system. Upon circulation through the body, these circulating tumor cells (CTC) must extravasate into distant site and proliferate. In 1889, Paget described the metastatic process as a seed-soil hypothesis[73]. According to his hypothesis, just like seeds of a plant that are dispersed will only grow when they land on good soil, tumor cells are selective for the best environment where they can colonize and grow. The first attempts to detect these rogue circulating tumor cells from peripheral blood dates back to the 19th century when Ashworth observed tumor-like cells in the blood of cancer patients after autopsy [74]. Almost 80% of all tumors are epithelial in origin and will need to alter their morphology to detach from the tumor site and display enhanced mobility. Unfortunately, by the time metastasis is apparent a large population of cells have already disseminated into body fluids such as urine, sputum, and blood. At this stage, patient prognosis is poor and the administration of therapy is often futile. Most of these cells exhibit the same genetic characteristics that are found in cells at the primary tumor site. Sensitive assays are available such as mass spectroscopy and PCR but some of these assays are expensive to run, complex and technically challenging. Prior to the appearance of morphologically distinct features in precancerous lesions, several genetic mutations have already been taking place.

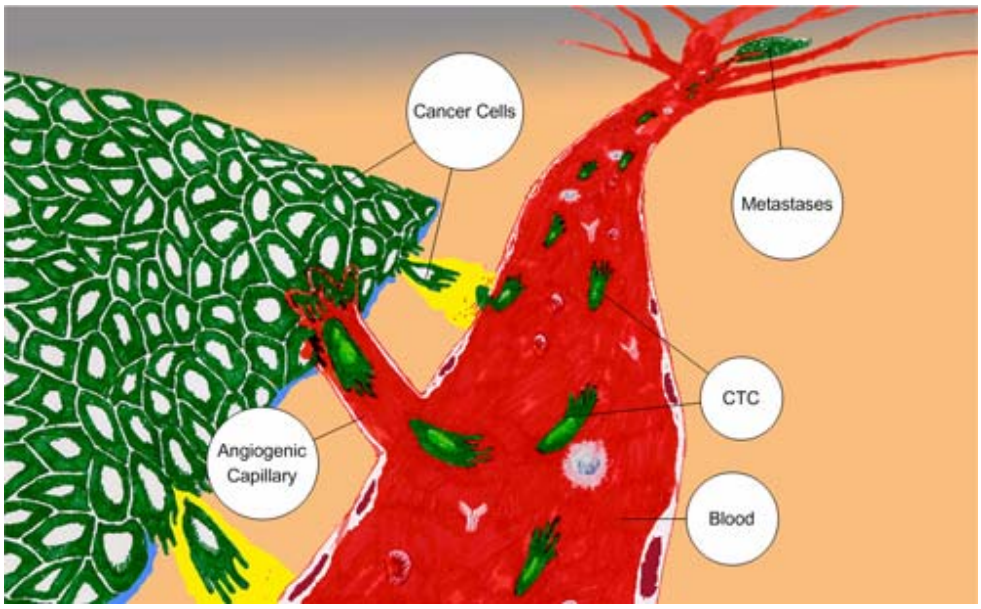

Figure 2.3: Schematic illustration of tumor cell dissemination from a local site to distant organs. The disseminated cells that are found in blood are called CTC (circulating tumor cells) and will eventually migrate from blood to a suitable environment and proliferate. Obtained from http://www.vitatex.com.

Therefore, a molecular assay needs to be developed that can intercept, enrich and perform molecular characterization of the cells undergoing a transition from precancerous to malignant phenotype. The National Cancer Institute (NCI) has outlined this transition phase as a "window of opportunity" that should be the focus of early detection assays. Needless to say, markers that can detect such cells need to be developed. In an important study conducted by Cristofanilli et al., levels of circulating tumor cells were quantified and correlated to disease progression and survival of metastatic breast cancer patients. The results showed that the number of CTC's before therapy and after the first follow-up are useful predictors of overall survival[75]. In particular, a fascinating conclusion of this study was the fact that having more than 5 cells per 7.5 ml of blood represented a cut-off point above which patient survival dropped drastically. Current methods for detecting circulating cells as tumor cells involve labor-intensive and highly subjective techniques such as immunohistochemistry, FISH and

PCR. However, before any of the techniques can be used, the cells need to be enriched since there is a large discrepancy between the population of tumor cell and normal MNC's in the blood. A significant challenge is the ability to isolate 1-10 tumor positive cells with a high degree of specificity[76]. Also it is imperative that no tumor cells are lost during enrichment. Flow cytometry has successfully been used for high-throughput analysis, but there is no morphological information that can be provided [77, 78]. Multiple color detection of cells with organic dyes is also possible but the inherent photostability problems associated with dye molecules make accurate quantitative analysis difficult. Overwhelming evidence suggests that there is an association between detection of tumor cell load and patient survival, and therefore it is worthwhile to invest efforts in developing tools to detect these cells [77, 79-83].

2.6 Components of Blood

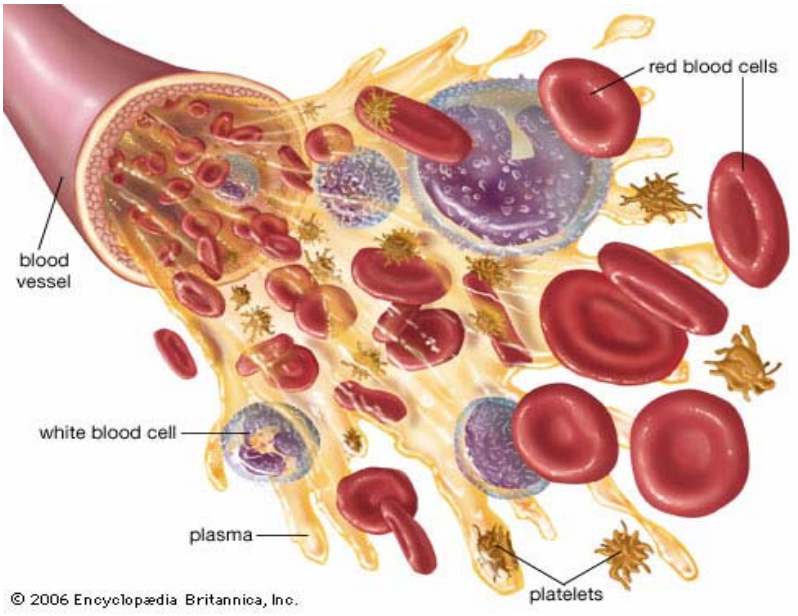

Figure 2.4: Schematic illustration showing components of human blood. Human blood consists of white blood cells (leukocytes), red blood cells (erythrocytes), platelets, and plasma. Courtesy http://www.britannica.com.

Blood is complex biological medium comprising plasma, white blood cells, red blood cells and platelets (**Figure 2.4**). Due to their small size, nanoparticles have distinct properties that are not available in the bulk form of the same material. When nanoparticles are introduced into whole blood there are a plethora of interactions possible with these components. In particular, the small size and the tremendous increase in surface area lead to increased interactions with soluble plasma proteins. It is surprising that despite significant developments made in nanoparticles for biomedicine and diagnostic applications, relatively little is known about interactions of nanoparticles such as QDs with immune cells and proteins [84].

Leukocytes are mobile units of the body's immune (protective) system. They are formed partially in the bone marrow and partially in lymph tissue. Most of them are specifically transported and activated in the presence of foreign agents, such as nanomaterials. There are six types of white blood cells normally found in the blood (**Figure 2.5**).

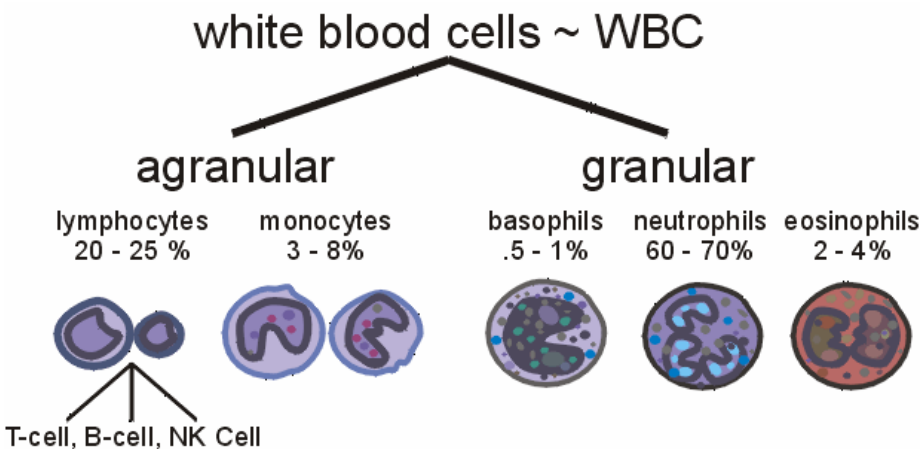

Figure 2.5: Composition of leukocytes in normal human blood. Obtained from http://www.lymphomation.org.

The leukocytes are typically classified either by their appearance (granular vs. agranular) or by the presence of multiple nuclei. There are three types of polymorphonuclear cells that have a granular appearance; these are eosinophils, basophils and neutrophils. These cells are commonly categorized as granulocytes. Lymphocytes and monocytes are agranular cells with single large nuclei that comprise mononuclear cells. Additionally, there are a large number of platelets that are cell fragments of megakaryocytes. The adult human being has about 7000 blood cells per microliter of blood and 5 million red blood cells. The approximate percentage of the cells is shown in **Figure 2.4**. The number of platelets in each microliter of blood is normally 300,000. It should be noted that these percentages are approximate and vary from person to person under different physiological conditions.

Phagocytes are cells that ingest debris, dead cells and foreign particles (bacteria, nanoparticles) from blood through a process called phagocytosis (described in Chapter 6). In the blood, the main phagocytes are neutrophils and macrophages/monocytes. Phagocytosis is an active process that helps to clear foreign substances from the circulatory system, and they play a crucial role in the removal of harmful substances. It is thought that the events mediating this process are closely connected to protein adsorption and tagging of the foreign agent with antibodies. Therefore, in order to design better nanoparticle probes for whole blood assays, and *in vivo* imaging, one needs to understand the relationship between these cells, the effector proteins and the nanoparticles. This will be explained in detail in Chapter 6.

2.7 References

[1] A. Smith and S. Nie, Chemical analysis and cellular imaging with quantum dots, *ANALYST* **129**: 672-677. (2004)

[2] A.M. Smith, X. Gao and S. Nie, Quantum dot nanocrystals for in vivo molecular and cellular imaging, *Photochem Photobiol* **80**: 377-385. (2004)

[3] A. Zajac, D. Song, W. Qian and T. Zhukov, Protein microarrays and quantum dot probes for early cancer detection, *Colloids Surf B Biointerfaces* **58**: 309-314. (2007)

[4] M.F. Kircher, U. Mahmood, R.S. King, R. Weissleder and L. Josephson, A multimodal nanoparticle for preoperative magnetic resonance imaging and intraoperative optical brain tumor delineation, *Cancer Res* **63**: 8122-8125. (2003)

[5] B.A. Moffat, G.R. Reddy, P. McConville, D.E. Hall, T.L. Chenevert, R.R. Kopelman*, et al.*, A novel polyacrylamide magnetic nanoparticle contrast agent for molecular imaging using MRI, *Mol Imaging* **2**: 324-332. (2003)

[6] A.S. Lubbe, C. Alexiou and C. Bergemann, Clinical applications of magnetic drug targeting, *J Surg Res* **95**: 200-206. (2001)

[7] J. Rehman, J. Landman, R.D. Tucker, D.G. Bostwick, C.P. Sundaram and R.V. Clayman, Ferromagnetic self-regulating reheatable thermal rod implants for in situ tissue ablation, *J Endourol* **16**: 523-531. (2002)

[8] A.C. Samia, S. Dayal and C. Burda, Quantum dot-based energy transfer: perspectives and potential for applications in photodynamic therapy, *Photochem Photobiol* **82**: 617-625. (2006)

[9] U. Hafeli, Magnetism in Medicine: A Handbook, Wiley-VCH, Berlin (1998).

[10] Q.A. Pankhurst, J. Connolly, S.K. Jones and J. Dobson, Applications of magnetic nanoparticles in biomedicine, *J. Phys. D-Appl. Phys.* **36**: R167-R181. (2003)

[11] C.J. Xu and S.H. Sun, Monodisperse magnetic nanoparticles for biomedical applications, *Polym. Int.* **56**: 821-826. (2007)

[12] K.B. Lee, S. Park and C.A. Mirkin, Multicomponent magnetic nanorods for biomolecular separations, *Angew Chem Int Ed Engl* **43**: 3048-3050. (2004)

[13] S. Miltenyi, W. Muller, W. Weichel and A. Radbruch, High-Gradient Magnetic Cell-Separation with Macs, *Cytometry* **11**: 231-238. (1990)

[14] R.S. Molday, S.P. Yen and A. Rembaum, Application of magnetic microspheres in labelling and separation of cells, *Nature* **268**: 437-438. (1977)

[15] Y. Jing, L.R. Moore, P.S. Williams, J.J. Chalmers, S.S. Farag, B. Bolwell*, et al.*, Blood progenitor cell separation from clinical leukapheresis product by magnetic nanoparticle binding and magnetophoresis, *Biotechnol Bioeng* **96**: 1139-1154. (2007)

[16] J.W. Choi, Fabrication of micromachined magnetic particle separators for bioseparation in microfluidic systems, *Methods Mol Biol* **321**: 65-81. (2006)

[17] S.J. Son, J. Reichel, B. He, M. Schuchman and S.B. Lee, Magnetic nanotubes for magnetic-field-assisted bioseparation, biointeraction, and drug delivery, *J Am Chem Soc* **127**: 7316-7317. (2005)

[18] J.M. Perez, L. Josephson, T. O'Loughlin, D. Hogemann and R. Weissleder, Magnetic relaxation switches capable of sensing molecular interactions, *Nat Biotechnol* **20**: 816-820. (2002)

[19] J.M. Perez, T. O'Loughin, F.J. Simeone, R. Weissleder and L. Josephson, DNA-based magnetic nanoparticle assembly acts as a magnetic relaxation nanoswitch allowing screening of DNA-cleaving agents, *J Am Chem Soc* **124**: 2856-2857. (2002)

[20] I. Hilger, R. Hergt and W.A. Kaiser, Use of magnetic nanoparticle heating in the treatment of breast cancer, *IEE Proc Nanobiotechnol* **152**: 33-39. (2005)

[21] I. Hilger, K. Fruhauf, W. Andra, R. Hiergeist, R. Hergt and W.A. Kaiser, Heating potential of iron oxides for therapeutic purposes in interventional radiology, *Acad Radiol* **9**: 198-202. (2002)

[22] J.W. Bulte, T. Douglas, B. Witwer, S.C. Zhang, E. Strable, B.K. Lewis*, et al.*, Magnetodendrimers allow endosomal magnetic labeling and in vivo tracking of stem cells, *Nat Biotechnol* **19**: 1141-1147. (2001)

[23] J.W. Bulte, S. Zhang, P. van Gelderen, V. Herynek, E.K. Jordan, I.D. Duncan*, et al.*, Neurotransplantation of magnetically labeled oligodendrocyte progenitors: magnetic resonance tracking of cell migration and myelination, *Proc Natl Acad Sci U S A* **96**: 15256-15261. (1999)

[24] M. Lewin, N. Carlesso, C.H. Tung, X.W. Tang, D. Cory, D.T. Scadden*, et al.*, Tat peptide-derivatized magnetic nanoparticles allow in vivo tracking and recovery of progenitor cells, *Nat Biotechnol* **18**: 410-414. (2000)

[25] D. Hogemann, L. Josephson, R. Weissleder and J.P. Basilion, Improvement of MRI probes to allow efficient detection of gene expression, *Bioconjug Chem* **11**: 941-946. (2000)

[26] E.A. Schellenberger, D. Hogemann, L. Josephson and R. Weissleder, Annexin V-CLIO: a nanoparticle for detecting apoptosis by MRI, *Acad Radiol* **9 Suppl 2**: S310-311. (2002)

[27] M.N. Widjojoatmodjo, A.C. Fluit, R. Torensma and J. Verhoef, Comparison of immunomagnetic beads coated with protein A, protein G, or goat anti-mouse immunoglobulins. Applications in enzyme immunoassays and immunomagnetic separations, *J Immunol Methods* **165**: 11-19. (1993)

[28] X.D. Tong, B. Xue and Y. Sun, A novel magnetic affinity support for protein adsorption and purification, *Biotechnol Prog* **17**: 134-139. (2001)

[29] S. Bucak, D.A. Jones, P.E. Laibinis and T.A. Hatton, Protein separations using colloidal magnetic nanoparticles, *Biotechnol Prog* **19**: 477-484. (2003)

[30] H. Gu, K. Xu, C. Xu and B. Xu, Biofunctional magnetic nanoparticles for protein separation and pathogen detection, *Chem Commun (Camb)*: 941-949. (2006)

[31] X.L. Su and Y. Li, Quantum dot biolabeling coupled with immunomagnetic separation for detection of Escherichia coli O157:H7, *Anal Chem* **76**: 4806-4810. (2004)

[32] M. Kuhara, H. Takeyama, T. Tanaka and T. Matsunaga, Magnetic cell separation using antibody binding with protein a expressed on bacterial magnetic particles, *Anal Chem* **76**: 6207-6213. (2004)

[33] K.J. Widder, A.E. Senyei, H. Ovadia and P.Y. Paterson, Magnetic protein A microspheres: a rapid method for cell separation, *Clin Immunol Immunopathol* **14**: 395-400. (1979)

[34] C.J. Pankhurst Q.A., Jones S.K., and J. Dobson, Applications of magnetic nanoparticles in biomedicine, *J. Phys. D: Appl. Phys.* **36**: R167-R181. (2003)

[35] S.H. Sun, C.B. Murray, D. Weller, L. Folks and A. Moser, Monodisperse FePt nanoparticles and ferromagnetic FePt nanocrystal superlattices, *Science* **287**: 1989-1992. (2000)

[36] T. Hyeon, S.S. Lee, J. Park, Y. Chung and H.B. Na, Synthesis of highly crystalline and monodisperse maghemite nanocrystallites without a size-selection process, *J Am Chem Soc* **123**: 12798-12801. (2001)

[37] S.H. Sun, H. Zeng, D.B. Robinson, S. Raoux, P.M. Rice, S.X. Wang*, et al.*, Monodisperse MFe2O4 (M = Fe, Co, Mn) nanoparticles, *Journal of the American Chemical Society* **126**: 273-279. (2004)

[38] B. Dabbousi, J. RodriguezViejo, F. Mikulec, J. Heine, H. Mattoussi, R. Ober*, et al.*, (CdSe)ZnS core-shell quantum dots: Synthesis and characterization of a size series of highly luminescent nanocrystallites, *JOURNAL OF PHYSICAL CHEMISTRY B* **101**: 9463-9475. (1997)

[39] M. Hines and P. Guyot-Sionnest, Synthesis and characterization of strongly luminescing ZnS-Capped CdSe nanocrystals, *JOURNAL OF PHYSICAL CHEMISTRY* **100**: 468-471. (1996)

[40] X. Peng, M. Schlamp, A. Kadavanich and A. Alivisatos, Epitaxial growth of highly luminescent CdSe/CdS core/shell nanocrystals with photostability and electronic accessibility, *JOURNAL OF THE AMERICAN CHEMICAL SOCIETY* **119**: 7019-7029. (1997)

[41] C.B. Murray, D.J. Norris and M.G. Bawendi, Synthesis and Characterization of Nearly Monodisperse Cde (E = S, Se, Te) Semiconductor Nanocrystallites, *Journal of the American Chemical Society* **115**: 8706-8715. (1993)

[42] W.C. Chan, D.J. Maxwell, X. Gao, R.E. Bailey, M. Han and S. Nie, Luminescent quantum dots for multiplexed biological detection and imaging, *Curr Opin Biotechnol* **13**: 40-46. (2002)

[43] M. Han, X. Gao, J.Z. Su and S. Nie, Quantum-dot-tagged microbeads for multiplexed optical coding of biomolecules, *Nat Biotechnol* **19**: 631-635. (2001)

[44] X. Wu, H. Liu, J. Liu, K.N. Haley, J.A. Treadway, J.P. Larson*, et al.*, Immunofluorescent labeling of cancer marker Her2 and other cellular targets with semiconductor quantum dots, *Nat Biotechnol* **21**: 41-46. (2003)

[45] X. Gao, L. Yang, J.A. Petros, F.F. Marshall, J.W. Simons and S. Nie, In vivo molecular and cellular imaging with quantum dots, *Curr Opin Biotechnol* **16**: 63-72. (2005)

[46] S.J. Rosenthal, Bar-coding biomolecules with fluorescent nanocrystals, *Nat Biotechnol* **19**: 621-622. (2001)

[47] M. Bruchez, M. Moronne, P. Gin, S. Weiss and A.P. Alivisatos, Semiconductor nanocrystals as fluorescent biological labels, *Science* **281**: 2013-2016. (1998)

[48] B.E. Yingyongnarongkul, S.E. How, J.J. Diaz-Mochon, M. Muzerelle and M. Bradley, Parallel and multiplexed bead-based assays and encoding strategies, *Combinatorial Chemistry & High Throughput Screening* **6**: 577-587. (2003)

[49] K. Braeckmans, S.C. De Smedt, M. Leblans, R. Pauwels and J. Demeester, Encoding microcarriers: Present and future technologies, *Nature Reviews Drug Discovery* **1**: 447-456. (2002)

[50] N.H. Finkel, X. Lou, C. Wang and L. He, Barcoding the microworld, *Anal Chem* **76**: 352A-359A. (2004)

[51] R.J. Fulton, R.L. McDade, P.L. Smith, L.J. Kienker and J.R. Kettman, Advanced multiplexed analysis with the FlowMetrix(TM) system, *Clinical Chemistry* **43**: 1749-1756. (1997)

[52] X. Gao and S. Nie, Quantum dot-encoded beads, *Methods Mol Biol* **303**: 61-72. (2005)

[53] X.H. Gao and S.M. Nie, Doping mesoporous materials with multicolor quantum dots, *Journal of Physical Chemistry B* **107**: 11575-11578. (2003)

[54] X. Gao and S. Nie, Quantum dot-encoded mesoporous beads with high brightness and uniformity: rapid readout using flow cytometry, *Anal Chem* **76**: 2406-2410. (2004)

[55] H. Gu, R. Zheng, X. Zhang and B. Xu, Facile one-pot synthesis of bifunctional heterodimers of nanoparticles: a conjugate of quantum dot and magnetic nanoparticles, *J Am Chem Soc* **126**: 5664-5665. (2004)

[56] A. Agrawal, T. Sathe and S. Nie, Nanoparticle Probes for Ultrasensitive Biomolecular Detection and Imaging, Wiley Interscience (2006).

[57] S. Santra, H.S. Yang, P.H. Holloway, J.T. Stanley and R.A. Mericle, Synthesis of water-dispersible fluorescent, radio-opaque, and paramagnetic CdS : Mn/ZnS

quantum dots: A multifunctional probe for bioimaging, *Journal of the American Chemical Society* **127**: 1656-1657. (2005)

[58] H. Kim, M. Achermann, L.P. Balet, J.A. Hollingsworth and V.I. Klimov, Synthesis and characterization of Co/CdSe core/shell nanocomposites: Bifunctional magnetic-optical nanocrystals, *Journal of the American Chemical Society* **127**: 544-546. (2005)

[59] F.X. Redl, K.S. Cho, C.B. Murray and S. O'Brien, Three-dimensional binary superlattices of magnetic nanocrystals and semiconductor quantum dots, *Nature* **423**: 968-971. (2003)

[60] X. Hong, J. Li, M.J. Wang, J.J. Xu, W. Guo, J.H. Li*, et al.*, Fabrication of magnetic luminescent nanocomposites by a layer-by-layer self-assembly approach, *Chemistry of Materials* **16**: 4022-4027. (2004)

[61] D.K. Yi, S.T. Selvan, S.S. Lee, G.C. Papaefthymiou, D. Kundaliya and J.Y. Ying, Silica-coated nanocomposites of magnetic nanoparticles and quantum dots, *J Am Chem Soc* **127**: 4990-4991. (2005)

[62] D.S. Wang, J.B. He, N. Rosenzweig and Z. Rosenzweig, Superparamagnetic Fe2O3 Beads-CdSe/ZnS quantum dots core-shell nanocomposite particles for cell separation, *Nano Letters* **4**: 409-413. (2004)

[63] H.Y. Xie, C. Zuo, Y. Liu, Z.L. Zhang, D.W. Pang, X.L. Li*, et al.*, Cell-targeting multifunctional nanospheres with both fluorescence and magnetism, *Small* **1**: 506-509. (2005)

[64] H.W. Gu, R.K. Zheng, H. Liu, X.X. Zhang and B. Xu, Direct synthesis of a bimodal nanosponge based on FePt and ZnS, *Small* **1**: 402-406. (2005)

[65] L. Josephson, M.F. Kircher, U. Mahmood, Y. Tang and R. Weissleder, Near-infrared fluorescent nanoparticles as combined MR/optical imaging probes, *Bioconjug Chem* **13**: 554-560. (2002)

[66] S.K. Mandal, N. Lequeux, B. Rotenberg, M. Tramier, J. Fattaccioli, J. Bibette*, et al.*, Encapsulation of magnetic and fluorescent nanoparticles in emulsion droplets, *Langmuir* **21**: 4175-4179. (2005)

[67] B. Zebli, A.S. Susha, G.B. Sukhorukov, A.L. Rogach and W.J. Parak, Magnetic targeting and cellular uptake of polymer microcapsules simultaneously

functionalized with magnetic and luminescent nanocrystals, *Langmuir* **21**: 4262-4265. (2005)

[68] N. Gaponik, I.L. Radtchenko, G.B. Sukhorukov and A.L. Rogach, Luminescent polymer microcapsules addressable by a magnetic field, *Langmuir* **20**: 1449-1452. (2004)

[69] T.R. Sathe, A. Agrawal and S. Nie, Mesoporous silica beads embedded with semiconductor quantum dots and iron oxide nanocrystals: dual-function microcarriers for optical encoding and magnetic separation, *Anal Chem* **78**: 5627-5632. (2006)

[70] D. Muller-Schulte, T. Schmitz-Rode and P. Borm, Ultra-fast synthesis of magnetic and luminescent silica beads for versatile bioanalytical applications, *Journal of Magnetism and Magnetic Materials* **293**: 135-143. (2005)

[71] V. Salgueirino-Maceira, M.A. Correa-Duarte, M. Spasova, L.M. Liz-Marzan and M. Farle, Composite silica spheres with magnetic and luminescent functionalities, *Adv Funct Mater* **16**: 509-514. (2006)

[72] P.S. Steeg, Tumor metastasis: mechanistic insights and clinical challenges, *Nat Med* **12**: 895-904. (2006)

[73] S. Paget, The distribution of secondary growths in cancer of the breast. 1889, *Cancer Metastasis Rev* **8**: 98-101. (1989)

[74] T.R. Ashworth, A case of cancer in which cells similar to those in the tumours were seen in the blood after death., *Aust Med J* **14**: 146. (1869)

[75] M. Cristofanilli, G.T. Budd, M.J. Ellis, A. Stopeck, J. Matera, M.C. Miller*, et al.*, Circulating tumor cells, disease progression, and survival in metastatic breast cancer, *N Engl J Med* **351**: 781-791. (2004)

[76] B.K. Zehentner, Detection of disseminated tumor cells: strategies and diagnostic implications, *Expert Rev Mol Diagn* **2**: 41-48. (2002)

[77] P.D. Beitsch and E. Clifford, Detection of carcinoma cells in the blood of breast cancer patients, *Am J Surg* **180**: 446-448; discussion 448-449. (2000)

[78] A.L. Allan, S.A. Vantyghem, A.B. Tuck, A.F. Chambers, I.H. Chin-Yee and M. Keeney, Detection and quantification of circulating tumor cells in mouse models

of human breast cancer using immunomagnetic enrichment and multiparameter flow cytometry, *Cytometry A* **65**: 4-14. (2005)

[79] P.L. Judson, M.A. Geller, R.L. Bliss, M.P. Boente, L.S. Downs, Jr., P.A. Argenta*, et al.*, Preoperative detection of peripherally circulating cancer cells and its prognostic significance in ovarian cancer, *Gynecol Oncol* **91**: 389-394. (2003)

[80] V. Muller, N. Stahmann, S. Riethdorf, T. Rau, T. Zabel, A. Goetz*, et al.*, Circulating tumor cells in breast cancer: correlation to bone marrow micrometastases, heterogeneous response to systemic therapy and low proliferative activity, *Clin Cancer Res* **11**: 3678-3685. (2005)

[81] R.A. Ghossein, S. Bhattacharya and J. Rosai, Molecular detection of micrometastases and circulating tumor cells in solid tumors, *Clin Cancer Res* **5**: 1950-1960. (1999)

[82] M.M. Reinholz, A. Nibbe, L.M. Jonart, K. Kitzmann, V.J. Suman, J.N. Ingle*, et al.*, Evaluation of a panel of tumor markers for molecular detection of circulating cancer cells in women with suspected breast cancer, *Clin Cancer Res* **11**: 3722-3732. (2005)

[83] E. Racila, D. Euhus, A.J. Weiss, C. Rao, J. McConnell, L.W. Terstappen*, et al.*, Detection and characterization of carcinoma cells in the blood, *Proc Natl Acad Sci U S A* **95**: 4589-4594. (1998)

[84] Dobrovolskaia MA and S.E. McNeil, Immunological properties of engineered nanomaterials, *Nature Nanotechnology* **2**: 469-478. (2007)

CHAPTER 3

DUAL FUNCTION MESOPOROUS MICROBEADS: OPTICALLY ENCODED AND MAGNETICALLY SEPARABLE FOR BIOLOGICAL DETECTION

3.1 Introduction

Diagnosing complex diseases such as cancer at an early stage requires the ability to detect and quantify disease molecules in a rapid, efficient and reproducible manner. As we gain a better understanding of the molecular basis of cancer, it will also be important to detect multiple tumor-associated molecules in a one-step assay. Such a technology should be able to probe patient samples, such as blood that is accessible and obtainable in a non-invasive manner. Next, the technology should be able to detect rare number of molecules from a large sample volume. Solid tumors are in constant interaction with body fluids such as human blood and lymph as they gain access to soluble nutrients. Detection of low copy numbers of target molecules like protein biomarkers may involve analysis of large sample volumes. As a result, there is a need to develop technology for ultrasensitive disease detection from complex heterogeneous biological samples.

High throughput and rapid assays that can detect multiple target molecules simultaneously with high sensitivity are desirable for many analytical applications. Micrometer-sized spherical beads are increasingly being used for such assays since their suspension in solution permits faster reaction kinetics [1-9]. Moreover, they can be physically manipulated and can offer a greater dynamic range of target detection (due to large surface area) compared to solid state microarray chip based assays. Enabling a

high throughput detection system requires encoding a set of beads uniquely so that they can bind to an assigned target, be captured and decoded accurately.

The application of magnetic beads for the isolation, or enrichment of a cell [10-12], protein [9, 13-15], or DNA [16, 17] of interest, has been well known. In fact, several commercial kits are now available for magnetic separation using beads[18]. In some instances, beads are in the nanometer size range whereas in others, they are in the micrometer range. Most beads are developed by loading superparamagnetic nanoparticles into a host material that is well sealed to prevent exposure and leakage of the nanoparticles to the environment. An important requirement of such beads is to have no magnetic remnance upon removal of a magnetic field.

In a similar vein, the development of optical beads has allowed for the multiplexed detection of several biomolecules in one step using spectroscopic methods and flow cytometry. Recently, there have been numerous reports of optical beads that can be encoded with QDs thereby making it possible to uniquely code several thousand beads [5, 19-22]. A similar approach using organic dye loaded microbeads has successfully been translated to the commercial sector and is widely used for high-throughput flow based detection of cytokines in solution [4]. Our *hypothesis* is that combining these two properties of magnetic and optical beads into one composite material will greatly enhance detection sensitivity due to magnetic enrichment strategies while still maintaining multiplexing capability. The magnetic properties of the bead will also allow for external manipulation and isolation of beads for other applications. Moreover, as flow-based magnetophoresis technology improves, our beads have the potential to increase the degree of multiplexing by adding a magnetic encoding parameter to existing optical encoding by QDs.

In this chapter, we describe the preparation of dual-function optical and magnetic beads, and also report two-color optical encoding and rapid magnetic bead separation.

In comparison with other work in this area [12, 19, 23-28], we have used mesoporous beads to incorporate both types of nanoparticles through hydrophobic interactions. Due to the highly porous internal structure and very large surface area [29], these mesoporous beads (with pore sizes ranging from 2-100 nm) allow up to one million nanoparticles to be incorporated into a single micrometer-sized bead.

3.2 Methods

Materials

(All chemicals were purchased from Sigma-Aldrich (St. Louis, MO) unless stated otherwise.) Iron oxide (Fe_3O_4) magnetite nanocrystals with an average diameter of 6 nm (4-5% size variations) and coated with oleic acid and oleylamine were synthesized according to the procedure by Sun et al. [30] The initial nanocrystals were dispersed in hexane. Core-shell ternary quantum dots [31] dispersed in toluene and coated with tri-n-octyl phosphine oxide (TOPO), were provided by Crystalplex Corporation (Pittsburgh, PA). In addition, CdSe/ZnS core-shell quantum dots were synthesized according to literature procedures. [32] C_{18} (octadecyl) chain derivatized mesoporous silica microbeads (3-5 μm) were obtained from Alltech Inc. (Deerfield, IL). The average pore diameter of these beads is about 30 nm, but the random pore size distribution means that a collection of small and large pores co-exist that may be “interconnected” with each other. This pore structure not only allows rapid partitioning of nanocrystals into the mesoporous structures, but provides nanocrystals with a larger surface area for binding. Bead concentrations were determined by using a hemacytometer.

Bead Encoding and Doping

The doping procedure for preparing dual-function beads involved addition of 10 μl of 32- nM iron oxide nanocrystals and 2 μl of 100 nM quantum dots (QD) either in

sequence or simultaneously to a well-mixed solution of 1.5 million silica beads dissolved in 0.5 mL butanol. The solution was vigorously stirred for 15-20 minutes, and was then placed on a 1.5 Tesla NdFeB permanent magnet (MCE Products, Torrance, CA). A brownish pellet was observed at the side of the tube within 10 seconds. Supernatant was removed and the sample was washed 2-3 times in ethanol to remove free nanocrystals. Free iron oxide nanocrystals that are not be incorporated in the beads experience a much lower magnetic force in presence of a magnet compared to several thousands packed in a bead. These nanoparticles will therefore not pellet as fast as the beads and can be pipetted out along with the supernatant. This washing step is essential as it aids in partitioning any remaining quantum dots into the highly hydrophobic porous sites of the bead. Non-magnetic beads used in bead separation efficiency studies were prepared according to Gao et al.[21]. These beads had to be pelleted by standard centrifugation since they cannot be magnetically manipulated. For sequential doping studies, a large batch of QD-doped beads were first prepared by mixing 5 µl of 100 nM QD with 50 µl bead solution (concentration of 5.15 x 10^5 beads /µl) in 0.5 mL 1-butanol. Each resulting bead contains approximately 13,000 QD's. The bead solution was then aliquoted into 8 equal volumes containing about 3.2 million beads and iron oxide nanocrystals were added in increasing amounts (i.e., 2 µl, 5 µl, 10 µl, 20 µl, 30 µl, 50 µl, 100 µl of 32 nM iron oxide) to each of the aliquots.

Optical Microscopy

Fluorescence images of individual beads spread on coverglass (Corning, Corning, NY) were obtained with an Olympus IX-70 inverted epifluorescence microscope (Olympus, Melville, NY) equipped with Nikon D1X digital CCD camera, broad-band 100W mercury arc lamp with a blue light BP460-490 excitation filter (Chroma Tech., Rockingham, VT), a DM500 dichroic mirror and 520LP long pass emission filter (Chroma

Tech, Rockingham, VT). Wavelength-specific single-bead fluorescence spectra were obtained with a single stage SpectraPro 150 spectrometer (Roper Scientific, Trenton, NJ) connected to the side port of the fluorescence microscope. A schematic of the setup is seen in Figure 3.1.

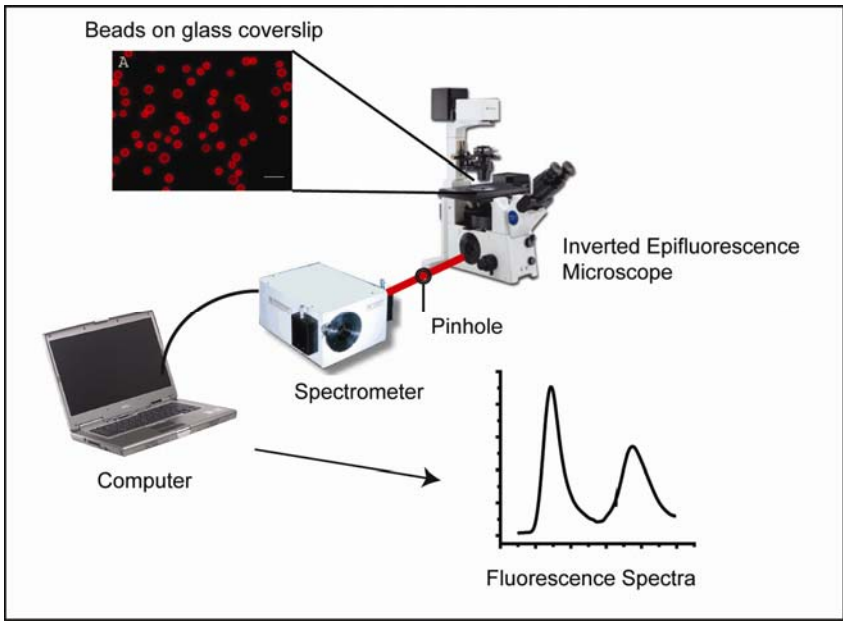

Figure 3.1: Single bead spectroscopy setup used for obtaining fluorescence spectra. By using a pinhole in between the microscope port and spectrometer, one can obtain fluorescence spectra from a single bead.

Polymer Coating

Hydrophobic bead surface was made hydrophilic by using octylamine poly (acrylic acid), an amphiphilic polymer prepared by modifying 40% of the carboxylic acid groups of polyacrylic acid with octylamine. Thus, hydrophobic beads were added to a 50:50 mixture of Triton X-100 and octylamine poly (acrylic acid). Absence of Triton X-100 surfactant led to poor bead stability and aggregation. The polymer-coated beads were dispersed in PBS with 0.02% Tween 20.

Bead Counting and Data Analysis

True color fluorescence images were obtained and beads counted using a data visualization and image analysis software package (Interactive Data Language or IDL, Research Systems Inc., Boulder CO). An astrophotometry package, DAOPHOT [33] which operates in IDL, was adapted for image processing to locate particles accurately. Threshold values were set for red and green channel images so that red and green beads could be accurately counted. Beads were then visually counted from the image to match up the results. The threshold settings led to an error of less than 3-4% in the number count. The separation efficiency is based on the removal of non-magnetic material from a solution containing magnetic beads. In our study, green non-magnetic beads were counted before and after separation. The number of beads before separation was divided by the initial number of beads, and multiplied by 100 to obtain the percentage.

Flow Cytometry

In order to assess the intensity-based encoding of the dual function beads, two sets of beads were created, having two different intensity levels of a single color. For this study, quantum dots with an emission maximum of 585 nm were used to encode the beads. The iron oxide nanoparticle concentration was kept constant and the beads were doped sequentially. QD intensity was obtained using a preset Phycoerythrin (PE) filter setting on a FACSAria flow cytometer (BD Biosciences, Franklin Lakes, NJ) as a function of side-scattering. The excitation source was a 405 nm violet laser. Scatter plots displaying side scattering as a function of PE signal intensity (QD) were plotted using Flowjo software.

Nanoparticle Toxicity

Precaution must be taken while handling QDs due to toxic nature of cadmium contained in the dots. Standard safety guidelines must be followed to prevent QDs from contact to skin. Supernatant containing excess QDs must be disposed off in organic solvent waste container according to OSHA guidelines. If the silica microbeads are provided in powder form, a respirator may help reduce possibility of silicosis through inhalation. There is no danger of inhalation of nanoparticles since they are synthesized in solution phase.

3.3 Results and Discussion

Bead Preparation

Silica beads derivatized with C18 alkyl chains offer a strongly hydrophobic environment for the incorporation of TOPO-coated QDs and oleic acid coated-iron oxide nanoparticles. The rapid partitioning and entrapment of nanoparticles throughout the bead make it possible to create a large number of uniformly doped beads in a short period (20-30 min). Bead doping can be accomplished in two ways: simultaneous incorporation by using pre-mixed nanoparticles, or sequential incorporation by adding QDs and iron oxide nanocrystals separately (**Figure 3.2A**). The choice of a particular doping scheme is largely determined by two factors: (i) the desired functionality and (ii) interaction amongst nanoparticles embedded in the bead. The physical size and surface chemistry of nanoparticles are important when incorporating them in a bead since dissimilar sizes or surface chemistries may lead to variations in doping kinetics and stability. Instead of traditional CdSe/ZnS core-shell QDs that have size-dependent photoluminescent properties, we have used ZnS capped ternary CdSSe alloyed TOPO-

coated QDs with composition-tunable optical properties at constant particle sizes [31]. Similarly, monodisperse iron oxide (magnetite; Fe_3O_4) nanocrystals, coated with hydrophobic oleic acid and oleylamine are synthesized such that they have the same physical size (6 nm) as QDs.

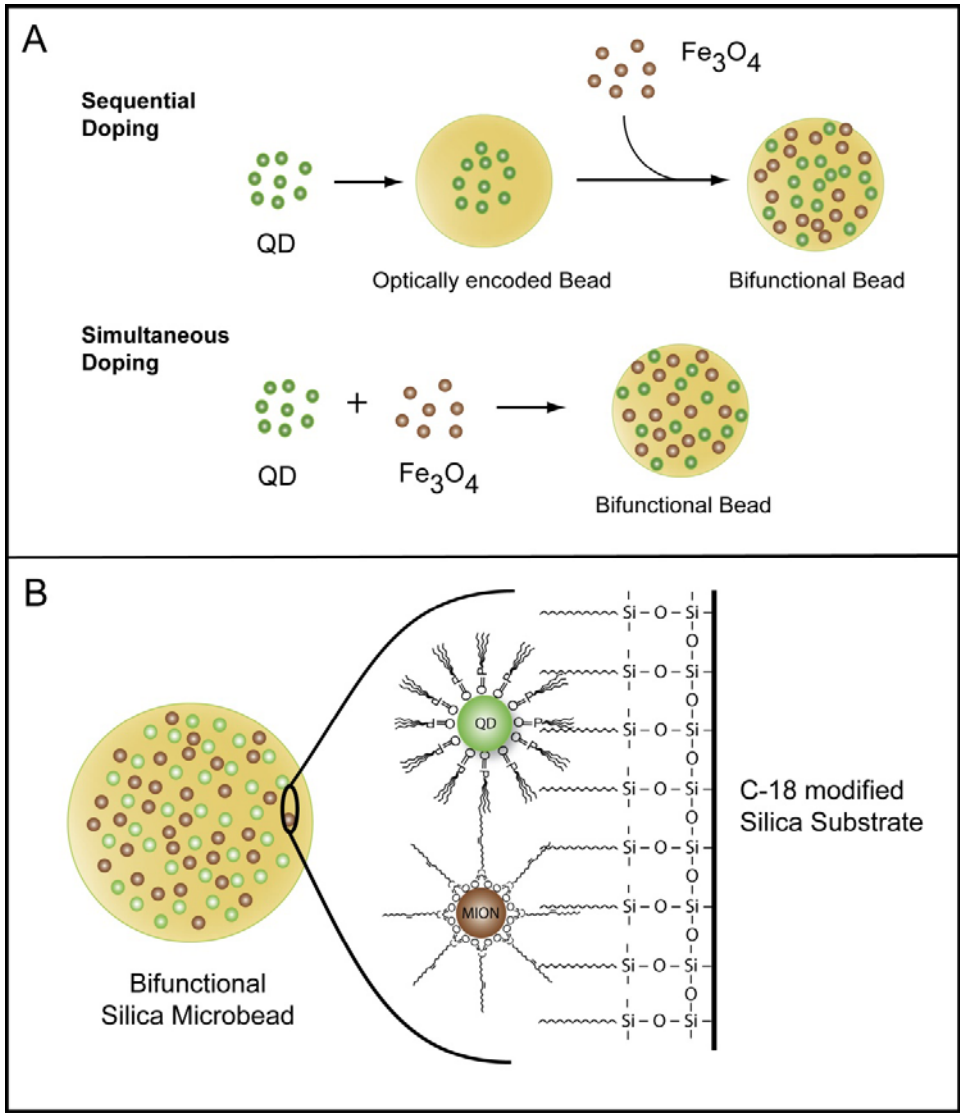

Figure 3.2: Schematic diagrams illustrating the preparation and the internal structure of dual-function optical and magnetic mesoporous beads. (A) Sequential and simultaneous incorporation of quantum dots and iron oxide nanocrystals into the nanoscale pores of silica beads. (B) Internal structure of encoded beads with strong interactions between hydrophobic surface ligands on the nanoparticles and long carbon chain (C-18) alkyl molecules on the silica pore walls.

The hydrophobic nanoparticles most likely interact strongly with the beads' porous network (**Figure 3.2B**). The internal structure, studied using TEM (**Figure 3.4**) of bead thin sections, reveals a highly porous structure with random pore size distribution. This random size may be beneficial for doping as the tortuosity and irregular surface of the pore allows stronger binding of nanoparticles to the pore surface by polyvalent interactions (that is, multiple ligands on the nanoparticle surface interacts with multiple C18 hydrocarbon molecules on the pore wall). Upon doping, beads suspended in solvent can be quickly washed by pulling them to the side of a microcentrifuge tube using an inexpensive permanent magnet and removing the supernatant. Consistent with this strong binding model, we found no trace of nanoparticle leakage from the beads into solvents such as water and ethanol (determined by fluorometric analysis of the solvent after washing). In the final step, the encoded hydrophobic beads are made hydrophilic by using an amphiphilic polymer, which is essential for conjugation to biomolecules and to minimize nonspecific binding.

For high throughput multiplexed analysis, the encoded beads should have uniform brightness. Fluorescence microscopy was performed on beads doped with QDs emitting at three wavelengths, either containing or not containing iron oxide (**Figure 3.3**). From the images, it is clear that the addition of iron oxide does not cause visible aggregation or clustering of QDs in the bead. Further, the superior QD brightness allows for easy visualization of beads that are magnetically addressable. Based on QD doping studies (performed by fluorometric analysis of QDs remaining in solution after bead doping), we have calculated that each bead, with 30 nm pore size, can roughly accommodate 0.3 to 0.4 million nanoparticles (diameter = 6 nm). This high loading capacity together with the high extinction coefficient of QDs implies that only a small fraction of binding sites need to be occupied by QDs. This permits other types of

nanoparticles to occupy the remaining binding sites. We estimate that occupation of 10-15% of sites with QDs is enough to accurately encode an optical signature.

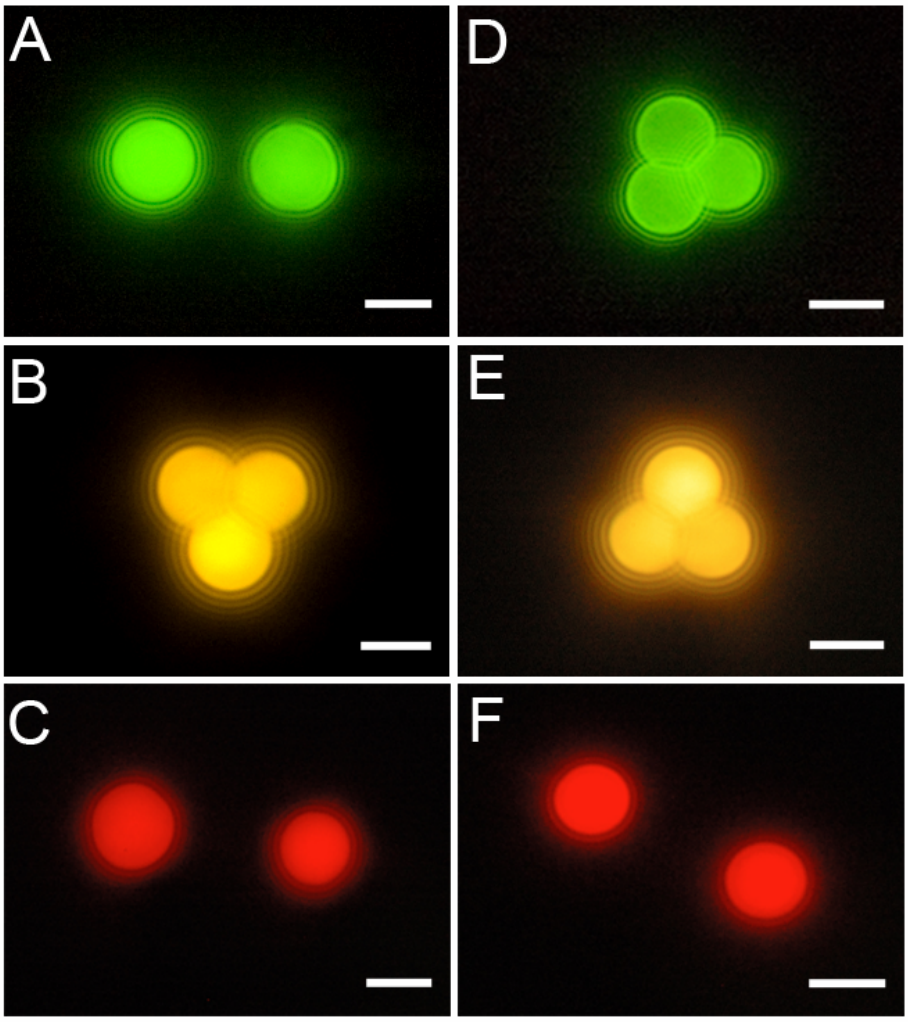

Figure 3.3: True color fluorescence images of encoded beads. (A-C) non-magnetic, and (D-F) magnetic QD-encoded beads. Mesoporous silica beads with a diameter of 4.0 nm were doped with single-color ternary quantum dots emitting at 530 nm (A,D), 590 nm (B,E), and 630 nm (C,F). White scale bar represents 4 μm.

Supplementing the encoded beads with extra functions through the addition of nanomaterials, could possibly compromise optical characteristics that are vital for decoding the spectroscopic signatures. In particular, coupling interactions between iron oxide and QDs is important to optimizing the optical and magnetic properties of the dual-function beads, as discussed below.

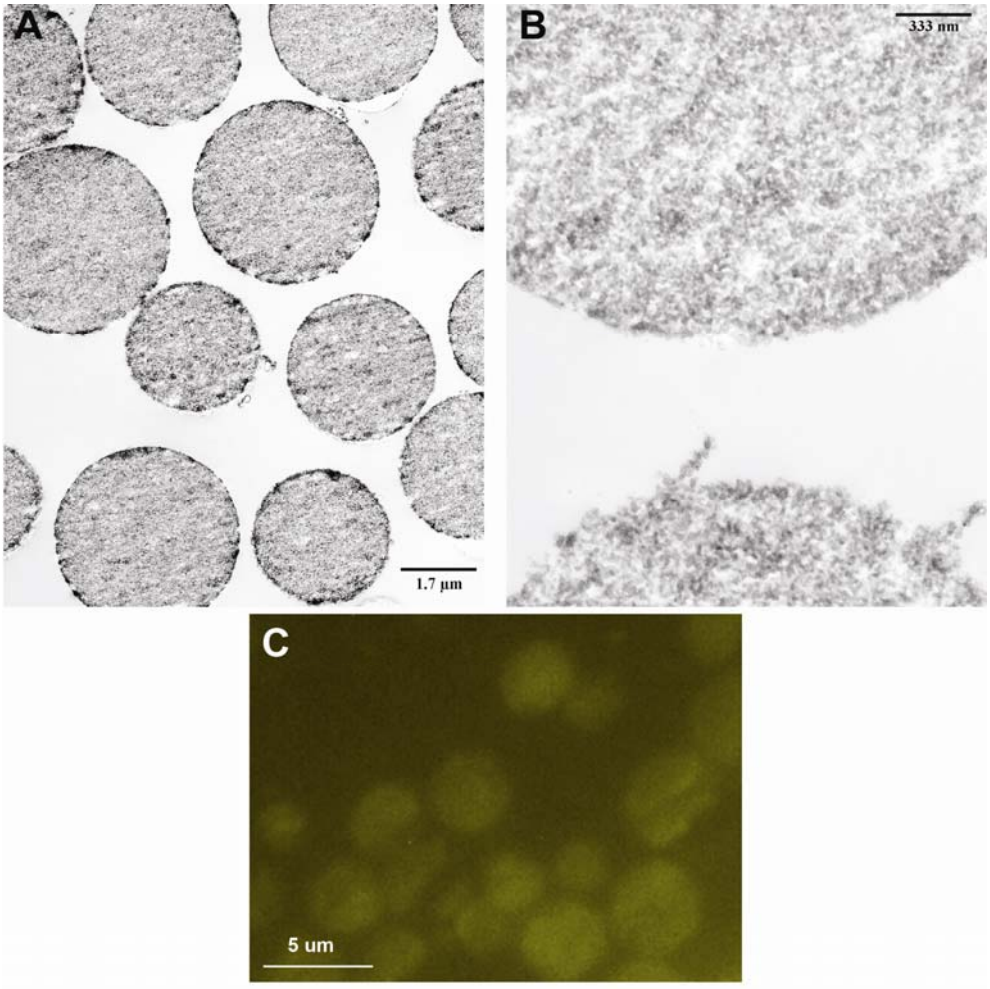

Figure 3.4: Transmission electron micrographs of magneto-optical bead sections. (A) Nanocrystals are distributed uniformly throughout the bead, although higher concentrations can be seen at the surface (B) High magnification image shows highly porous structure of beads necessary for allowing doping of high number of nanocrystals. (C) Fluorescence image of 200 nm thick sections of beads in immobilizing resin. Yellow color QD encoded beads were used but show weak signal due to background autofluorescence. Beads appear to be uniformly doped with QD although there are some variations in intensity possibly due to non-uniform internal structure of beads.

Upon preparation, beads were sectioned to reveal internal distribution of nanoparticles. **Figure 3.4A** shows a TEM image of 60-70 nm thick bead sections, with a magnified view (**Figure 3.4B**) showing the highly porous structure of the beads. Although these beads have an average pore size of 30 nm, the random pore size is evident from the TEM images. Also, pores inside the bead appear to be interconnected,

forming a porous network, which would explain the incredibly fast rate (15-20 mins) at which nanoparticles partition into the beads. Moreover, the porosity of the bead doesn't seem to vary from the center to the periphery, which is important for uniform distribution of nanoparticles. From Figure 3.4A and 3.4B it is hard to confirm nanoparticles distribution in the interior due to high background from electron dense silicon. Therefore, bead sections of dual-functional beads were imaged under wide-field fluorescence illumination (**Figure 3.4C**) and show even distribution across the diameter, although net fluorescence may vary from bead to bead.

Effect of Iron Oxide on QD Fluorescence

To examine the effect of iron oxide on QD signal intensity, increasing concentrations of iron oxide were added to QD-doped beads in a sequential manner, and fluorescence spectra **(Figure 3.5A)** were recorded using single-bead spectroscopy. Statistical error analysis of the fluorescence intensity measurement was obtained from at least 25 single-bead spectra for each bead sample **(Figure 3.5B)**. The results indicate that the embedded iron oxide significantly reduces the QD fluorescence intensity. A parallel study using the simultaneous doping procedure yielded a similar drop in fluorescence intensity. Although there is no shift in the emission spectra, they are not as symmetric as that for free QDs. This is evident by the longer tail towards the red-end of the visible spectrum. There are several possible explanations for this effect: first, the embedded iron oxide nanocrystals could quench QD fluorescence through electronic coupling and energy transfer; second, the embedded QDs could be replaced by iron oxide nanocrystals during sequential incorporation; and third, the embedded iron oxide absorbs broadly in the visible spectrum, and could thus attenuate both the excitation light and the emitted QD fluorescence.

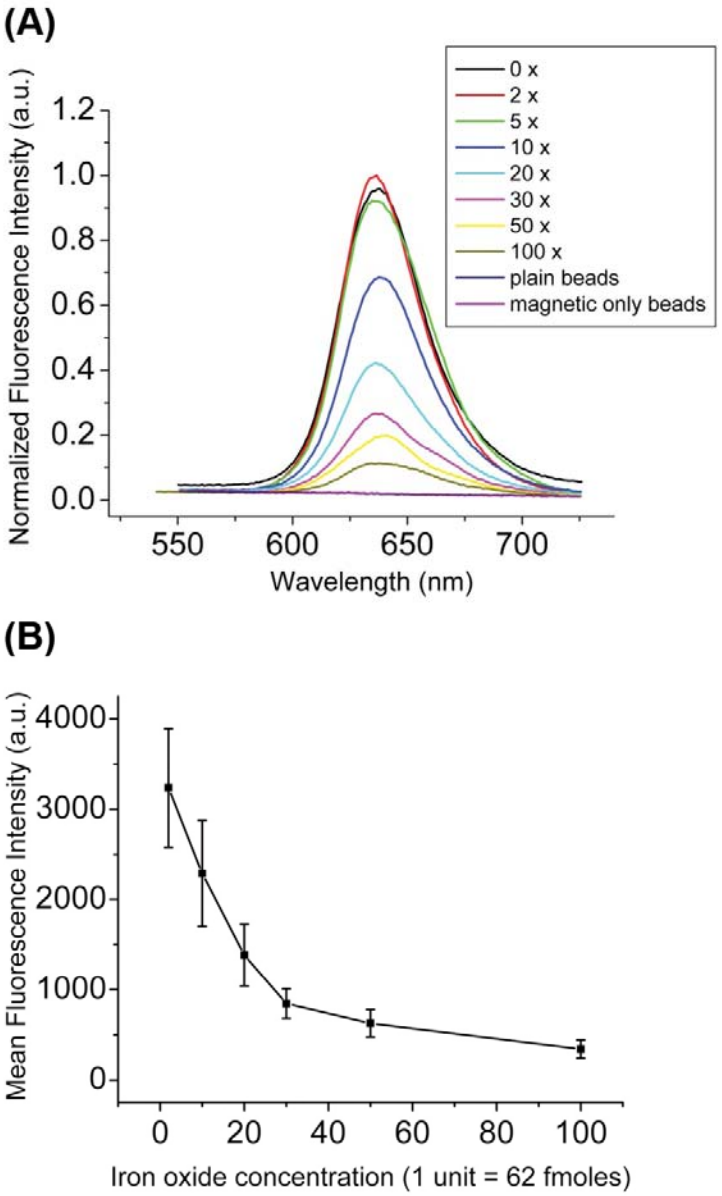

Figure 3.5: Effect of embedded iron oxide nanocrystals on QD fluorescence in dual-function mesoporous beads. (A) Fluorescence emission spectra obtained from single beads doped with increasing amounts of iron oxide. (B) Statistical analysis of bead (n = 25) fluorescence intensity as function of iron oxide concentration. For both (A) and (B), one unit (1x) is equal to 62 femtomoles of iron oxide nanocrystals, corresponding to 6,000 nanocrystals per bead. Error bars signify standard deviation. All beads contained the same amount of QDs (approximately 13,000 QDs per bead).

The first possibility can be ruled out because similar decreases were observed in dilute solutions of simple QD and iron oxide mixtures. In this case, the large distances

between QD and iron oxide particles should prevent energy transfer. Also, a quenching mechanism does not explain the non-symmetric fluorescence peak.

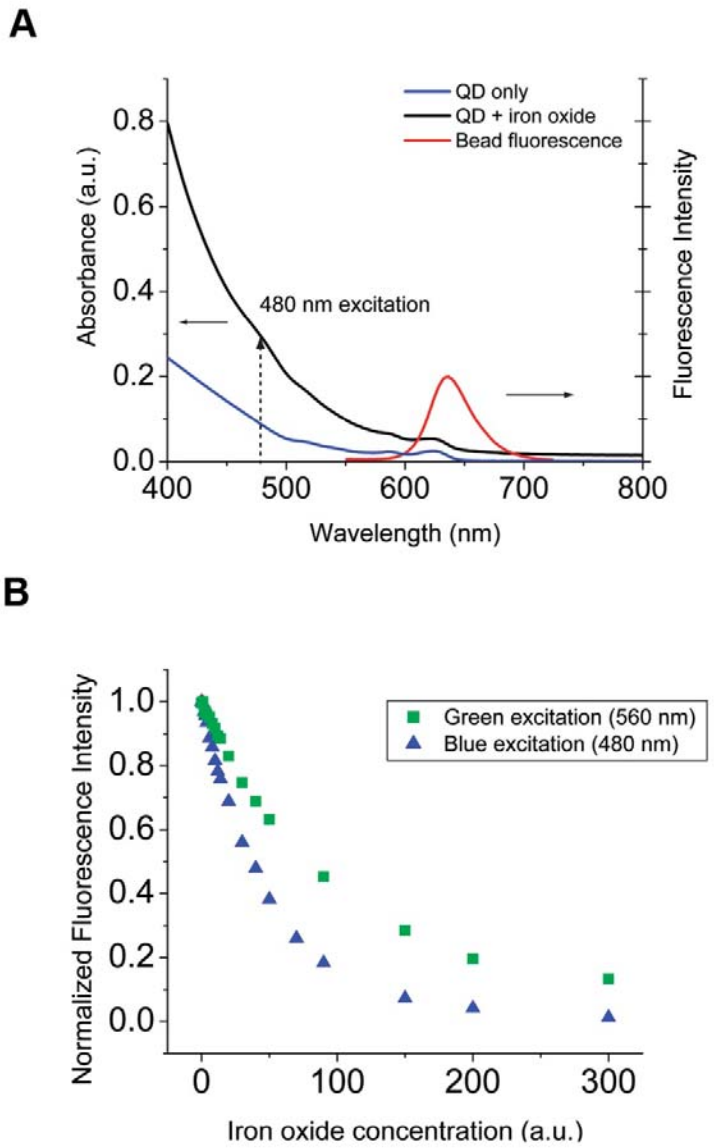

Figure 3.6: Spectroscopic analysis of quantum dots in the presence of iron oxide (A) Absorption profiles of quantum dots in the absence and presence of iron oxide. Also shown is the emission spectrum of a dual-function optical and magnetic bead. (B) Fluorescence intensity as a function of iron oxide concentration for two excitation wavelengths, blue (480 nm) and green (560 nm).

The second possibility can also be ruled out because no replaced QDs were detected in the supernatant. Furthermore, simultaneous incorporation of QDs and iron oxide particles leads to similar fluorescence decreases. We believe that the iron oxide optical absorption is mainly responsible for the observed interference of iron oxide on QD fluorescence. To further study this effect, we obtained fluorescence spectra and absorption profiles of QDs mixed in solution with increasing levels of iron oxide. In agreement with previous studies, [34] iron oxide nanocrystals show a broad absorption spectrum in the visible range (400 nm – 600 nm) **(Figure 3.6A)**, perhaps due to charge transfer transitions in this mixed-valence compound. As expected, excitation light in this window will be strongly absorbed by iron oxide, thus attenuating the light intensity reaching the embedded QDs. Because the iron oxide absorption spectrum decreases gradually to the red, excitation at longer wavelengths should lead to smaller intensity attenuations. Indeed, when excited with green (560 nm) light instead of blue (480 nm) there is significantly less attenuation of fluorescence intensity **(Figure 3.6B)**. In addition, a fraction of photons emitted by QDs could be absorbed by iron oxide in a wavelength dependent manner. This absorption is most likely responsible for the slight asymmetric shape ("tailing" at longer wavelengths) of QD fluorescence in dual-function optical and magnetic beads.

Ratiometric Bead Encoding

Figure 3.7 shows representative spectra from beads doped with QDs emitting in the green and red wavelengths. Based on two intensities, there are three ratios that can be used to encode beads. Variations in the ratio for the beads are roughly 15% and can be attributed to two factors. First, there could be differential adsorption of iron oxide in beads as a result of size differences. Second, given that iron oxide absorbs strongly in the blue region, variations in iron oxide concentration could lead to a population of beads

with variable green QD signal intensities. This proof-of-concept study demonstrates that it is indeed possible to prepare dual-function optical and magnetic beads encoded with three different and discernable spectroscopic signatures.

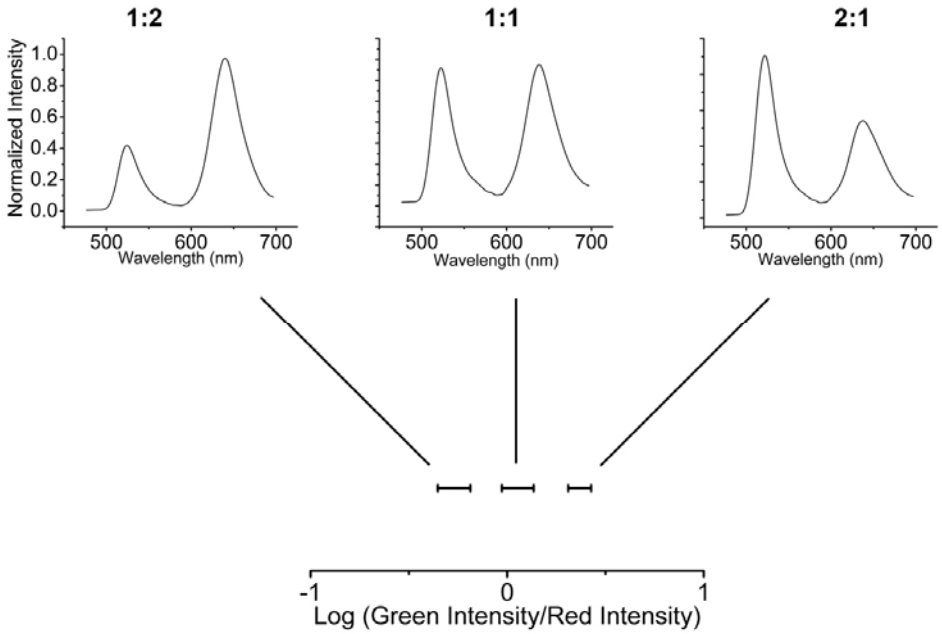

Figure 3.7: Two-color QD encoding of dual-function beads using green (530 nm) and red (630 nm) emitting dots. Horizontal error bars indicate variances in the ratio of green to red fluorescence intensities of single beads on a logarithmic scale. Log error bars were computed by calculating standard deviation of the log of intensity ratios and representing as a horizontal bar in logarithmic scale. As a reference, log of 1:2, 1:1 and 2:1 ratios are -0.301, 0, and 0.301 respectively.

Flow Cytometry Analysis

So far, we have demonstrated that mesoporous beads can be uniquely encoded by emission wavelength of QDs or by intensity of each emission color. We decided to test the ability to discriminate dual function beads encoded with a low or high intensity of a single color using flow cytometry. Biologists, immunologists and biochemists routinely use flow cytometry as it can be used to quantify the number or expression patterns of mammalian cells. Microbeads used in our studies are similar in size to these cells and

can be easily detected by the PMT's and filter sets in standard flow cytometers. Two sets of beads either having low or high fluorescence intensity of QDs emitting at 580 nm were prepared and verified visually under an epifluorescence microscope. Three samples, each of the sets and one containing a 50:50 mixture of both were prepared and run. A phycoerythrin (PE) filter set and channel was used to analyze side scatter and a scatter plot was generated (**Figure 3.8**).

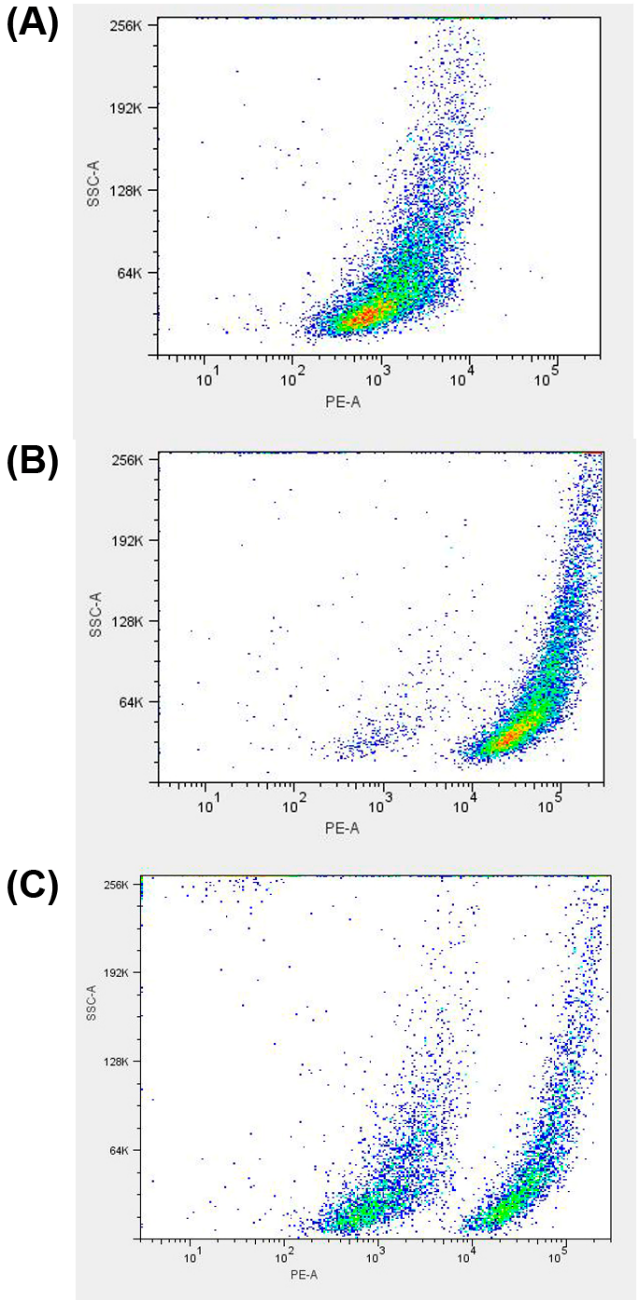

Figure 3.8: Flow cytometry analysis of dual function beads encoded by color intensity. Side scatter plots of beads exhibiting (A) low and (B) high fluorescence intensity and (C) a mixture of both low and high intensity.

Magnetic Bead Separation

To study the efficiency of magnetic bead separation, we mixed red-QD encoded magnetic beads with green non-magnetic beads **(Figure 3.9A)**. Upon placing the

solution on a magnet for 5 minutes, and removing the supernatant, beads were re-constituted to the initial volume and imaged using a standard fluorescence microscope with blue-light excitation.

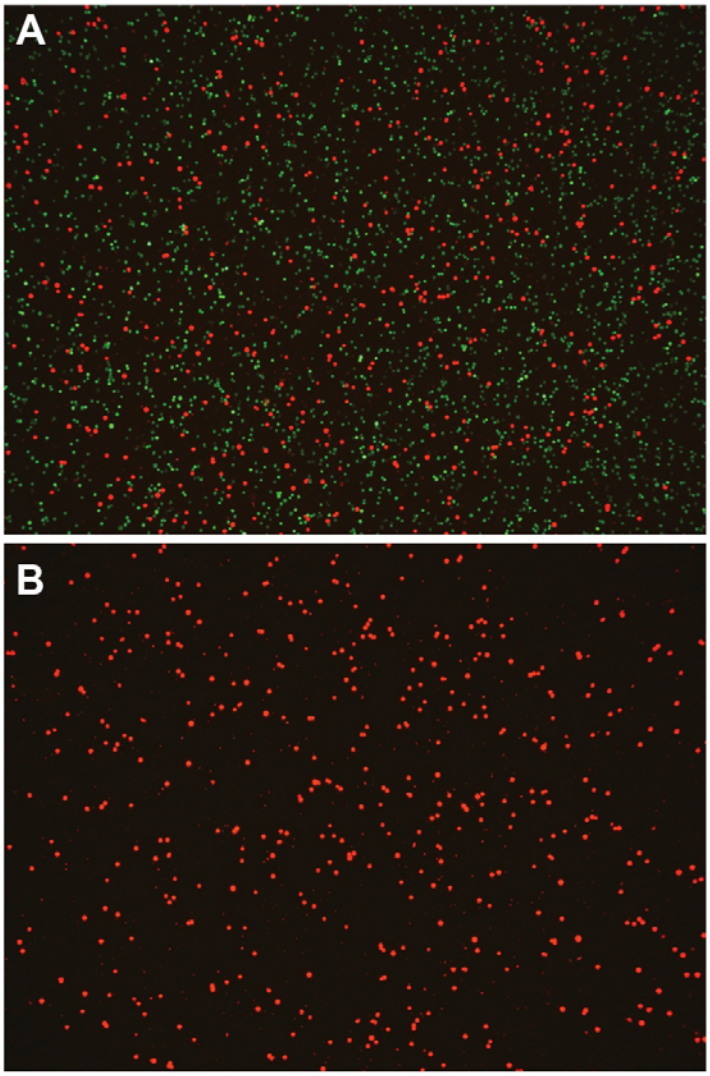

Figure 3.9: Fluorescence microscope images showing efficient separation of magnetic and nonmagnetic QD-encoded beads. (A) Mixture of magnetic red-QD beads and nonmagnetic green-QD beads spread on a glass coverslip. (B) After magnetic separation and washing to remove the nonmagnetic beads.

Prior to this, beads were water solubilized for two reasons. Firstly, bead separation efficiency cannot be calculated when using ethanol as a solvent since the hydrophobic beads tend to cluster and can bind to a cluster of non-magnetic beads. A

non-polar solvent cannot be used either because nanoparticles could leach out of the bead. Secondly, viscosity of the solvent affects magnetophoretic mobility (See Stokes' drag force ($F_{D)}$ relationship, Equation 4, Chapter 2). Therefore time of separation in various solvents may provide misleading data. Ultimately, it is essential to calculate the efficiency in an aqueous solution as we see great promise for this technology in biological separation of cells and molecules. In order to calculate the efficiency in a fast and accurate manner, magnetic and non-magnetic beads were color coded and mixed such that non-magnetic beads were in large excess. Figure 3.9A is an image of the bead mixture prior to separation. Using an NdFeB permanent magnet, beads were allowed to be pulled towards the magnet for 5 minutes. In reality, a large bead pellet was seen near the magnet wall within 20-30 seconds, unlike the 20 minutes[35] and few hours[25] reported elsewhere. After a single wash with PBS buffer, an equal volume of bead sample was immobilized on a coverslip and imaged as shown in Figure 3.9B. The images were quantified for total bead populations using a particle counting software.

The results were matched with manual counting to confirm veracity of the data. From the results shown in **Figure 3.9**, the efficiency of bead separation is almost 99% after a single wash. Additional washes were not performed but a total of three washes will ensure that essentially all non-magnetic material is removed. The results clearly show separation of the red and green beads. We used a computer program to count the number of red and green pixels above an intensity threshold, and the automated counting data show that the separation efficiency is better than 99% (calculated by dividing the number of non-magnetic beads after separation by the initial number of beads before separation, and multiplying this by 100).

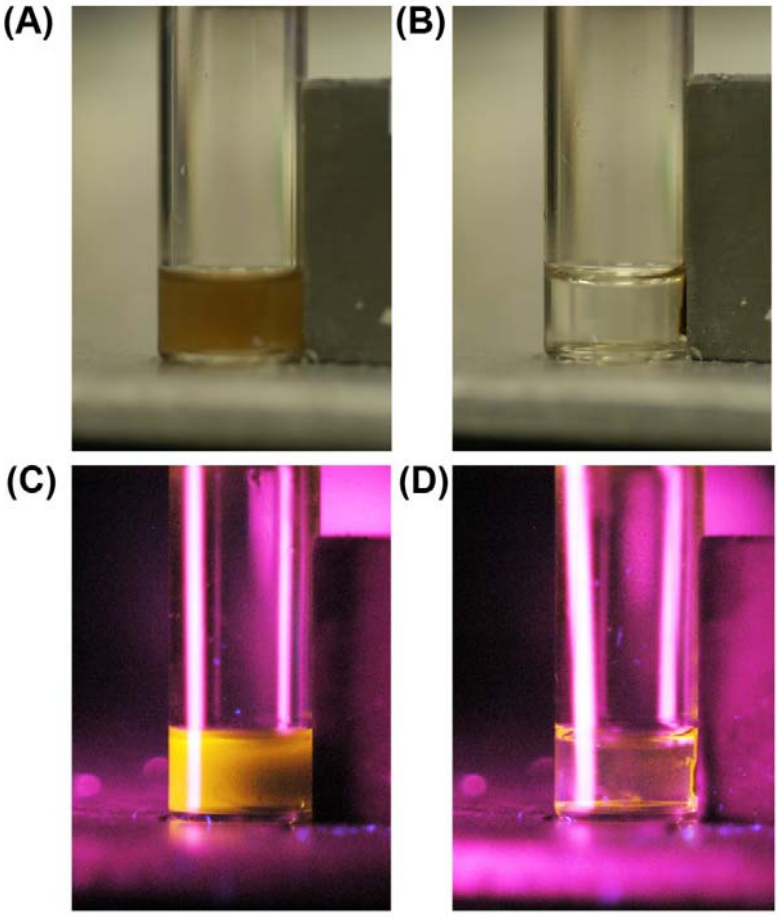

Figure 3.10: Rapid separation of dual function magnetic and optically (QD585) encoded beads. Bright field image of bead suspension in water at (A) t = 0 seconds and (B) t = 50 seconds. (C, D) Dual function beads under UV excitation initially, and after placing next to a permanent magnet.

The efficiency of magnetic separation will of course depend on the iron oxide concentration in the beads. Beads containing more iron oxide nanocrystals (3×10^5) and encoded with ternary QDs emitting at 580 nm were prepared. These beads were rapidly pulled towards the permanent magnet and the corresponding images are shown in **Figure 3.10**. As more iron oxide nanocrystals are packed into a bead, the total magnetic force experienced by the bead increases, thereby increasing net magnetization. We estimate that about 10^5 iron oxide nanocrystals per bead, as used in this experiment, are ideal for manipulating micron-sized beads.

Water Solubilization

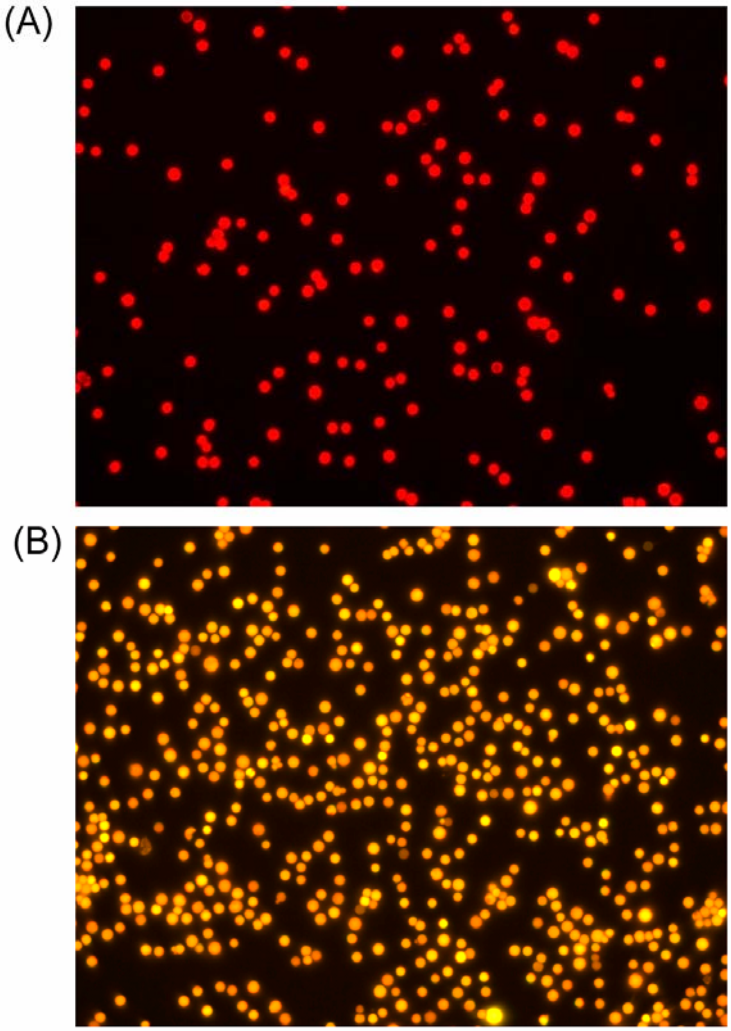

Figure 3.11: Water soluble dual function beads. Magnetic and optical beads coated with poly (acrylic acid) modified with octyl amine and encoded with (A) 630 nm emission ternary QDs and (B) 580 nm ternary QDs.

Beads were solubilized in water by adding them to a 50:50 mixture of Triton X-100: Poly(acrylic acid) with 40% carboxyl groups modified with Octylamine using Dicyclohexylcarbodiimide (DCC) based coupling. Beads were precipitated with a magnet and solvent was removed before the addition of surfactant-amphiphilic polymer mixture. Absence of Triton X-100 surfactant results in poor bead stability and particles begin to aggregate. The resultant beads are dispersed in PBS with 0.02% Tween 20 and have

functional groups that can be used for conjugating biomolecules to the surface. Additionally, electrostatic interaction can be employed to attach positively charged biomolecules to the surface consisting of negatively charged carboxyl functional groups.

In conclusion, we have prepared dual-function optical and magnetic beads by incorporating monodisperse QD and iron oxide nanocrystals into mesoporous silica beads. Iron oxide nanocrystals provide superparamagnetic properties for bead separation and target enrichment, but also attenuate the QD fluorescence intensity. Nonetheless, we have prepared and characterized highly uniform dual-functions beads with three ratiometric signatures. We have also achieved rapid separation of magnetic and nonmagnetic beads at better than 99% efficiencies, allowing enrichment of targets and reduction of background signals. Development of more complex multifunctional beads is also possible due to the large doping capacity of porous beads. In addition, we expect that encoded mesoporous beads could be used for automated detection technology, as well as microfluidic devices for multiplexed and ultrasensitive detection of cancer biomarkers from body fluid samples. In the following chapter, we discuss a bead-based assay using magnetic beads and luminescent nanoparticles to demonstrate the effect of magnetic isolation coupled with ultrasensitive fluorescence-based detection of a protein.

3.4 References

[1] K. Braeckmans, S.C. De Smedt, M. Leblans, R. Pauwels and J. Demeester, Encoding microcarriers: present and future technologies, *Nat Rev Drug Discov* **1**: 447-456. (2002)

[2] A. Fan, C. Lau and J. Lu, Magnetic bead-based chemiluminescent metal immunoassay with a colloidal gold label, *Anal Chem* **77**: 3238-3242. (2005)

[3] N.H. Finkel, X. Lou, C. Wang and L. He, Barcoding the microworld, *Anal Chem* **76**: 352A-359A. (2004)

[4] R.J. Fulton, R.L. McDade, P.L. Smith, L.J. Kienker and J.R. Kettman, Advanced multiplexed analysis with the FlowMetrix(TM) system, *Clinical Chemistry* **43**: 1749-1756. (1997)

[5] N. Gaponik, I.L. Radtchenko, G.B. Sukhorukov, H. Weller and A.L. Rogach, Toward encoding combinatorial libraries: Charge-driven microencapsulation of semiconductor nanocrystals luminescing in the visible and near IR, *Advanced Materials* **14**: 879-882. (2002)

[6] R.C. Jin, Y.C. Cao, C.S. Thaxton and C.A. Mirkin, Glass-bead-based parallel detection of DNA using composite Raman labels, *Small* **2**: 375-380. (2006)

[7] M.T. McBride, S. Gammon, M. Pitesky, T.W. O'Brien, T. Smith, J. Aldrich*, et al.*, Multiplexed liquid arrays for simultaneous detection of simulants of biological warfare agents, *Anal Chem* **75**: 1924-1930. (2003)

[8] J.M. Nam, C.S. Thaxton and C.A. Mirkin, Nanoparticle-based bio-bar codes for the ultrasensitive detection of proteins, *Science* **301**: 1884-1886. (2003)

[9] J.M. Nam, A.R. Wise and J.T. Groves, Colorimetric bio-barcode amplification assay for cytokines, *Anal Chem* **77**: 6985-6988. (2005)

[10] E. Schulze, C. Siewert, M. Herber, J. Schmitz, M. Assenmacher and S. Miltenyi, Highly sensitive detection of disseminated tumor cells using MACS technology, *Cytometry* **46**: 193-194. (2001)

[11] R.S. Molday, S.P. Yen and A. Rembaum, Application of magnetic microspheres in labelling and separation of cells, *Nature* **268**: 437-438. (1977)

[12] D.S. Wang, J.B. He, N. Rosenzweig and Z. Rosenzweig, Superparamagnetic Fe2O3 Beads-CdSe/ZnS quantum dots core-shell nanocomposite particles for cell separation, *Nano Lett* **4**: 409-413. (2004)

[13] A.R. Ahmed, G.W. Olivier, G. Adams, M.E. Erskine, R.G. Kinsman, S.K. Branch, *et al.*, Isolation and partial purification of a melanocyte-stimulating hormone receptor from B16 murine melanoma cells. A novel approach using a cleavable biotinylated photoactivated ligand and streptavidin-coated magnetic beads, *Biochem J* **286 (Pt 2)**: 377-382. (1992)

[14] M. Han, X. Gao, J.Z. Su and S. Nie, Quantum-dot-tagged microbeads for multiplexed optical coding of biomolecules, *Nat Biotechnol* **19**: 631-635. (2001)

[15] B.I. Haukanes and C. Kvam, Application of Magnetic Beads in Bioassays, *Bio-Technology* **11**: 60-63. (1993)

[16] S.I. Stoeva, F. Huo, J.S. Lee and C.A. Mirkin, Three-layer composite magnetic nanoparticle probes for DNA, *J Am Chem Soc* **127**: 15362-15363. (2005)

[17] H. Xu, H.P. Wu, F. Huang, S.P. Song, W.X. Li, Y. Cao, *et al.*, Magnetically assisted DNA assays: high selectivity using conjugated polymers for amplified fluorescent transduction, *Nucleic Acids Research* **33**: -. (2005)

[18] S. Miltenyi, W. Muller, W. Weichel and A. Radbruch, High-Gradient Magnetic Cell-Separation with Macs, *Cytometry* **11**: 231-238. (1990)

[19] P.S. Eastman, W. Ruan, M. Doctolero, R. Nuttall, G. de Feo, J.S. Park, *et al.*, Qdot Nanobarcodes for Multiplexed Gene Expression Analysis, *Nano Lett* **6**: 1059-1064. (2006)

[20] X.H. Gao, W.C.W. Chan and S.M. Nie, Quantum-dot nanocrystals for ultrasensitive biological labeling and multicolor optical encoding, *Journal of Biomedical Optics* **7**: 532-537. (2002)

[21] X.H. Gao and S.M. Nie, Doping mesoporous materials with multicolor quantum dots, *J Phys Chem B* **107**: 11575-11578. (2003)

[22] X.H. Gao and S.M. Nie, Quantum dot-encoded mesoporous beads with high brightness and uniformity: Rapid readout using flow cytometry, *Anal Chem* **76**: 2406-2410. (2004)

[23] B. Zebli, A.S. Susha, G.B. Sukhorukov, A.L. Rogach and W.J. Parak, Magnetic targeting and cellular uptake of polymer microcapsules simultaneously functionalized with magnetic and luminescent nanocrystals, *Langmuir* **21**: 4262-4265. (2005)

[24] D. Muller-Schulte, T. Schmitz-Rode and P. Borm, Ultra-fast synthesis of magnetic and luminescent silica beads for versatile bioanalytical applications, *Journal of Magnetism and Magnetic Materials* **293**: 135-143. (2005)

[25] V. Salgueirino-Maceira, M.A. Correa-Duarte, M. Spasova, L.M. Liz-Marzan and M. Farle, Composite silica spheres with magnetic and luminescent functionalities, *Adv Funct Mater* **16**: 509-514. (2006)

[26] J. Kim, J.E. Lee, J. Lee, J.H. Yu, B.C. Kim, K. An*, et al.*, Magnetic fluorescent delivery vehicle using uniform mesoporous silica spheres embedded with monodisperse magnetic and semiconductor nanocrystals, *J Am Chem Soc* **128**: 688-689. (2006)

[27] S.P. Mulvaney, H.M. Mattoussi and L.J. Whitman, Incorporating fluorescent dyes and quantum dots into magnetic microbeads for immunoassays, *Biotechniques* **36**: 602-+. (2004)

[28] S.K. Mandal, N. Lequeux, B. Rotenberg, M. Tramier, J. Fattaccioli, J. Bibette*, et al.*, Encapsulation of magnetic and fluorescent nanoparticles in emulsion droplets, *Langmuir* **21**: 4175-4179. (2005)

[29] D. Zhao, J. Feng, Q. Huo, N. Melosh, G.H. Fredrickson, B.F. Chmelka*, et al.*, Triblock copolymer syntheses of mesoporous silica with periodic 50 to 300 angstrom pores, *Science* **279**: 548-552. (1998)

[30] S.H. Sun, H. Zeng, D.B. Robinson, S. Raoux, P.M. Rice, S.X. Wang*, et al.*, Monodisperse MFe2O4 (M = Fe, Co, Mn) nanoparticles, *Journal of the American Chemical Society* **126**: 273-279. (2004)

[31] R.E. Bailey and S.M. Nie, Alloyed semiconductor quantum dots: Tuning the optical properties without changing the particle size, *Journal of the American Chemical Society* **125**: 7100-7106. (2003)

[32] D.V. Talapin, A.L. Rogach, A. Kornowski, M. Haase and H. Weller, Highly luminescent monodisperse CdSe and CdSe/ZnS nanocrystals synthesized in a hexadecylamine-trioctylphosphine oxide-trioctylphospine mixture, *Nano Letters* **1**: 207-211. (2001)

[33] P.B. Stetson, Daophot - a Computer Program for Crowded-Field Stellar Photometry., *Publications of the Astronomical Society of the Pacific* **99**: 191-222. (1987)

[34] R.F. Ziolo, E.P. Giannelis, B.A. Weinstein, M.P. Ohoro, B.N. Ganguly, V. Mehrotra*, et al.*, Matrix-Mediated Synthesis of Nanocrystalline Gamma-Fe2O3 - a New Optically Transparent Magnetic Material, *Science* **257**: 219-223. (1992)

[35] N. Gaponik, I.L. Radtchenko, G.B. Sukhorukov and A.L. Rogach, Luminescent polymer microcapsules addressable by a magnetic field, *Langmuir* **20**: 1449-1452. (2004)

CHAPTER 4

SINGLE-BEAD BASED ASSAYS USING MAGNETIC MICROBEADS AND LUMINESCENT NANOPARTICLES

4.1 Introduction

As discussed in previous chapters, there is a need to develop an assay that can detect low copy number of molecules from a large sample volume (low concentration). Although solid-phase assays such as Enzyme-Linked Immunosorbent Assay (ELISA) and DNA microarrays are tools that are increasingly being used for basic research, pharmacological screening and clinical diagnostics, they suffer from limitations in flexibility, cost, and sensitivity. Our hypothesis for this work is that bead-based assay has the potential for high sensitivity screening of DNA fragments and proteins in solution. In the previous chapter, we discussed the development of bead-based technology with the potential for multiple molecule detection by combining unique properties of magnetic and optical nanoparticles. Here, we demonstrate application of similar technology towards detection of rare protein and DNA molecules using magnetic-bead and optical readout sandwich assay.

Magnetic beads have been used in the past decade for target enrichment. In fact, magnetic beads with different functional groups (-NH2, -COOH, Streptavidin, Tosyl group) are commercially available from a variety of sources [1, 2]. The major advantage of magnetic beads is that it allows for captured target molecules to be isolated and enriched without the need of centrifugation or column chromatography. This allows for fragile biomolecules to be enriched without causing any damage [2]. Enrichment of target and reduction of sample volume leads to increased local target concentration and

improved detection sensitivity. Further, improvements in bead synthesis chemistry have made it possible to produce beads with high degree of uniformity, smooth surface for attachment of targeting ligands, and elevated target binding kinetics (reaction limited as opposed to diffusion limited) compared to solid-state arrays such as ELISA [3]. Antibody-coated magnetic beads have been successfully used in capture and quantitative analysis of proteins [1, 4-10], nucleic acids [3, 11, 12], and infectious diseases [13-17].

Most of these studies have depended on chromophores or fluorescent molecules to quantify target concentrations. Fluorescence-based assays offer much higher detection sensitivities compared to colorimetric assays, however the inherently poor photostability of commonly used organic dyes diminishes this sensitivity. Fluorescent nanoparticles such as QDs and dye-doped nanoparticles have been successfully demonstrated in ultrasensitive detection formats [18] due to their extended photostability and greater brightness [19, 20]. In this chapter, QD and dye-doped nanoparticles (hereon referred as Luminescent Nanoparticles; LNP) are used as external probes for target quantification. A bead-based sandwich immunoassay for detection of tumor-associated protein TNF-alpha is demonstrated here. Standard fluorescence microscopy, spectroscopy and image analysis is used to analyze and quantify single beads and determine target concentration based on total fluorescence intensity. Additionally, we also report preliminary results for oligonucleotide detection at nano-molar concentrations using a similar setup.

4.2 Materials and Methods

Magnetic bead conjugation

Approximately 6.7 million magnetic beads (Streptavidin-coated magnetic Dynabeads M-270 (Invitrogen) 2.8 um in diameter, were first washed with washing buffer composed of 10 mM Tris-HCl (pH 7.5), 1mM EDTA and 2.0 M NaCl, followed by blocking buffer (BlockAid Buffer, Invitrogen). All washing steps were performed in a 1.5 mL Eppendorf tube by pulling beads to the side-wall of the tube with a permanent magnet (1.5 T Sintered Neodymium Iron Boron Magnet, MCE Magnets Inc., Torrance, CA) and removing supernatant. This was followed by incubation at room temperature with either biotinylated anti-TNF-alpha antibodies (20 ul of TNF-alpha antibody (concentration = 0.5 mg/mL, T-9160-14d, U.S.Biologicals, Swampscott, MA) for protein detection assay, or with biotinylated oligonucleotides (get sequence from lab, TriLink Biotechnologies, San Diego, CA) for DNA detection. Upon incubation for 30 minutes under gentle shaking, beads were washed three times with PBS Buffer (10 mM, pH 7.4) to remove unbound antibody or DNA molecules. An excess of avidin was added to saturate any free biotin sites at this point.

Optical probe conjugation

For QD conjugation, 10nM of streptavidin-coated QDs (Invitrogen) with emission maxima of 525 nm were coupled with biotinylated oligonucleotides having a sequence complimentary to that attached on the magnetic bead. A 1:5 molar feed ratio of QD:oligo was used for reactions. After incubation at room temperature for 1 hour, unbound oligos were purified by filtration through an S-300HR size-exclusion chromatography filtration column (GE Healthcare, Piscataway, NJ). Purified samples were qualitatively tested by running them through a 0.8% agarose gel in 0.5X TBE Buffer for 1 hour at 100V. Compared to plain streptavidin-coated QDs, the DNA-conjugated QDs migrated faster to

the cathode. (Tetramethylrhodamine and biotin-labeled dextran (Invitrogen Inc.) were also used to test the detection limit using identical experimental procedures.

Carboxylate-modified yellow/green FluoSpheres (F8795, excitation/emission 505/515, 43 nm diameter, Invitrogen Inc.) were conjugated to monoclonal murine TNF-alpha antibody (T9160-16A, 1 mg/mL, U.S. Biologicals Inc.) using an aqueous-based 1-ethyl-3-(3-dimethylaminopropyl) carbodiimide hydrochloride (EDC; Sigma-Aldrich) coupling reaction [21]. Specifically, 5 µL of the FluoSphere stock solution was added to 40 µL of 25 mM MES buffer (pH 5.9), and the mixture was sonicated for 15 min. Next, the EDC solution at a concentration of 5 mg/mL (20 µL, 100 µg total) was added to the bead solution and was vortexed for 15 min. Similarly, 11 µL of *N*-hydroxysulfosuccinimide (sulfo-NHS; Thermo-Fisher Scientific, Rockford, IL) at 14 mg/mL concentration was added to the bead solution and was vortexed for 15 min. Thereafter, 2.5 µL of TNF-R antibody at a stock concentration of 1 mg/mL was added to the solution and vortexed for 1 h. Next, 100 µg of EDC (as freshly prepared solution in MES buffer) was added, and the solution was vortexed for 75 min (total reaction volume was 100 µL). Finally, the reaction product was filtered by using an S-400 HR size exclusion filtration column (GE Healthcare, Piscataway, NJ) to remove unreacted antibody molecules.

Assay procedure

One microliter of magnetic microparticle (MMP)-antibody conjugates was mixed with recombinant murine TNF-alpha molecule (R&D Systems Inc., Minneapolis, MN) in various concentrations (from 6×10^{-9} to 10^{-17} M) in 1 mL of PBS buffer (10 mM PBS, pH 7.4 + 0.1% BSA + 0.02% sodium azide +0.02% Tween 20) and was allowed to react with vigorous stirring at room temperature for 2 hours. The MMPs were pulled down using a 1.5 T magnet (Sintered Neodymium Iron Boron Magnet, MCE Magnets Inc.) and

were washed three times with the PBS buffer. The MMPs with TNF-alpha molecules captured on their surfaces were resuspended in 90 µL of PBS buffer and were allowed to react with 10 µL of Fluosphere-antibody conjugate with vigorous vortexing for 1 h at room temperature. Finally, the reaction product was pulled down using magnet, washed two times with the PBS buffer, and concentrated to 10 µL before imaging.

For oligonucleotide hybridization assay, DNA hybridization was performed using 4 × SSC- sodium dodecyl sulfate (SDS) (1X SSC: 0.15 M sodium chloride and 0.015 M sodium citrate, pH 7.0) for 30 min at 42°C. Care was taken not to exceed this temperature as QD coating is not stable at temperatures greater than 46°C for prolonged periods.

Data Acquisition and Analysis

All images were taken using an Olympus IX-71 microscope (Center Valley, PA) that was equipped with a mercury lamp for excitation, a Nikon D70 color digital camera, and a 100 x objective (NA 1.25, oil). The hybridized or control sample (1-3 µL) was spread between two clean cover slips (no. 1 coverglass, Corning Inc., Corning, NY) and was placed on an epi-fluorescence microscope. True color fluorescence images were obtained by using 488-nm excitation and a long pass filter (505 nm, Chroma Technology Corp., Brattleboro, VT). The exposure times were 0.2-2 seconds. The fluorescence spectra of the QDs and the fluospheres (excitation = 505 nm, emission = 515 nm; Invitrogen Inc.) were recorded by using a standard fluorometer (FluoMax; Jobin Yvon, Edison, NJ), and the spectra of single MMPs were recorded by using a spectrophotometer (SpectraPro 150, Roper Scientific, Trenton, NJ) attached to the side port of the microscope. All images were analyzed by using NIH Image J software [22].

4.3 Results and Discussion

The basic principle of the single-bead sandwich assay is shown in **Figure 4.1**. In this procedure, antibody-conjugated magnetic microbeads capture target molecules (DNA or protein) from solution by binding them either through antigen-antibody recognition or oligonucleotide hybridization. For DNA fragment isolation, oligonucleotides are conjugated to the beads (see **Figure 4.5**). The beads are then separated using a permanent magnet and subjected to several washing steps to remove non-target molecules. Luminescent nanoparticles (LNP) with recognition molecules specific to a different epitope or sequence on the target bind and "sandwich" the captured targets. Following a second washing step to remove unbound LNPs, beads are then imaged under a microscope by placing them on a thin glass coverslip. Target concentration is quantified based on the intensity of the integrated fluorescence signal from LNPs on each bead. This integrated intensity is then acquired from several beads and the values are averaged. It must be noted that unlike other assays in which targets are directly tagged, this two step assay removes the need to perform direct target tagging, which can be a time-consuming and highly inefficient when target concentrations are low. Further, the ability to manipulate samples with a magnet makes it possible to perform assays with minimum sample handling and contamination. For this study, we detected TNF-alpha since it is secreted by immune cells in response to inflammatory responses and is highly expressed in many cancers.

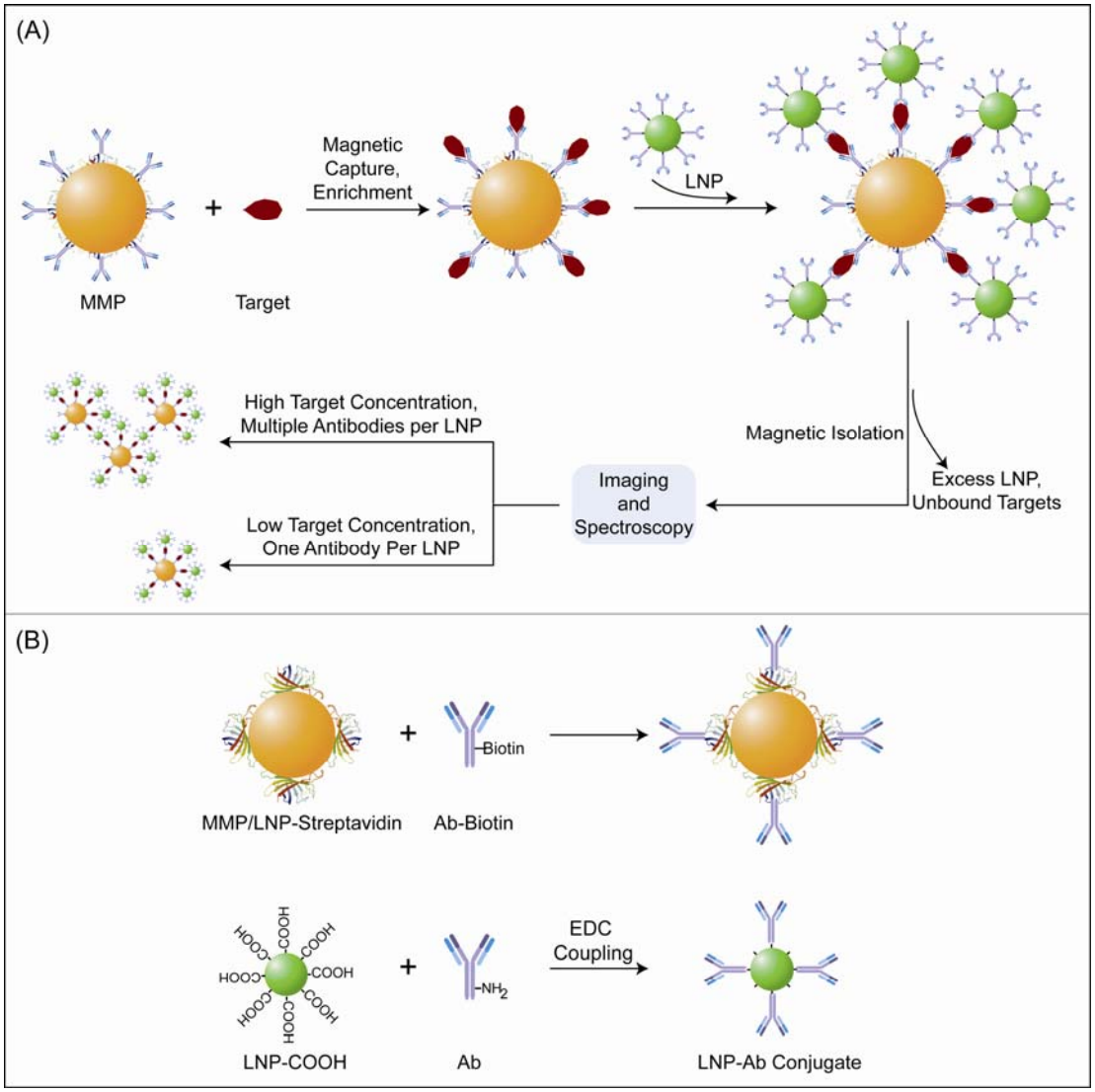

Figure 4.1: Schematic illustration of bead-based sandwich immunoassay using magnetic beads (MMP) and luminescent nanoparticles (LNP). (A) MMPs are added to a solution containing target molecules (protein shown here). Upon target enrichment, LNPs are added and bind to the target molecules captured on the bead. (B) Conjugation strategies used to couple recognition biomolecules to MMPs and LNPs.

Another advantage of this assay is the ability to perform washing steps to increase specificity and reduce non-specific binding of target or fluorescent probe to the bead.

Initially, our imaging setup and detection sensitivity was tested using dye-labeled biotin (tetramethyl-rhodamine conjugated to biotinylated dextran molecule) as a reporter probe. High-resolution single-bead images were captured at decreasing concentrations

of the probe. The average integrated intensity from several beads at each probe concentration was obtained and is shown in **Figure 4.2**.

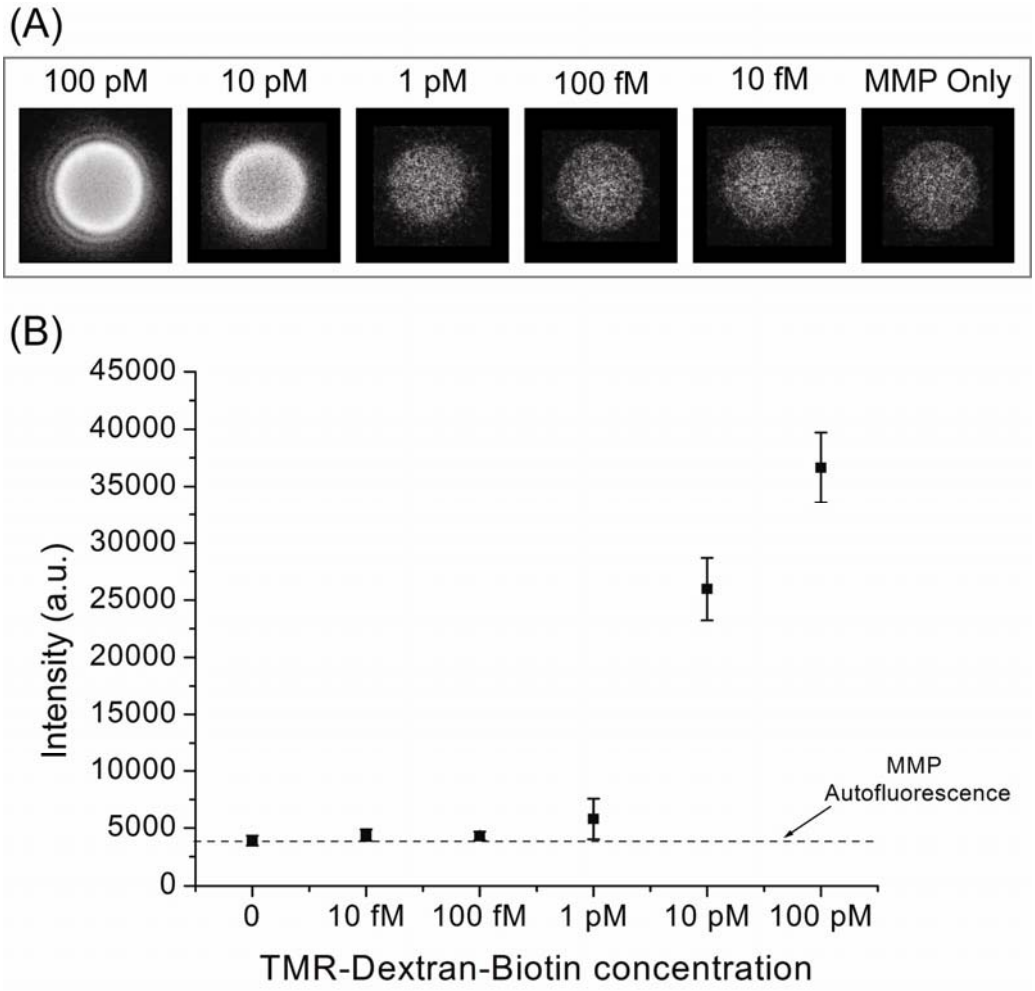

Figure 4.2: Single-bead assay and fluorescence detection as a function of TMR-labeled probe concentration. (A) High resolution single-bead fluorescence images at varying concentrations of TMR dye. (B) Plot of average bead fluorescence intensity versus TMR-dextran-biotin concentration (n=5).

From the results, it is clear that although one can detect 10 pM probe concentration, below 1 pM the fluorescence signal from beads was not detected and was similar to that of bare beads. This observation was attributed to the probe signal (emission peak ~590 nm) being buried under the visible autofluorescence from the beads.

In order to determine the best probes for labeling captured targets on the bead, it was important to obtain the autofluorescence spectrum of bare magnetic beads (streptavidin-beads without any dye on surface) when excited under blue light (excitation wavelength = 488 nm).

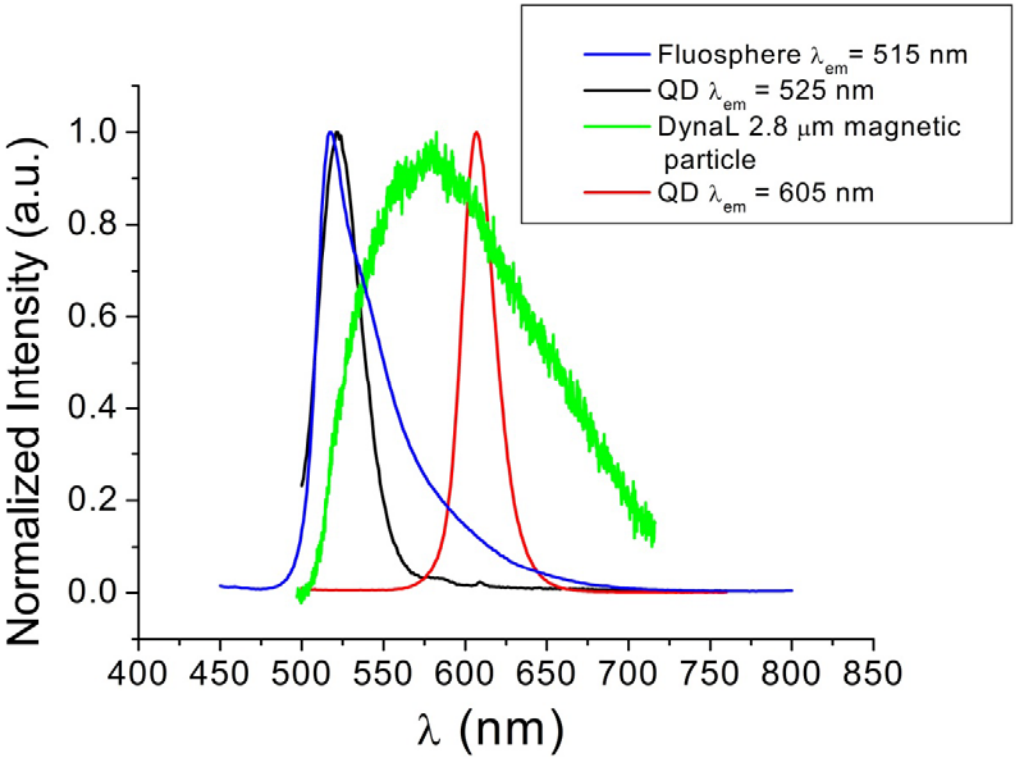

Figure 4.3: Autofluorescence spectrum of beads juxtaposed with fluorescence spectra of luminescent nanoparticles. QD525 and Fluosphere515 were used due to less overlap with bead autofluorescence peak.

In addition, we obtained fluorescence spectra of three nanoparticle probes, QD605, QD525 and Fluospheres emitting at 515 nm. From the spectra (**Figure 4.3**), it is clear that the broad bead autofluorescence spectrum tapers sharply at shorter wavelengths (around 510 nm) and more gently at longer wavelengths (in the near-infrared region). Both QD525 and 515 nm emitting fluospheres do not overlap with bead autofluorescence as much as QD605. It should be noted that TMR dye that was used to obtain data shown earlier (see **Figure 4.2**) has a broad non-symmetric emission peak

with a maxima at 590 nm. This peak strongly overlaps with the autofluorescence peaks and further confirms the low detection sensitivity observed due to signal being buried under bead autofluorescence. An interesting property of QDs is that unlike dye molecules, they exhibit a large Stokes' shift, whereby single light sources (such as blue light) can excite QDs emitting multiple colors. This unique property makes it possible to design probes so that they are "spectrally-shifted" from the autofluorescence of materials such as polymer magnetic beads.

Although, the autofluorescence peak also tapers in the near-infrared (near-IR) region, we did not evaluate near-IR probes for the following reasons. There is lesser availability of near-IR nanoparticle probes compared to that in the visible region. Second, commonly used and affordable CCD cameras and detectors are more efficient in the visible region compared to near-IR CCD detectors. Therefore, the LNPs we decided to use for our studies were either QD525 or TransFluospheres (dye-doped polystyrene nanoparticles) that emit at 515 nm. Dye-embedded Fluospheres are 43 nm in size and also bright like QDs. They also resist photobleaching to a greater extent than standard organic fluorophores and are excellent alternatives to QDs.

Next, the assay was tested by adding varying concentrations of TNF-alpha as the target molecule. Beads coupled-with anti-TNF-alpha antibodies (**Figure 4.1**) were used to capture the target molecules. This was followed by the addition of antibody-labeled green emitting Fluosphere to the sample volume. Both antibodies coupled to beads and Fluospheres were monoclonal but targeted to different epitopes on TNF-alpha target molecule. **Figure 4.4** shows the results we obtained.

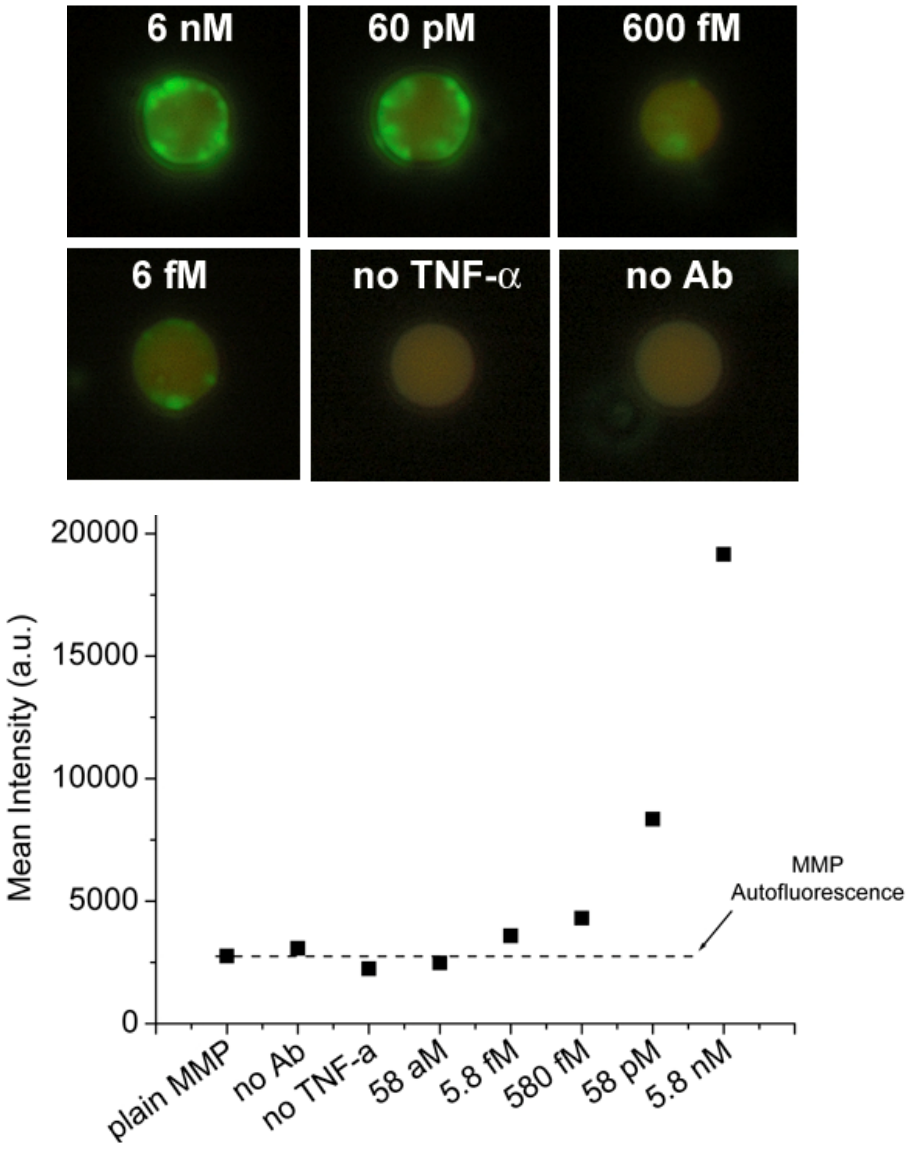

Figure 4.4: Single-bead immunoassay for TNF-alpha detection using luminescent nanoparticles (dye-doped particles). Fluorescence microscope images (top figure) obtained at varying concentrations of target. Plot of the integrated fluorescence intensity as a function of target concentration (bottom figure). Spectral shift of nanoparticles from bead autofluorescence is evident.

Upon using spectrally-shifted LNPs, a dramatic increase in detection sensitivity was observed. Compared to TMR-labeled probes where the detection limit was in the picomolar range, we see a 2-3 order of magnitude increase in detection sensitivity. This

is clearly evident from the green-signal visible in the single-bead fluorescence microscope images obtained at 6 fM target concentration (**Figure 4.4**, top figure). When comparing integrated fluorescence intensity to the background signal (shown by dotted line in **Figure 4.4**), signal was detected at the femtomolar range. Controls for this experiment consisted of plain beads, bead-antibody conjugates with no target present, and beads without any antibodies. No signal was detected from the controls.

DNA detection

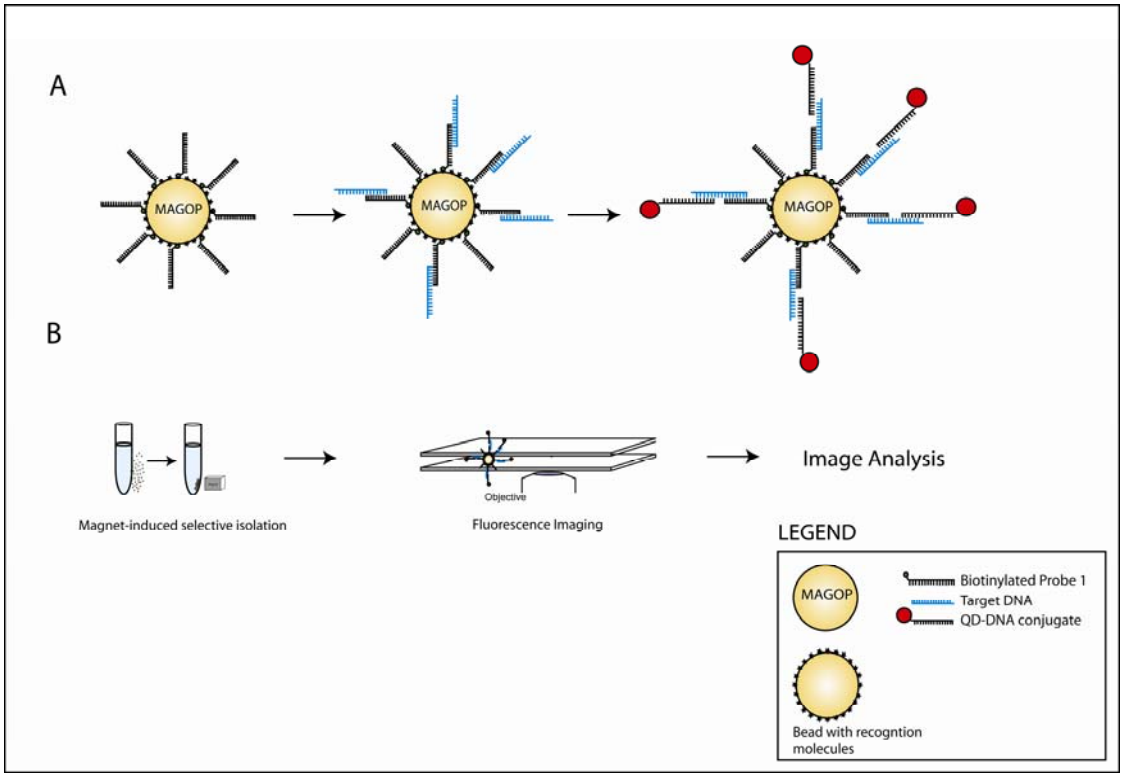

Figure 4.5: Schematic illustration of methods for oligonucleotide detection.

Detecting DNA molecules from bodily fluids by using a similar bead-based assay holds promise for performing multiplexed genotyping and diagnosis of diseases at an early stage. In theory, a similar bead-based assay can be used to detect fragments in solution through hybridization of complimentary DNA strands. Using streptavidin-coated

beads and the same basic principles as discussed for protein detection, we performed a DNA detection assay **(Figure 4.5)**. Unlike TNF-alpha immunoassay described previously, oligonucleotide having a sequence complimentary to the target sequence was directly labeled using QD525. The QD:DNA molar ratio at the time of conjugation was 1:5.

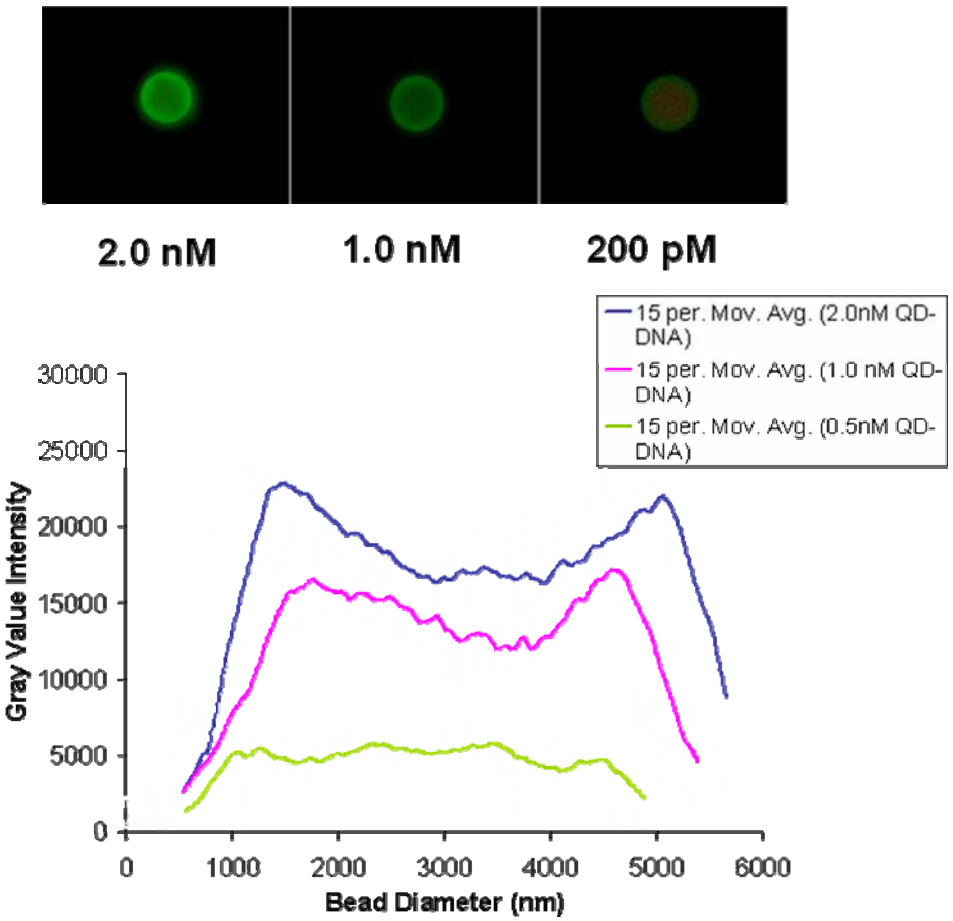

Figure 4.6: Single-bead imaging and quantitative analysis of fluorescence signal obtained by detecting QD-labeled oligonucleotides.

This ratio was estimated because conjugation reactions are seldom 100% efficient. Assuming an efficiency of 50%, the final conjugation ratio would be ca. 1:2, therefore this ratio was chosen. Results of the assay are shown in **Figure 4.6**. From single-bead microscope images, we were able to detect a signal at 200 pM target

concentration. However, below this concentration no signal was detected. The integrated bead signal was obtained and is plotted as a function of concentration. When comparing DNA detection assay results with protein detection assay results, it should be remembered that the recognition molecules used to capture targets are entirely different in size, charge, function, and affinity. DNA oligonucleotide coupled to the bead was a 25 bp sequence with a 16-carbon spacer on the terminal end. Hybridization conditions are generally tuned towards a particular assay but typically involve varying salt concentration and temperature of hybridization [23]. However, steric inhibition may prevent hybridization. Compared to micron sized bead surface, the oligo sequence is only a few nanometers. A possible solution to this problem is to introduce PEG spacer with a functional group at one end so that oligonucleotide can be conjugated.

It should be noted that a sandwich assay for DNA detection was performed in a similar fashion to immuno-sandwich assay described in this chapter, but despite several attempts under several conditions, the experiments were unsuccessful. A significant challenge was obtaining the right conditions for DNA triplex-hybridization, where target sequence is hybridized to two sequences complimentary to each half of the target. Each of these two sequences were conjugated to the bead and LNP. Future studies and solutions to address this problem are discussed in Chapter 7.

In conclusion, we have demonstrated a bead-based sandwich assay using magnetic beads and luminescent QD and dye-doped nanoparticles as probes. Further, we have shown that using spectral-shifting properties of QDs it is possible to by-pass issues of autofluorescence from beads and also from biological media where such tests may be applicable. This technology has potential in automated biomolecule screening in labs where high detection sensitivity is required. Combined with encoding technology discussed in Chapter 3, we believe that bead-based immunoassays using QDs as bright fluorescent probes can improve current detection limits obtained from ELISAs.

4.4 References

[1] S.P. Mulvaney, H.M. Mattoussi and L.J. Whitman, Incorporating fluorescent dyes and quantum dots into magnetic microbeads for immunoassays, *Biotechniques* **36**: 602-+. (2004)

[2] B.E. Yingyongnarongkul, S.E. How, J.J. Diaz-Mochon, M. Muzerelle and M. Bradley, Parallel and multiplexed bead-based assays and encoding strategies, *Comb Chem High Throughput Screen* **6**: 577-587. (2003)

[3] M.R. Henry, P. Wilkins Stevens, J. Sun and D.M. Kelso, Real-time measurements of DNA hybridization on microparticles with fluorescence resonance energy transfer, *Anal Biochem* **276**: 204-214. (1999)

[4] A. Agrawal, T. Sathe and S. Nie, Single-bead immunoassays using magnetic microparticles and spectral-shifting quantum dots, *J Agric Food Chem* **55**: 3778-3782. (2007)

[5] T.R. DeCory, R.A. Durst, S.J. Zimmerman, L.A. Garringer, G. Paluca, H.H. DeCory*, et al.*, Development of an immunomagnetic bead-immunoliposome fluorescence assay for rapid detection of Escherichia coli 0157 : H7 in aqueous samples and comparison of the assay with a standard microbiological method, *Applied and Environmental Microbiology* **71**: 1856-1864. (2005)

[6] A. Fan, C. Lau and J. Lu, Magnetic bead-based chemiluminescent metal immunoassay with a colloidal gold label, *Anal Chem* **77**: 3238-3242. (2005)

[7] R.J. Fulton, R.L. McDade, P.L. Smith, L.J. Kienker and J.R. Kettman, Advanced multiplexed analysis with the FlowMetrix(TM) system, *Clinical Chemistry* **43**: 1749-1756. (1997)

[8] T.T. Hansel, I.J. De Vries, T. Iff, S. Rihs, M. Wandzilak, S. Betz*, et al.*, An improved immunomagnetic procedure for the isolation of highly purified human blood eosinophils, *J Immunol Methods* **145**: 105-110. (1991)

[9] K.S. Kim and J.K. Park, Magnetic force-based multiplexed immunoassay using superparamagnetic nanoparticles in microfluidic channel, *Lab Chip* **5**: 657-664. (2005)

[10] J.M. Nam, C.S. Thaxton and C.A. Mirkin, Nanoparticle-based bio-bar codes for the ultrasensitive detection of proteins, *Science* **301**: 1884-1886. (2003)

[11] P.S. Eastman, W. Ruan, M. Doctolero, R. Nuttall, G. de Feo, J.S. Park*, et al.*, Qdot Nanobarcodes for Multiplexed Gene Expression Analysis, *Nano Lett* **6**: 1059-1064. (2006)

[12] H. Xu, H.P. Wu, F. Huang, S.P. Song, W.X. Li, Y. Cao*, et al.*, Magnetically assisted DNA assays: high selectivity using conjugated polymers for amplified fluorescent transduction, *Nucleic Acids Research* **33**: -. (2005)

[13] T. Aytur, J. Foley, M. Anwar, B. Boser, E. Harris and P.R. Beatty, A novel magnetic bead bioassay platform using a microchip-based sensor for infectious disease diagnosis, *J. Immunol. Methods* **314**: 21-29. (2006)

[14] A.G. Gehring, C.G. Crawford, R.S. Mazenko, L.J. VanHouten and J.D. Brewster, Enzyme-linked immunomagnetic electrochemical detection of Salmonella typhimurium, *J. Immunol. Methods* **195**: 15-25. (1996)

[15] J.M.C. Luk and A.A. Lindberg, Rapid And Sensitive Detection Of Salmonella (O-6,7) By Immunomagnetic Monoclonal Antibody-Based Assays, *J. Immunol. Methods* **137**: 1-8. (1991)

[16] C. Monceyron and B. Grinde, Detection Of Hepatitis-A Virus In Clinical And Environmental-Samples By Immunomagnetic Separation And PCR, *J. Virol. Methods* **46**: 157-166. (1994)

[17] J.A.W. Morgan, C. Winstanley, R.W. Pickup and J.R. Saunders, Rapid Immunocapture Of Pseudomonas-Putida Cells From Lake Water By Using Bacterial Flagella, *Applied and Environmental Microbiology* **57**: 503-509. (1991)

[18] A. Agrawal, C. Zhang, T. Byassee, R.A. Tripp and S. Nie, Counting single native biomolecules and intact viruses with color-coded nanoparticles, *Anal Chem* **78**: 1061-1070. (2006)

[19] P. Alivisatos, The use of nanocrystals in biological detection, *Nat Biotechnol* **22**: 47-52. (2004)

[20] A. Smith and S. Nie, Chemical analysis and cellular imaging with quantum dots, *Analyst* **129**: 672-677. (2004)

[21] G.T. Hermanson, Bioconjugate Techniques, Academic Press, San Diego (1996).

[22] W.S. Rasband. ImageJ. 1997-2006, Accessed 10/15/2006, 2005.

[23] L.M. Demers, C.A. Mirkin, R.C. Mucic, R.A. Reynolds, 3rd, R.L. Letsinger, R. Elghanian, *et al.*, A fluorescence-based method for determining the surface coverage and hybridization efficiency of thiol-capped oligonucleotides bound to gold thin films and nanoparticles, *Anal Chem* **72**: 5535-5541. (2000)

CHAPTER 5

SELECTIVE CAPTURE AND MULTICOLOR PROFILING OF RARE CIRCULATING TUMOR CELLS USING MAGNETIC NANOPARTICLES AND QUANTUM DOTS

5.1 Introduction

Metastasis is the major cause of cancer-related deaths and involves the dissemination of tumor cells from a primary tumor to different organs of the body[1]. Upon diagnosis and resection of a primary tumor, the oncologist's decision to administer follow-up treatment is usually dependent on whether the disease has spread or metastasized to other organs in the body. This is because metastatic tumor cells are considered to be the source of disease relapse after surgery[2]. The most efficient way for the cells to spread is through the blood and lymph circulatory systems. As these circulating tumor cells (CTC) disseminate, most are detected as aberrant and destroyed by the immune system, however, a small fraction can evade these regulatory mechanisms and proliferate at a distant site. Not all of these disseminated tumor cells will develop into distant tumors. In fact, there is new evidence that suggests that a significant fraction of these cells are either apoptotic (dead) or do not have stem cell like properties [3]. By capturing and scrutinizing these cells before they metastasize, one can obtain a real-time cellular biopsy of the tumor without using invasive needle biopsy techniques. Therefore, there is a need to identify and characterize tumor cells *ex vivo* for viability, aggressiveness, and invasive potential. With a better understanding of the nature of disseminated cells it is possible to improve disease staging and administer tailored therapy for cancer patients.

Even though MRI, computed tomography, and serum protein MALDI-TOF analysis can be used to detect residual disease, the presence of circulating tumor cells has been shown to correlate most sensitively with cancer progression, metastasis and overall patient survival [4, 5]. Detection of CTC's from peripheral blood in patients with localized and metastatic breast cancer is associated with poor outcome [4-6]. In a seminal study by Cristofanilli et al.[4], peripheral blood of 177 patients with metastatic breast cancer was examined for the presence of CTC's and observed that CTC's were frequently detected in almost all patients. 60% had at least two CTC's in 7.5 mL of whole blood, 49% had more than five and 21% had more than 50.

Current methods for detecting circulating tumor cells include histopathological staining, immunofluorescence [7, 8], RT-PCR[9], FISH[10], flow cytometry[8, 11, 12], and FAST (fiber-optic array scanning technology)[13, 14] . PCR-based assays have been used by exploiting expression of epithelial or cancer-specific genes to detect CTC's. Although they provide unrivalled sensitivity, the major limiting factor is the illegitimate low-level transcription of tumor-associated or epithelial genes in normal cells[15, 16]. Quantitative RT-PCR, may be able to resolve these problems but will not provide information on the number of tumor cells detected, which is an important indicator of patient survival. Further, RT-PCR methods require destruction of cells and loss of morphological information, which can be valuable to validate tumor cell origin and metastatic potential. For example, it is known that cells with stem-cell like properties like self-renewal and increased mobility have distinctly different morphology to normal epithelial cells. Finally, it is not clear whether these methods can provide clinically relevant information such as treatment monitoring. Similarly, flow cytometry provides quantitative information about cell surface protein expression but provides no morphological information. FAST is technically challenging requiring carefully tuned

optics and requires spreading of whole blood onto 100 cm^2 microscope slides, which is messy and a health hazard to the user when handling infected blood.

Phenotyping captured CTC's has not been easy and is not a well established. Two methods, namely immunohistochemistry (IHC), and flow cytometry are often used to characterize rare cells. Although IHC stains cell surface markers, it is not quantitative. Further it is time consuming and highly subjective. Therefore, IHC cannot be used for routine screening of large number of patients. On the other hand, flow cytometry can be used to detect circulating tumor cells from non-cancerous cells through surface staining, but cannot provide morphological data. Although, one may argue about the value of morphological information in CTC characterization, the spatial location of proteins may offer clues to the cell's invasive potential.

There is no doubt that the sensitivity of all these techniques can be improved by enriching target cells and eliminating background cell populations. The ratio of tumor:non-tumor cell in blood of early metastatic cancer patients is usually $1:10^6$ for 1 mL of blood. There are two ways to address this problem. First, there must be a concerted effort in developing separation technology for specifically isolating and characterizing target cells such that there are virtually no background blood cells. A second approach is to use existing techniques and develop imaging probes that can recognize tumor from non-tumor and eliminate or rule them out through image algorithms. Several approaches for CTC capture from blood have been pursued in the past. Normally, cell enrichment and volume reduction techniques are applied by isolating mononuclear cells from blood using red blood cell lysis or gradient separation techniques (Ficoll gradient separation). However, both of these approaches can lead to a loss of tumor cells either due to lysis, or due to variations in density. Cells are easily lost during Ficoll separation as the larger dense epithelial cells are lost in the granulocyte fraction.

Another method used is positive selection or negative depletion of cells using immunomagnetic particles. In this approach, particles are labeled with monoclonal antibodies specific to epithelial cell surface markers such as the glycoprotein, EpCAM. However, due to heterogeneity of antigen expression across tumor and blood cells, there is a possibility of false positives. Negative hematopoietic cell depletion is also widely used to improve sensitivity in large sample volumes of blood. In this procedure, immunomagnetic beads conjugated with antibodies against pan-leukocyte CD (Clusters of Differentiation) markers such as CD45 are used to remove leukocytes. Unfortunately, this techniques does not completely remove all the non-tumor cells. The focus is on developing standardized technology that will enable selective capture of target cells, and elimination of false positives. Although, such nanoparticles have been used in the past for cell capture, advances in nanoparticle synthetic chemistry[17] have made it possible to synthesize a large batch of highly monodisperse magnetic nanoparticles [18-20]. The magnetic properties of the uniform nanoparticles can be tuned precisely and also enable more efficient biological tagging and separation.

There were two goals for this study; (1) to demonstrate application of QDs in identifying and profiling magnetically enriched tumor cells artificially spiked in blood using spectroscopic methods (2) to compare separation efficiency of uniform and single magnetic nanoparticles to larger commercial polydisperse magnetic nanoparticles in isolating tumor cells. Using this integrated approach, we believe it will be possible to monitor patient response to therapy and predict disease invasiveness. Therefore, our *hypothesis* is that a combination of immunomagnetic isolation and QD-based multiplexed cell protein profiling will provide quantitative and morphologically relevant data in establishing patient prognosis with circulating tumor cell phenotype and load. Here, we describe the integration of magnetic iron oxide and Quantum Dot (QD) optical

nanoparticles for selectively isolating and analyzing multiple biomarkers expressed inside and on the cells.

5.2 Materials and Methods

Tumor cell line culture

Adherent breast cancer cell lines (BT-474, MCF-7 and MDA-MB-231) of epithelial origin were obtained from American Type Culture Collection (ATCC, Manassas, VA) and were used to artificially spike media and normal human blood samples. The above mentioned cell lines were grown in RPMI-1640 (MDA-MB-231) and Minimum Essential Medium (BT-474 and MCF-7). Both types of media were supplemented with 10% Fetal Bovine Serum (Invitrogen, Carlsbad, CA) and 1% Penicillin/Streptomycin antibiotic. Cells were harvested upon reaching ~80-90% confluency using 0.05% Trypsin (containing EDTA) (Mediatech Inc., Herndon, VA), followed by washing steps before seeding them into 25 cm^2 culture flasks (Corning, Corning, NY) at a high seeding density. Due to the tendency of MCF-7 and BT-474 cells to clump, the trypsinized cells were passed through a 30 μm filter (BD Biosciences, San Jose, CA). In addition, two prostate cancer cell lines that were cultured at Emory University from ascites fluid of prostate cancer patients, 1A8 and 1F11 were used. These cells display an epithelial-to-mesenchymal transition (EMT) and are morphologically and phenotypically distinct. We used these cells to demonstrate multicolor molecular profiling upon isolation. Similar culture procedures were used for these cells with T-medium (Mediatech Inc., Herndon, VA) used instead. Prior to spiking cells, they were counted manually by adding fixed volume of cell suspension to a 96-well transparent plate and recording cell number. Approximately 300-400 cells were used per mL of blood/media for efficiency calculations.

Blood Collection

Normal human blood was collected using standard veni-puncture practices into 2-3 CellSave (Immunicon Inc. Huntington Valley, PA) evacuated 10 mL glass tubes. The first tube containing blood was discarded to reduce contamination from skin epithelial cells. CellSave tubes contain disodium EDTA anti-coagulant, polyethylene glycol and a proprietary preservative. According to vendor documentation, the preservative is used to preserve morphology and cell surface antigen expression over a period of 72 hours. Cultured cells were then enumerated and spiked into whole blood solutions (typically 1-2 mL) and used for further experiments. Whole blood was kept at room temperature, opened under sterile condition, and used immediately.

Magnetic Nanoparticles and Microbeads

Magnetic particles were either obtained from a commercial vendor, Invitrogen Inc. (Carlsbad, CA) and Immunicon Inc. (Huntington Valley, PA) for cell isolation experiments. The particles from Invitrogen were CELLection Dynal Microbeads (4.5 μm in diameter) and are conjugated to mouse anti-EpCAM (BER-EP4 epitope) antibodies. The antibodies on the bead can be cleaved from the bead surface via a cleavable DNA linker conjugated on one end to the Fc portion of the IgG molecule and on the other end to the carboxylated bead surface. The nanoparticles were either pre-conjugated to antibodies specific to tumor cells or were pre-coated with streptavidin. In addition uniform magnetic nanoparticles prepared using a method developed by Yu and co-workers [21] were provided by Ocean Nanotech Corp. (Fayeteville, AK). These nanoparticles were 30 nm in diameter and coated with hydrophobic ligands. In order to be used in biological medium, they were coated with two types of polymers to phase-transfer into the aqueous phase, (i) poly (maleic anhydride co-alt-1-octadecene) amphiphilic polymer (M_n ~ 30,000-50,000) with 30% carboxyl groups coupled to PEG,

using modified procedure originally described by Yu et al. [22], and a (ii) poly(acrylic acid, tetradecene modified) amphiphilic polymer (MW ~ 3,500, provided by Brad Kairdolf, Nie group). Concentration of hydrophobic magnetic nanoparticles was measured through absorbance and a standard curve provided by Ocean Nanotech. Additionally, amphiphilic polymer coated nanoparticles concentration was measured by Inductively Coupled Plasma (ICP-MS) analysis (UGA Chemical Analysis Lab, Athens, GA).

Magnetic Tagging and Isolation

Cells grown in culture were detached using 0.05% Trypsin. After manual counting, a fixed number of cells were spiked either into normal human blood or cell culture media. The spiked blood was centrifuged at 800xg for 10 minutes to remove interfering serum proteins. 25 ul of 100 ug/mL biotin-EpCAM IgG (R&D Systems, Minneapolis, MN) was added per 500 ul of blood solution. After incubating this solution at 4°C for 30 minutes, (to prevent endocytosis of IgG molecules) 35 ul of streptavidin-coated magnetic nanoparticles was added and the solution was incubated at room temperature for 60 minutes. Afterwards, the magnetically-labeled cells were isolated by placing the sample on a permanent magnet (NdBFe 1.5T, MCE, Torrance, CA) and washed three times with PBS (Phosphate Buffered Saline, 10 mM, pH 7.4) buffer containing 0.1% BSA (Bovine Serum Albumin). The cell solution was either transferred manually to superfrost microscope slides, or spun down using a cytospin device.

When using Dynal microbeads pre-coated with anti-EpCAM antibodies, beads were first incubated with cell suspension for 30 minutes at 4C to minimize phagocytosis or uptake by cells. Following washing steps with PBS containing 0.1% BSA, the tagged cells were then transferred into RPMI-1640 medium

Cell transfer to microscope slides

Cell suspension was transferred onto Superfrost slides (Fisher Scientific, Waltham, MA) using a Cytospin 3 cytocentrifuge machine (Thermo Shandon, Waltham, MA) for 6 minutes at 700 rpm using medium acceleration. The superfrost slides are specially coated slides so that cells adhere to the surface electrostatically. Also, there is reduced background fluorescence. The cytocentrifuge speed was determined after testing cytospun slides at various speeds for nuclear integrity. At speeds above 800 rpm, cell shearing and nuclear disintegration was visible. We also observed that when cells tagged with magnetic nanoparticles were cytospun, the cells were shredded and the plasma membrane and nuclear membrane were severely disrupted. This may be because the highly dense nanoparticles are strongly influenced by the centrifugal forces. When cells were isolated using magnetic nanoparticles, cell suspensions were transferred manually onto the slide, which was placed on a permanent magnet customized to fit 4 slides in parallel on it. The slides on magnet were kept at 4°C for 1 hour until cells had settled onto the slide. Washes using PBS Buffer (10 mM, pH 7.4) were performed with great care and while making sure that the slides were firmly secured to the magnet.

Cell staining using Quantum Dots

After transferring the cells on to the microscope slides, they were fixed and permeabilized for 20 minutes using a mixture of 3.7% formaldehyde and 0.1% Triton X-100 surfactant in 10mM PBS (pH 7.4), followed by washing with PBS. A blocking buffer (Goat serum + BSA) was added to prevent non-specific protein binding. Subsequently, antibodies specific to antigens of choice were added either simultaneously or in sequence. The concentration of antibody varied between 5-10 ug/mL. For breast cancer profiling, antibodies against ER (Estrogen Receptor), HER2, PR (Progesterone Receptor), CD45 (for staining white blood cells) were used, whereas anti-Vimentin and anti-E-Cadherin antibodies were used for prostate cancer cell profiling. Upon incubating

the antibodies for 2 hours at room temperature, excess antibodies were washed from samples, and 20 nM of QD-secondary antibody conjugates (Invitrogen, Carlsbad, CA) were added. These QDs are coated with antibodies specific to the species in which the above four were raised. As some are raised in the same animal, the QDs are added in sequence with a washing step in between to remove excess unbound QDs. The QD staining step can either be done at room temperature for 2 hours or overnight at 4°C. Finally, the samples were counterstained with DAPI (4',6-diamidino-2-phenylindole) a nuclear staining dye and mounted for long term storage.

Single-cell spectroscopy and imaging

Molecular profile and relative abundance of stained protein markers were obtained using a spectrometer (Acton SP-150, Acton Research, Acton, MA) fitted to the side port of a epifluorescent microscope (Olympus IX-70, Olympus, Center Valley, PA). Exposure times for the acquisition of spectra ranged from 0.1-1 s. Images were acquired using a CCD camera (Olympus, Center Valley, PA) and a 20x PlanApo or 100x oil (NA 1.3) immersion objective (Olympus, Center Valley, PA). The true color fluorescence images were obtained using a 460-490 nm band pass excitation filter and a 505 nm long pass filter (Chroma Tech. Brattleboro, VT). The exposure times varied from 0.2- 4 seconds.

5.3 Results and Discussion

Magnetic Separation

Epithelial cells strongly express Epithelial Cell Adhesion Molecules (EpCAM) glycoprotein on their surface. Since the vast majority of metastasized cancer cells in peripheral blood are epithelial in origin [23], we decided to use anti-EpCAM antibody coated magnetic particles for our experiments. Most commercial kits also provide

EpCAM antibody conjugated nanoparticles/microparticles for epithelial cell enrichment. The general enrichment strategy (**Figure 5.1**) is very easy, relatively quick (depending on magnetic nanoparticle size) and allows for non-target cells to be washed off and reduce sampling volume. Although an excess of anti-EpCAM magnetic particles can be added to the sample, the optimum ratio of magnetic particle to cell is dependent on the size of particles. Larger beads used in our studies were detached from the cell surface after isolation through a DNA linker between the bead and antibody that was cleavable using DNAse enzyme (see Methods section). When isolating artificially spiked tumor cells from whole blood, a range of 2×10^7 to 1×10^8 beads per mL of blood was used. Upon isolation, magnetically labeled cells can be transferred to microscope slides using cytospin centrifugation to transfer cells from solution to slide. Although this method is convenient, it may result in cell loss, or shearing of cells if spun down at high g forces. An alternative but intricate method is to manually transfer the cell suspension onto a positively charged microscope slide with a magnet held underneath it. This method works with higher cell transfer efficiency but is tedious and error-prone. Since our main focus was to reduce total CTC cell loss, we decided to use cytospin when dealing with more than 200 cells per sample, and the manual method was used for lower concentrations.

After cell transfer is complete, QDs are stained using an indirect immunostaining procedure commonly used for staining cells with dye-conjugated antibodies. In this procedure, primary antibodies produced in various species bind to targeted antigens either on the cell surface, or in the cytoplasm (following permeabilization of the cell membrane).

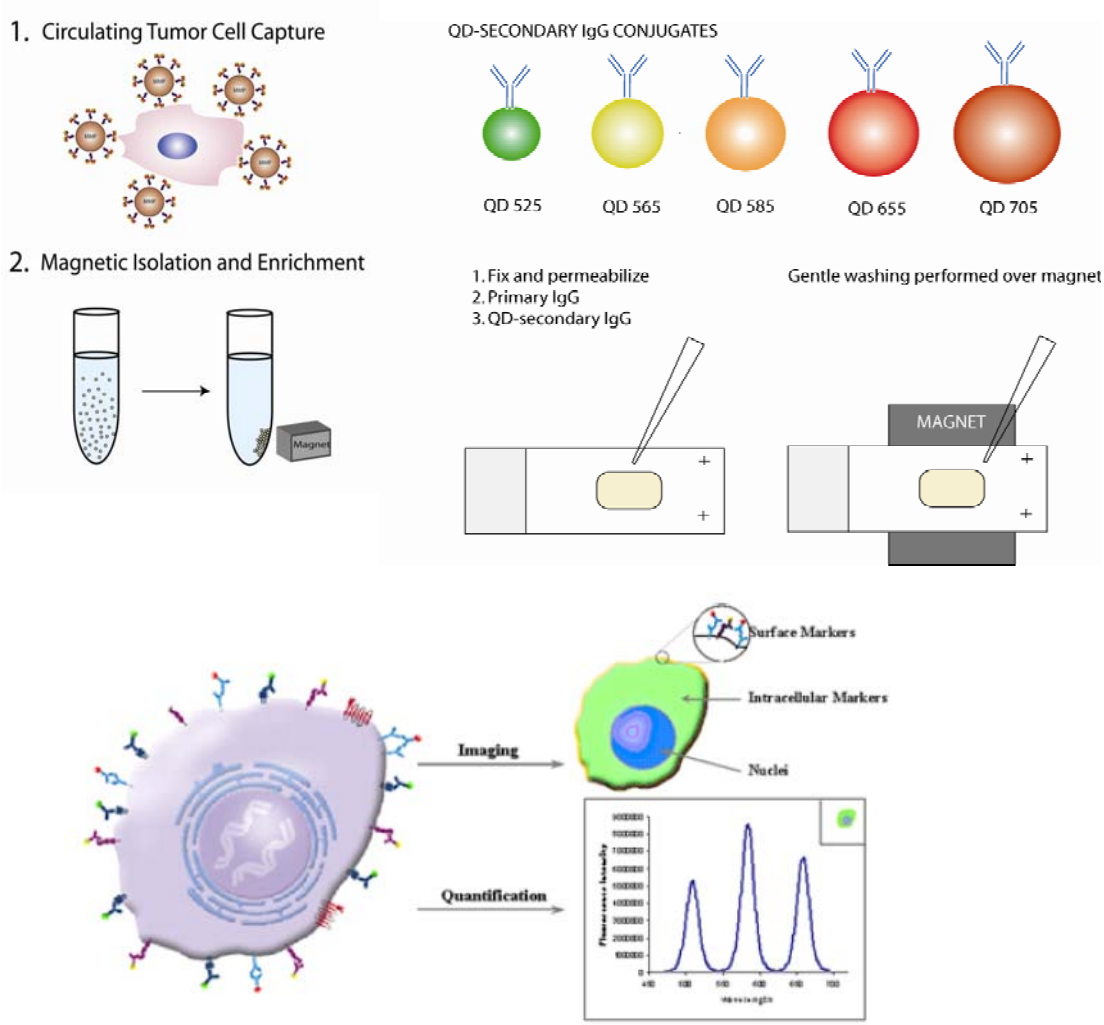

Figure 5.1: Schematic illustration of tumor cell isolation and profiling using magnetic nanoparticles and QDs.

QDs conjugated with antibodies raised in the same species as the primary antibodies are then added to the cells. Therefore, one indirectly labels the antigens being targeted. Finally, after counterstaining with 4',6-diamidino-2-phenylindole (DAPI), a nuclear staining dye, the samples are mounted and imaged under a microscope. Using single-cell spectroscopy methods similar to those used to obtain spectra from dual-function encoded beads (see Materials and Methods section in Chapter 3), the spectral

signature of the cell can be obtained to obtain cell phenotype while preserving morphology and other spatial information from the cell.

Isolation and Profiling of Morphologically and Phenotypically Distinct Prostate Cancer Cells

To determine whether cells artificially spiked in blood could be enriched and profiled for molecular expression, Prostate cancer cell lines that showed an epithelial-to-mesenchymal transition (EMT) were chosen. Epithelial cells are restricted in their ability to grow outside their normal environment. For an epithelial cell tumor to metastasize, the cellular signaling pathways must undergo dramatic changes that permit cell survival and proliferation at non-physiological locations[23]. Initiation of metastasis in primary tumors requires loss of cell adhesion through repression of certain adhesion molecules, such as E-Cadherin. For epithelial cells to become metastatic, they must change their morphology and acquire the ability to escape the control of these survival signals, that is, undergo an EMT (Epithelial-Mesenchymal Transition)[24, 25].

Also, these cells are known to acquire increased mobility, so that upon dissemination, they can invade into distant organs and proliferate. This change in phenotype is typical of EMT where cells acquire “stem-cell like” characteristics. Before proceeding to blood-based studies, two cell lines, 1F11 (epithelial phenotype) and 1A8 (mesenchymal phenotype) were spiked into culture medium, isolated and stained with QDs emitting at 525 nm and 655 nm (**Figure 5.2**). Two proteins were stained, E-Cadherin and Vimentin. Vimentin is an intermediate filament and is closely associated with the cytoskeleton. More importantly, it was chosen as it is a commonly used marker for mesenchymal cells [26].

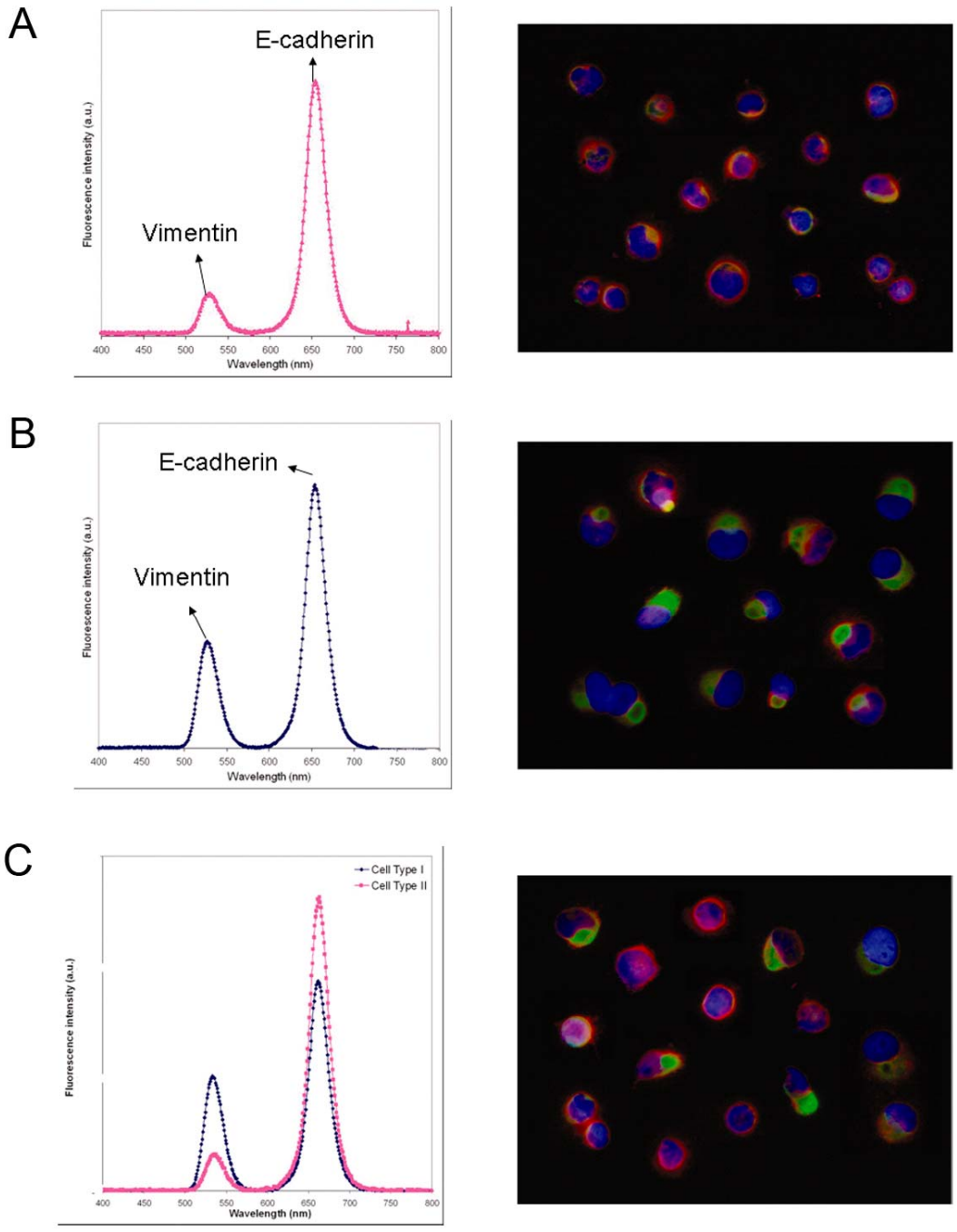

Figure 5.2: Molecular profile and true color fluorescence image of prostate cancer cells that have undergone EMT using QD525 (Vimentin) and QD655 (E-Cadherin). (A) Mean fluorescence spectra (n=10) and microscopy of 1F11 (Epithelial phenotype) cells isolated and stained (B) Mean fluorescence spectra (n=10) and microscopy of 1A8 (mesenchymal phenotype) cells isolated and stained. (C) Mixed sample containing both 1F11 and 1A8. DAPI counterstain shown in blue.

As expected, we were able to isolate and obtain molecular spectral signature of cells enriched from the media. 1F11 cells showed high expression of E-Cadherin and moderate expression of Vimentin, whereas 1A8 cells showed increased Vimentin expression with a down regulation of E-cadherin. The difference in molecular profiles is clear when juxtaposed with each other (**Figure 5.2C** spectra) for a mixed sample of 1F11 and 1A8 cells. The isolation efficiency for this test was 56% on average, which is quite low. There are two reasons that may explain the poor efficiency. First, since magnetic microbeads with cleavable DNA linker was used, the efficiency of the DNAse enzyme will strongly determine cell isolation efficiency. This is because after cleaving beads from the cells, a magnet is used to remove beads and allow the cell solution to be transferred for further use. However, if the bead release is unsuccessful or partially successful, it will result in loss of isolated cells. Large micron-sized beads have such a great magnetic sedimentation velocity that it permits rapid cell isolation even if only one bead binds to the cell. Based on microscopy of cells prior to bead release, several beads (10-20) will bind to one cell. As a result, incomplete cleavage of the DNA linker between beads and antibody will result in loss of cells.

Isolation of Tumor Cells from Blood using Magnetic beads

Subsequently, the same Prostate cancer cells (1F11 and 1A8) were spiked into whole blood and isolated (**Figure 5.3**). From the figure, it is clear that although tumor cells were detected there was interference from leukocytes. The inability to completely remove leukocytes after immunomagnetic cell isolation from whole blood has also been reported by others [27, 28]. Typically, normal human blood contains between 5,000 to 10,000 white blood cells (WBC) per ul of whole blood. Studies were performed with 1mL of blood, which would contain somewhere between 5-10 million WBC's. For this

particular study, the number of cells varied between 521±39 (1F11) and 588±36 (1A8) cells per sample.

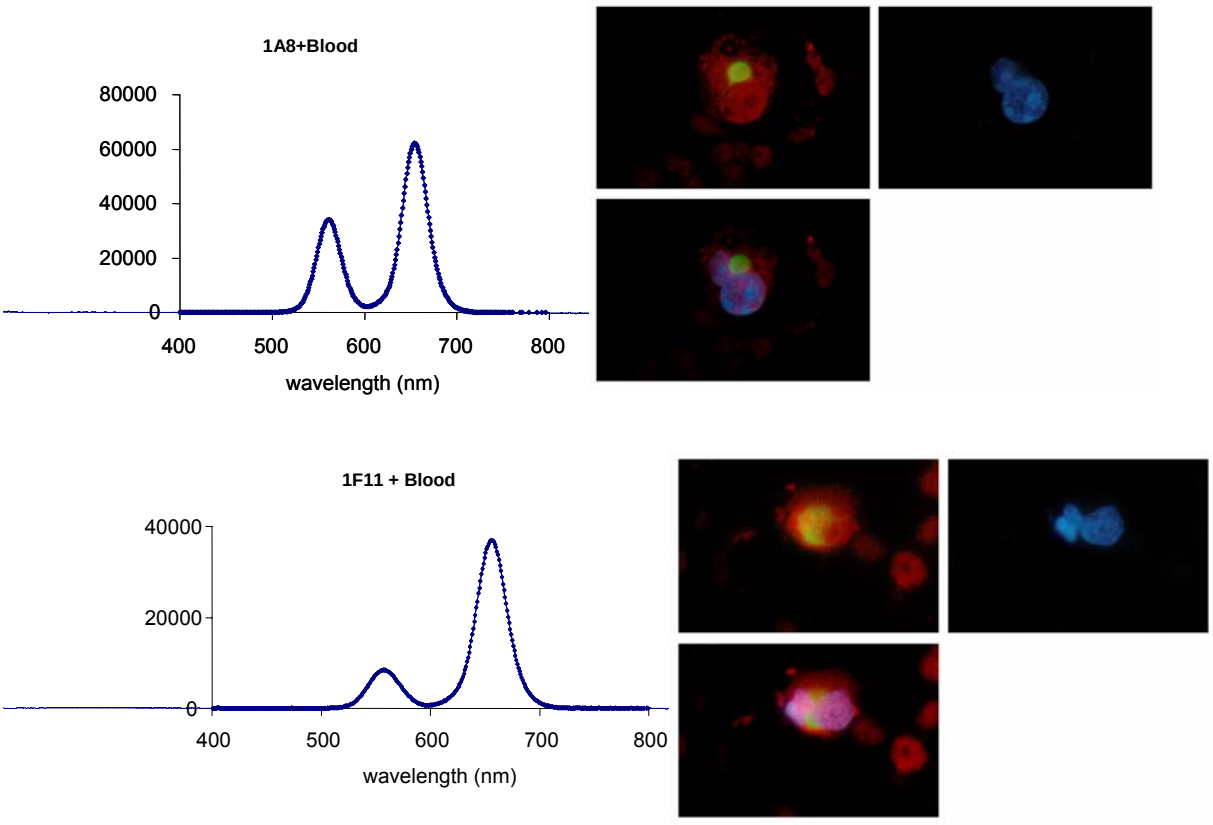

Figure 5.3: Multicolor QD imaging and spectral analysis of 1F11 (epithelial phenotype) and 1A8 cells (mesenchymal phenotype) isolated from whole blood and stained with QD525 (Vimentin) and QD655 (E-Cadherin).

This means that the ratio of WBC:tumor cell is roughly 10,000:1. There are two possible scenarios that would explain the presence of leukocytes. First, there is non-specific interaction between the bead and WBCs. Second, the shear number of cells would make it difficult to completely remove all cells even after 4 rounds of washing with buffer. Images showing beads non-specifically bound to polymorphonuclear cells (PBMC) would suggest that the former scenario is responsible for presence of leukocytes. Interestingly, the spectral signature or pattern of leukocytes is different from 1F11 and 1A8 spectral signatures (**Figure 5.4**). Therefore, a solution to the problem may

involve identifying non-tumor cells from their spectral profiles and subtracting them from the image using image processing algorithms.

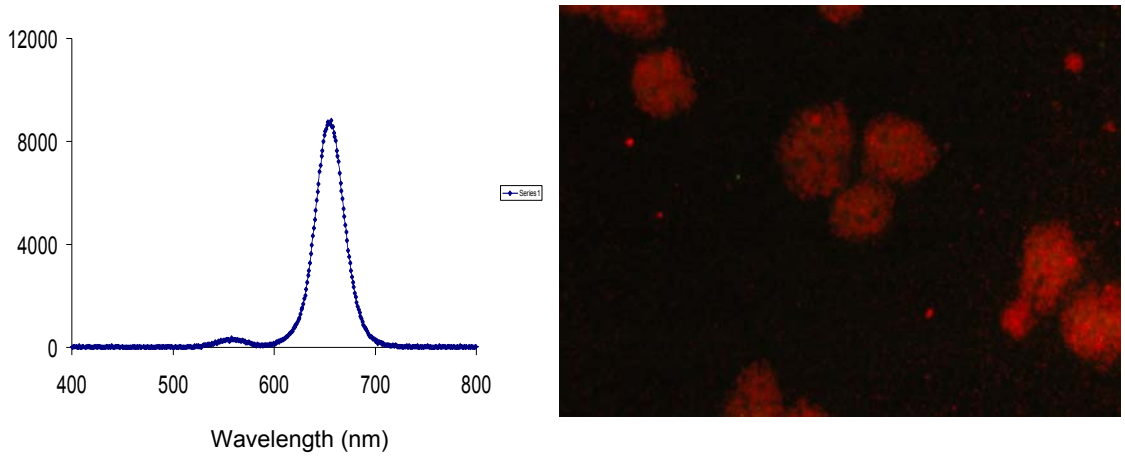

Figure 5.4: Spectral profile and fluorescence image of non-specifically isolated leukocytes.

Isolation of Tumor Cells using Magnetic nanoparticles

An alternative to magnetic microbeads is magnetic nanoparticles. Unlike microbeads that consist of a polymer matrix containing several nanoparticles packed into the core, nanoparticles that were used for the next studies were 200 nm diameter polystyrene particles containing 20-30 iron oxide magnetic nanocrystals. The rationale for testing them was that having many smaller particles binding with the cell would allow better control over leukocyte presence upon isolation (see Background, Chapter 2). The assumption was that the anti-EpCAM IgG conjugated magnetic nanoparticles would bind to more tumor cells than leukocytes, and would allow discrimination between strongly labeled cells and weakly-labeled leukocytes. However, upon isolation and staining, the results showed a greater presence of leukocytes (**Figure 5.5**). Looking at the DAPI and QD fluorescence images, the prostate cancer cell (1A8) can be clearly distinguished due to the obviously larger size and staining pattern, but the presence of blood cells was

concerning. In fact, leukocyte population was so overwhelming that it was difficult to image captured tumor cells due to overlap and in some cases cells on the microscope slide were in multiple layers.

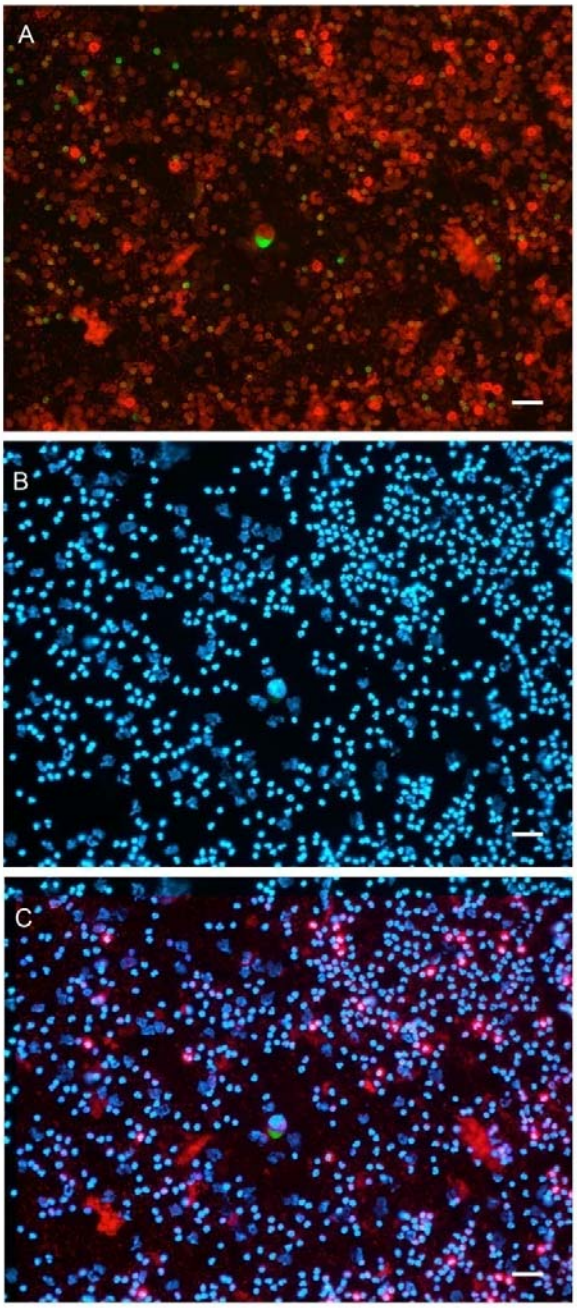

Figure 5.5: Fluorescence images of isolated cells stained with QD525 (Vimentin) and QD 655 (E-Cadherin). (A) Images obtained using 20 x objective and 488 nm excitation with 505 nm emission filter. A single tumor cell (1A8) is visible in the center of the image. (B) DAPI channel of the same image. (C) Overlay of DAPI emission and QD emission.

Profiling of Breast Cancer Cells

In order to demonstrate 3-4 color multiplexed profiling of tumor cells, three commonly available breast cancer cell lines were chosen, MDA-MB-231, MCF-7 and BT-474. Treatment decisions in breast cancer are commonly made based on the expression of three target proteins, namely estrogen receptor (ER), progesterone receptor (PR) and HER2/neu (HER2). ER and PR expression clearly predict for benefit from endocrine therapy while HER2 expression is a prerequisite for response to trastuzumab [29, 30].

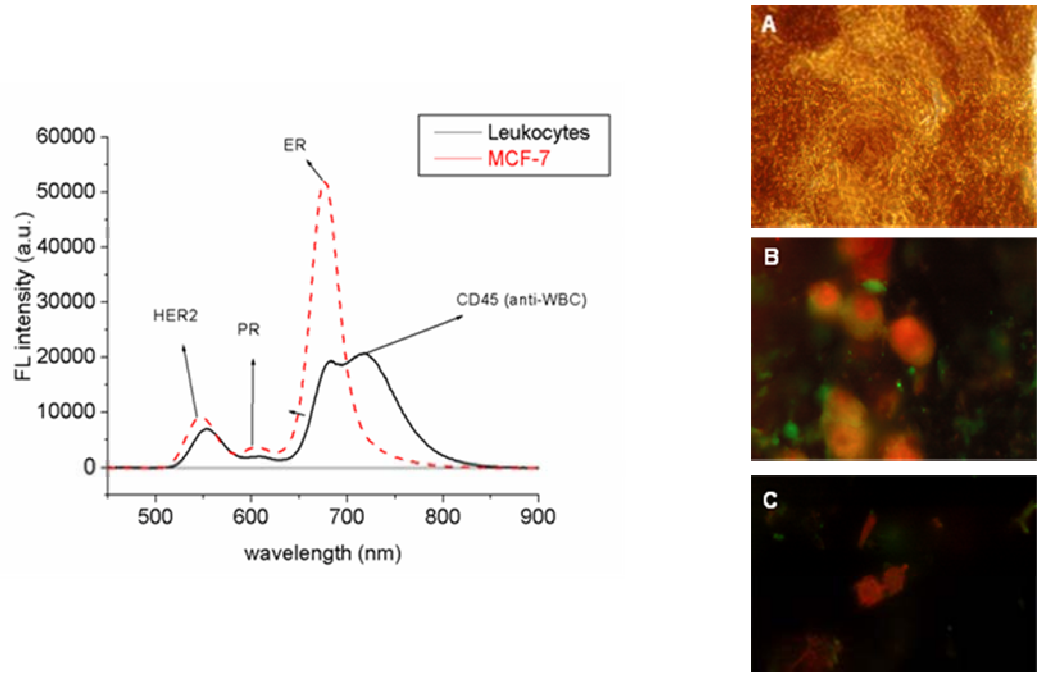

Figure 5.6: Molecular Profile and fluorescence image of isolated MCF-7 cells. Also included is the profile from leukocytes non-specifically labeled with the same QDs (n=5). (A) Bright field image clearly shows magnetic nanoparticles (brown color) (B) Fluorescence image of MCF-7 cells (C) Image of non-specifically captured leukocytes. 60x oil immersion objective used.

These three cells differentially express or lack the three mentioned biomarkers, and were labeled after isolation from whole blood. Additionally, a pan-leukocyte extracellular marker (CD45) was used as a positive marker for all types of leukocytes.

Unlike the microbead isolation procedure, cytospin was not used to transfer cells to glass slides as there was shredding of the cell and loss of morphology even at

reasonable rcf values (300 x g). The surface of magnetic nanoparticles was coated with streptavidin, a glycoprotein that has a strong affinity for biotin.

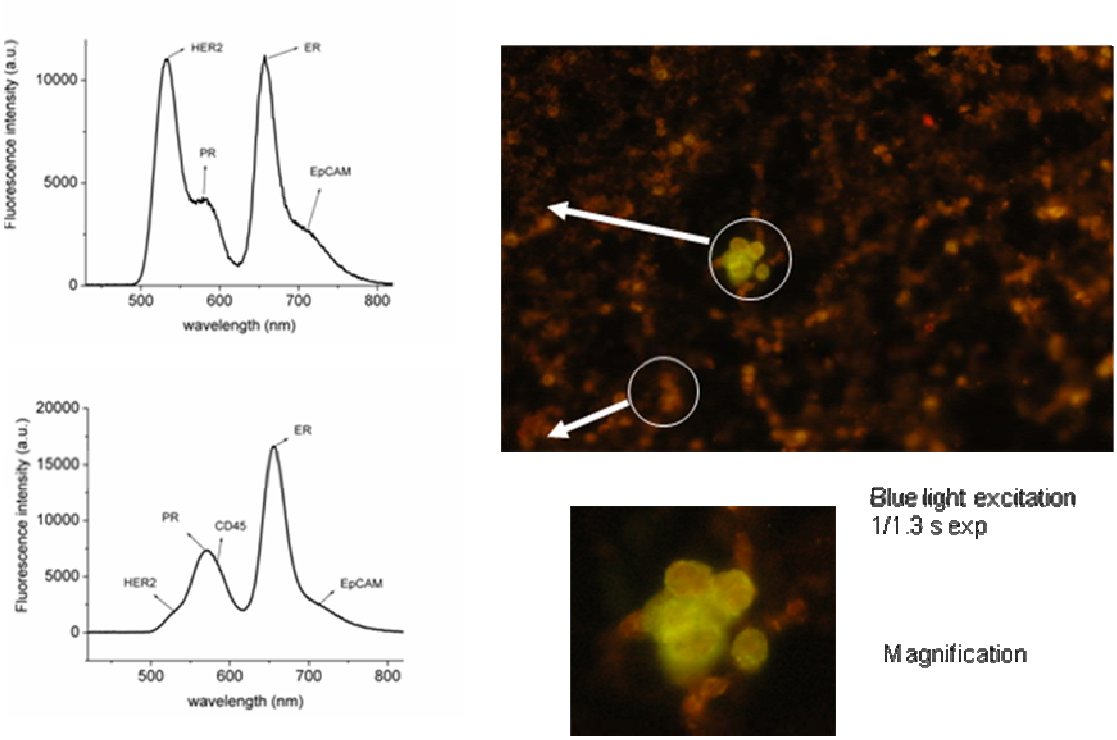

Figure 5.7: Molecular Profile and fluorescence image of isolated BT-474 breast tumor cells. Also included is the spectral profile of leukocytes after isolation from human blood. (n=3)

Biotinylated anti-EpCAM antibodies were incubated with the sample, followed by addition of the streptavidin-nanoparticles. Consistent to previous findings, leukocytes were ubiquitous on all slides that were prepared. Negative isolation steps are occasionally used to remove leukocytes, but due to addition of several extra steps and increase in duration of assay, no merit was seen in this. The distinct spectral signatures of MCF-7 cells and leukocytes were used to differentiate the two as seen in **Figure 5.6**. MCF-7 cells strongly express ER compared to HER2 and PR, and we see the same in the spectra. Also evident in the bright-field image (**Figure 5.6A**) is the inability to see the cell outline due to dense layer of magnetic nanoparticles (brown color due to strong

absorption of light). Likewise, BT-474 cells were profiled and it was possible to identify tumor cells and differentiate them from leukocytes (**Figure 5.7**). BT-474 cells overly express HER2 with weaker expression of ER and PR as can be seen from the spectra.

Comparison of non-specific binding of leukocytes by magnetic nanoparticles

In order to address the issue of non-specific association and capture of magnetic nanoparticles to leukocytes we mixed equal concentration of three types of magnetic nanoparticles with equal volume of whole blood. These three types were (a) Immunicon Inc. nanoparticles that are 150 nm in diameter and are streptavidin-coated (b) PAA-TDA (Poly(acrylic acid)-tetradecylamine) coated magnetic nanoparticles that are 30 nm in diameter, and (c) PMAO-PEG (Poly(maleic anhydride-alt-1-octadecene) –PEG) coated 30 nm magnetic nanoparticles. It is known that PEG groups sterically stabilize nanoparticles and prevent non-specific uptake. Upon magnetic sedimentation and several washing steps under magnetic field, the samples were cytocentrifuged onto microscope slides, counterstained with DAPI and imaged (**Figure 5.8**). From the results, we observe that both streptavidin coated nanoparticles (Immunicon) and carboxylated nanoparticles (PAA-OA coated) were strongly associated with leukocytes, as is evident from the large presence of cells with DAPI-stained nuclei (**Figure 5.8 A & B**). Non-specific binding of PMAO-PEG particles was drastically reduced as seen from this image.

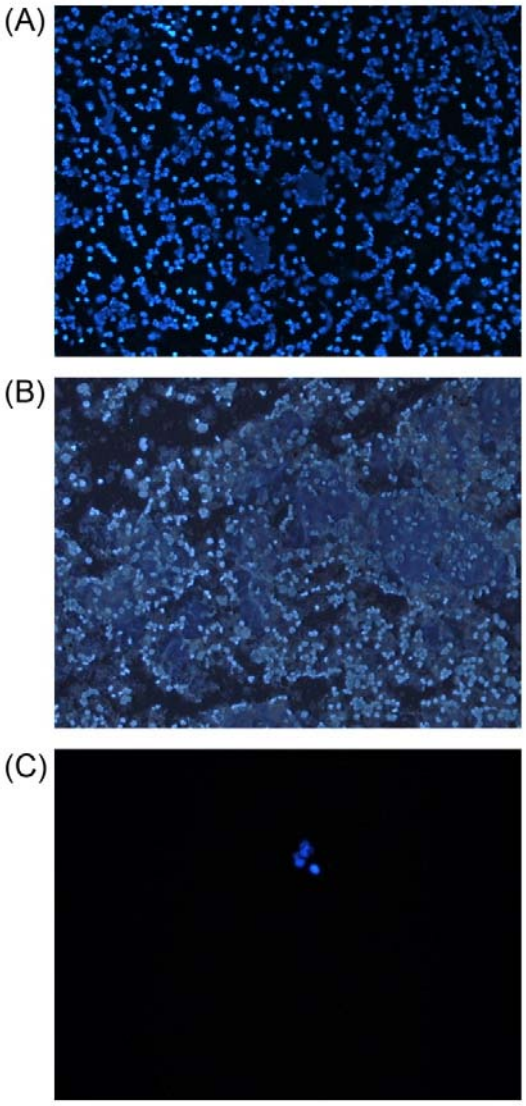

Figure 5.8: DAPI fluorescence images of leukocytes non-specifically captured. (A) Immunicon 150 nm magnetic nanoparticles (B) 30 nm polyacrylic acid coated magnetic nanoparticles (C) 30 nm PEGylated magnetic nanoparticles. A 10 x objective was used.

	Immunicon (150 nm)	Dynabeads (4.5um)	Uniform PAA-TDA coated MNP (30 nm)
Separation Efficiency (~500 cells/mL)	73%	56%	78%

Table 5.1. Comparison of cell separation efficiencies. Average cell count obtained from triplicates (n=3). MCF-7 cells (EpCAM positive) captured from culture media.

During isolation, we recorded the separation efficiencies (**Table 5.1**) for each of the magnetic separation. Compared to the microbead separation procedure, both nanoparticles, although different in size were comparable in separation efficiency. We can also conclude from the values that even though the efficiency of the 30 nm particles is fractionally better, such nanoparticles hold greater promise for post-capture multi-spectral analysis using QDs since they are smaller than the larger Immunicon nanoparticles. Invariably, one is going to face a situation where larger nanoparticles allow faster separation, but may not be ideal for one's application. It should be noted that these efficiency values were obtained from 1 cell line and by isolating them from culture medium. Further studies need to determine this efficiency across a number of epithelial tumor cell lines having varying expression of EpCAM. Also, studies should determine isolation efficiency from whole blood samples. It is hoped that this initial work will provide the foundation for further improvements in cell separation.

In conclusion, we have demonstrated multicolor QD spectral profiling of magnetically isolated tumor cells. Prostate cancer cells with distinctly different morphologies and protein expression levels were isolated with magnetic microbeads and labeled with QDs successfully. However, isolation of cells in blood posed a technical challenge due to the overwhelming number of leukocytes. We tried to address this issue by distinguishing tumor cells from leukocytes by obtaining fluorescence spectral profiles and showed that this could be done. In some cases we observed that number of leukocytes was so great that they were physically obstructing tumor cells and prevented spectral profiling. To address leukocyte non-specific binding, we have recently developed PEGylated polymer coatings that drastically reduce this problem. Hpwever, further tests need to be performed after conjugation to EpCAM antibody, as illegitimate expression of small amounts of EpCAM on leukocytes may still prevent elimination of leukocytes after magnetic isolation.

In the following chapter, we attempt to understand nanoparticle-leukocyte interactions as a function of surface coatings using QDs instead of magnetic nanoparticles. This is because the superior fluorescent properties of QDs permit imaging and fluorescence-based quantitative assays to examine nanoparticle behavior in blood.

5.4 References

[1] K. Pantel and R.H. Brakenhoff, Dissecting the metastatic cascade, *Nat Rev Cancer* **4**: 448-456. (2004)

[2] B.K. Zehentner, Detection of disseminated tumor cells: strategies and diagnostic implications, *Expert Rev Mol Diagn* **2**: 41-48. (2002)

[3] S. Braun, F.D. Vogl, B. Naume, W. Janni, M.P. Osborne, R.C. Coombes*, et al.*, A pooled analysis of bone marrow micrometastasis in breast cancer, *N Engl J Med* **353**: 793-802. (2005)

[4] M. Cristofanilli, G.T. Budd, M.J. Ellis, A. Stopeck, J. Matera, M.C. Miller*, et al.*, Circulating tumor cells, disease progression, and survival in metastatic breast cancer, *N Engl J Med* **351**: 781-791. (2004)

[5] M. Cristofanilli, D.F. Hayes, G.T. Budd, M.J. Ellis, A. Stopeck, J.M. Reuben*, et al.*, Circulating tumor cells: a novel prognostic factor for newly diagnosed metastatic breast cancer, *J Clin Oncol* **23**: 1420-1430. (2005)

[6] N. Xenidis, M. Perraki, M. Kafousi, S. Apostolaki, I. Bolonaki, A. Stathopoulou*, et al.*, Predictive and prognostic value of peripheral blood cytokeratin-19 mRNA-positive cells detected by real-time polymerase chain reaction in node-negative breast cancer patients, *J Clin Oncol* **24**: 3756-3762. (2006)

[7] T.E. Witzig, B. Bossy, T. Kimlinger, P.C. Roche, J.N. Ingle, C. Grant*, et al.*, Detection of circulating cytokeratin-positive cells in the blood of breast cancer patients using immunomagnetic enrichment and digital microscopy, *Clin Cancer Res* **8**: 1085-1091. (2002)

[8] E. Racila, D. Euhus, A.J. Weiss, C. Rao, J. McConnell, L.W. Terstappen*, et al.*, Detection and characterization of carcinoma cells in the blood, *Proc Natl Acad Sci U S A* **95**: 4589-4594. (1998)

[9] R.A. Ghossein and J. Rosai, Polymerase chain reaction in the detection of micrometastases and circulating tumor cells, *Cancer* **78**: 10-16. (1996)

[10] I.A. Sokolova, K.C. Halling, R.B. Jenkins, H.M. Burkhardt, R.G. Meyer, S.A. Seelig*, et al.*, The development of a multitarget, multicolor fluorescence in situ hybridization assay for the detection of urothelial carcinoma in urine, *J Mol Diagn* **2**: 116-123. (2000)

[11] A.L. Allan, S.A. Vantyghem, A.B. Tuck, A.F. Chambers, I.H. Chin-Yee and M. Keeney, Detection and quantification of circulating tumor cells in mouse models of human breast cancer using immunomagnetic enrichment and multiparameter flow cytometry, *Cytometry A* **65**: 4-14. (2005)

[12] P.D. Beitsch and E. Clifford, Detection of carcinoma cells in the blood of breast cancer patients, *Am J Surg* **180**: 446-448; discussion 448-449. (2000)

[13] H.B. Hsieh, D. Marrinucci, K. Bethel, D.N. Curry, M. Humphrey, R.T. Krivacic*, et al.*, High speed detection of circulating tumor cells, *Biosens Bioelectron* **21**: 1893-1899. (2006)

[14] R.T. Krivacic, A. Ladanyi, D.N. Curry, H.B. Hsieh, P. Kuhn, D.E. Bergsrud*, et al.*, A rare-cell detector for cancer, *Proc Natl Acad Sci U S A* **101**: 10501-10504. (2004)

[15] V. Muller, D.F. Hayes and K. Pantel, Recent translational research: circulating tumor cells in breast cancer patients, *Breast Cancer Res* **8**: 110. (2006)

[16] A.E. Ring, L. Zabaglo, M.G. Ormerod, I.E. Smith and M. Dowsett, Detection of circulating epithelial cells in the blood of patients with breast cancer: comparison of three techniques, *Br J Cancer* **92**: 906-912. (2005)

[17] C.J. Xu and S.H. Sun, Monodisperse magnetic nanoparticles for biomedical applications, *Polym. Int.* **56**: 821-826. (2007)

[18] T. Hyeon, S.S. Lee, J. Park, Y. Chung and H.B. Na, Synthesis of highly crystalline and monodisperse maghemite nanocrystallites without a size-selection process, *J Am Chem Soc* **123**: 12798-12801. (2001)

[19] S.H. Sun, C.B. Murray, D. Weller, L. Folks and A. Moser, Monodisperse FePt nanoparticles and ferromagnetic FePt nanocrystal superlattices, *Science* **287**: 1989-1992. (2000)

[20] S.H. Sun, H. Zeng, D.B. Robinson, S. Raoux, P.M. Rice, S.X. Wang*, et al.*, Monodisperse MFe2O4 (M = Fe, Co, Mn) nanoparticles, *Journal of the American Chemical Society* **126**: 273-279. (2004)

[21] W.W. Yu, J.C. Falkner, C.T. Yavuz and V.L. Colvin, Synthesis of monodisperse iron oxide nanocrystals by thermal decomposition of iron carboxylate salts, *Chem Commun (Camb)*: 2306-2307. (2004)

[22] W. Yu, E. Chang, J. Falkner, J. Zhang, A. Al-Somali, C. Sayes*, et al.*, Forming biocompatible and nonaggregated nanocrystals in water using amphiphilic polymers., *J Am Chem Soc* **129**: 2871-2879. (2007)

[23] V.H. Cowling and M.D. Cole, E-cadherin repression contributes to c-Myc-induced epithelial cell transformation, *Oncogene* **26**: 3582-3586. (2007)

[24] J.P. Thiery, Epithelial-mesenchymal transitions in tumor progression, *Nat Rev Cancer* **2**: 442-454. (2002)

[25] C. Birchmeier, W. Birchmeier and B. Brand-Saberi, Epithelial-mesenchymal transitions in cancer progression, *Acta Anat (Basel)* **156**: 217-226. (1996)

[26] O.W. Petersen, H. Lind Nielsen, T. Gudjonsson, R. Villadsen, L. Ronnov-Jessen and M.J. Bissell, The plasticity of human breast carcinoma cells is more than epithelial to mesenchymal conversion, *Breast Cancer Res* **3**: 213-217. (2001)

[27] A.G. Tibbe, B.G. de Grooth, J. Greve, G.J. Dolan, C. Rao and L.W. Terstappen, Magnetic field design for selecting and aligning immunomagnetic labeled cells, *Cytometry* **47**: 163-172. (2002)

[28] P.A. Liberti, C. Rao and L.W. Terstappen, Optimization of ferrofluids and protocols for the enrichment of breast tumor cells in blood, *Journal of Magnetism and Magnetic Materials* **225**: 301-307. (2001)

[29] G. Konecny, G. Pauletti, M. Pegram, M. Untch, S. Dandekar, Z. Aguilar*, et al.*, Quantitative association between HER-2/neu and steroid hormone receptors in hormone receptor-positive primary breast cancer, *J Natl Cancer Inst* **95**: 142-153. (2003)

[30] C.L. Vogel, M.A. Cobleigh, D. Tripathy, J.C. Gutheil, L.N. Harris, L. Fehrenbacher*, et al.*, Efficacy and safety of trastuzumab as a single agent in first-line treatment of HER2-overexpressing metastatic breast cancer, *J Clin Oncol* **20**: 719-726. (2002)

CHAPTER 6

EXAMINING THE BEHAVIOR OF QUANTUM DOTS IN HUMAN BLOOD AS A FUNCTION OF SURFACE COATINGS

6.1 Introduction

In the previous chapter we observed non-specific association of magnetic nanoparticles with leukocytes. In order to understand these interactions and the types of cells involved we used QDs to study nanoparticle behavior in whole blood as a function of surface coatings. The emergence of Quantum Dot nanocrystals (QD) [1, 2] as an alternative to traditional fluorescent dyes has seen a tremendous rise in biomedical applications such as single-molecule imaging[3], *in vivo* imaging [4], live cell imaging [5, 6] and cell and tissue labeling[7]. Much of this rise can be attributed to the QD's distinct and robust size-tunable optical properties that are only seen in the nano-scale size regime [8-11]. From a structural perspective, QDs and similar-sized nanomaterials are in the same size scale as biological molecules and therefore a small number of nanoparticles can interact with many proteins due to the large surface-to-volume ratio. With this increased interaction comes growing concern about nanoparticle toxicity, biodistribution, and blood circulation half-life[12-14]. Even though there have been promising developments in the application of QD probes for *in vivo* targeting and imaging[4, 15], the behavior of QDs and other nanoparticles in human blood where there is first contact with soluble proteins and immune cells is not well understood.

Depending on surface properties, such as charge and hydrophobicity, nanoparticles have been shown to be coated by proteins (opsonins) within a few minutes. It is thought that the nature of this protein adsorption (opsonization) will

ultimately decide the fate of the nanoparticles, causing removal from circulation by mononuclear phagocyte system (MPS) and polymorphonuclear phagocytes[16]. A recent study by Cedervalli et al.[17] indicates that the initial adsorption of proteins, which depends on the surface chemistry, shape and size of nanoparticles, results in a corona that will determine further interactions with other proteins and cells. More generally, the primary forces behind protein adsorption on nanoparticles in blood are thought to be hydrophobic and electrostatic interactions, together with conformational changes and associated changes in entropy in adsorbed proteins.[18-20] Plasma proteins implicated in the clearance of nanoparticles have been shown to include, fibronectins, complement (C3), albumin, fibrinogen, IgG, immunoglobulin light chains and apolipoproteins (Apo A-I and ApoE).[12, 16, 21-23].

Developments in biomaterials for biocompatible non-fouling medical devices have led to emergence of PEG (polyethylene glycol) and polysaccharide-grafted nanomaterials. These nanoparticles resist protein adsorption and significantly improve circulation half-life through a steric repulsion effect [24, 25]. PEG, in particular has become popular as it is hydrophilic, non-immunogenic and enables straight-forward conjugation chemistry[26]. A detailed study by Luck et al. discussed possible correlations between physicochemical characteristics and protein adsorption and showed that particles with neutral hydroxyl groups had ten times lower protein adsorption compared to charged particles.

In this chapter, we have examined interactions of three types of QD surface coatings with three different types of leukocytes (granulocytes, monocytes, and lymphocytes) in the presence and absence of plasma proteins. The three QD surface coatings in order of decreasing negative zeta-potential are QD-COOH (a highly anionic surface coating); QD-OH (anionic surface coating modified with propane-diols to yield hydroxyl groups) and QD-PEG-Micelle (a dense micellar encapsulation of QDs with

amphiphilic PEO-PMMA). In order to quantify association of these QDs with the three cell types, we performed flow cytometric measurements. Further, protein adsorption studies were conducted using gel shift assays. Single-cell fluorescence microscopy was performed to study the non-specific binding, uptake and spatial localization of QDs. Time-dependent studies on the association of QDs with cells are also reported. We report for the first time, the application of QDs to study the interactions of nanoparticles with three types of immune cells as a function of nanoparticle surface properties. These findings will enable a new generation of nanoparticles and nanodrug formulations for *in vivo* imaging and targeted delivery of therapeutic agents. Additionally, we hope these results will also lead to the development of non-interacting nanoparticles for assays such as magnetic capture of rare cells from human blood.

6.2 Materials and Methods

Nanoparticle coatings

Monodisperse, fluorescent red-emitting CdSe/ZnS core-shell Quantum Dots (emission peak = 633 nm) coated with organic ligands were synthesized using established procedures [27] and purified by precipitation and re-dispersion in Acetone (Sigma-Aldrich) and Hexane (Sigma-Aldrich) respectively. The nanoparticles were made water soluble by self-assembly of an amphiphilic polymer on the nanoparticle surface. Two types of polymers were used for surface coating, (i) a polyacrylic acid polymer (MW 3500) modified with tetradecylamine, (PAA-TDA) and (ii) a poly(methyl methacrylic acid) polymer backbone with poly(ethylene oxide) grafted (PMMA-PEO). Upon self-assembly and phase transfer the hydrophilic carboxylic acid groups in PAA-TDA are exposed to the aqueous environment, whereas the long-carbon alkyl chains (TDA) interact strongly with hydrophobic surface ligands on the QD surface. Similarly, the amphiphilic PMMA-PEG block copolymer encapsulates the nanoparticle to form a micelle-like structure.

Hydroxyl-modified QDs (QD-OH) were prepared by conjugating 2-amino 1, 3-propanediol (Acros, Morris Plains, NJ) to the PAA-TDA coated QDs using EDC (1-ethyl-3-(3-dimethylaminopropyl) carbodiimide hydrochloride, Pierce Biotech, Rockford, IL) coupling procedures[28]. Hydrodynamic size of all three types of nanoparticles was determined using a Dynamic Light Scattering (DLS) machine (Brookhaven 90Plus, Worcestershire, UK). Zeta potential measurements were obtained using a Zetasizer instrument (Zetasizer Nano ZS90, Malvern Instruments, Worcestershire, UK).

Blood Collection and FACS

Healthy donor blood was obtained through standard venipuncture technique using 20-gauge needle (BD Medical, Franklin Lakes) and 10 mL CellSave vacutainer collection tubes (Immunicon Inc., Huntington Valley, PA) containing anti-coagulant disodium EDTA. Blood samples were stored at room temperature until use. It should be noted that all experiments were performed on fresh blood (no longer than 2 hours post-collection) to ensure maximum blood cell viability and minimum perturbations to the cells. Leukocytes in the whole blood were labeled with dye-conjugated antibodies (Biolegend) targeted to CD ligands specific to granulocytes (FITC-anti-CD66b), monocytes/macrophages (PE-anti-CD14) and lymphocytes (APC-anti-CD5) for 20-30 minutes in the dark at 4°C. A 5:1 (v/v) ratio of 1x RBC Lysis Buffer (Ebiosciences, San Diego, CA) to blood to selectively lyse RBC's. After adding the lysis buffer, blood sample was kept in the dark for no more than 10 minutes. Upon hemolysis, the sample was centrifuged at 400 x g using a swinging-bucket rotor for 7-10 minutes, followed by removal of supernatant and re-dispersion of pelleted cells in 10mM PBS (formula) containing 2mM EDTA. Using a BD FACSAria (BD Biosciences, San Jose CA) flow cytometry machine, the leukocyte suspension was sorted into three tubes containing granulocytes, monocytes and lymphocytes. QDs with different coatings were then

incubated with the cells either in the presence or absence of plasma at 4°C or 37°C. A 488 nm blue laser excitation source together with a PE-Alexa 610 emission channel was used for the analysis. Quantitative analysis of QD adsorption/uptake to cells was performed using the same flow cytometry system, however instead of performing RBC (red blood cell) lysis and then incubating cells in plasma, QDs were added to whole blood and quantified directly with the flow cytometer. In the case where QD uptake/binding was examined in the absence of plasma, RBC lysis was performed as described above. Cell concentration was determined from cell count events obtained during the cell sort and by measuring the total volume of cell suspension. Plasma was obtained from a second vial of blood by centrifugation for 15 minutes at 5000 x g followed by transfer of the supernatant. Plasma used in all experiments was from the same batch of blood as that used for leukocyte sorting.

Gel Mobility Shift Assay

Agarose gel (0.8% w/v) was prepared in 0.5 x TBE Buffer (Tris-HCl + Borate Buffer + EDTA, pH 8.0) and heated for 75 seconds in a microwave at maximum power until a clear solution was obtained. The agarose solution was cast in a refrigerator for 30 minutes and placed into an electrophoresis tray containing 0.5 x TBE Buffer. Upon loading the QD samples, a voltage of 100V was applied for 1 hour. The gel was then imaged using a UV transillumination system (BioRad, Hercules, CA).

Single-cell fluorescence microscopy

FACS (Fluorescence Assisted Cell Sorting) was performed as mentioned earlier to obtain the three cell types. The cells were incubated with QD samples either containing plasma solution or PBS Buffer. Upon incubation in certain specific conditions, such as 4°C or 37°C temperature, the cells were washed twice by centrifugation at 400 x g for 5 minutes followed by removal of the supernatant. The washes were important to

remove unbound QDs from the solution as they will increase background interference and make it difficult to image single leukocytes. Following the last washing step, the sample volume was reduced to increase cell concentration. To a clean No. 1 Cover Glass (Corning), 4 ul of cell suspension was added and gently spread uniformly in circular motions. The solution was not spread too thin to prevent quick drying of sample. Images were obtained using a 100 x oil immersion objective (NA 1.35, infinity-corrected), a mercury-arc lamp with bandpass excitation filter (BP460-490) and emission filter (510LP). Images were captured using an Olympus CCD Camera (Model, Olympus, WA) attached to an Olympus IX-71 inverted epifluorescence microscope. Bright field, fluorescence, and combination images (bright field + fluorescence) were obtained by varying exposure settings based on signal intensity. Prior to taking images, cell type was confirmed by signal from fluorescent dye attached to cell surface, i.e. in case of granulocytes labeled with FITC-anti CD66b antibodies, green signal confirmed positive cell sample. In order to make sure that certain samples (QD-OH and QD-Micelles) indeed didn't have any QDs bound or internalized, fluorescence images were taken at high exposure times.

Bulk fluorescence measurements

Uptake or non-specific adsorption of QDs to the cells was measured in bulk by a mass balance analysis on QDs in solution. QDs at a specific concentration (ranging from 50 pM to 5 nM) were added to a solution of 10 mM PBS (pH 7.4) containing a fixed number of cells. The initial fluorescence intensity of the solution at the peak emission wavelength of QDs (633 nm) was measured using a PTI QuantaMaster NIR QM5 spectrofluorometer (PTI, Birmingham, NJ) followed by a reading after a fixed time interval. Both concentration-dependent and time-dependent studies were conducted in

this manner. The difference or loss in fluorescence intensity was calculated to understand dynamics of nanoparticle uptake/non-specific binding.

6.3 Results and Discussion

Nanoparticle-cell interactions

Blood is a complex and diverse biological medium containing as many as 3,700 types of proteins[23], platelets, erythrocytes (Red Blood Cells) and leukocytes (White Blood Cells). The advantages of nanoparticles from a functional and physical perspective are now evident and applications in biological systems in vitro and in vivo are exponentially growing. Currently, the mechanism by which nanoparticles (10-50 nm in diameter) interact with cells in whole blood is not well understood. Studies focused on understanding them will be important not only to engineer better nanoparticles for imaging and therapeutic applications, but to assess their overall toxicity at a cellular and tissue-level.

Numerous reports [20, 29-35] have demonstrated the effects of surface charge on protein adsorption and subsequent phagocytosis. In fact, there is agreement that surface characteristics and size are the major factors [36] in clearance and biodistribution. Polycationic nanoparticles (positively charged) are toxic and immunogenic due to their membrane disrupting properties[37] and are generally not considered for in vivo/whole blood applications. Anionic nanoparticles, although less toxic, have been consistently shown to bind strongly to plasma proteins and are rapidly cleared by cells of MPS. In cultured cells, anionic nanoparticles have been observed to non-specifically attach to the cell membrane (Kairdolf and Nie, unpublished results). Preventing this non-specificity has been achieved through the attachment of high molecular weight (>2000 Da) PEG chains to the nanoparticle surface. PEGylation of nanoparticles is known to reduce protein adsorption due to the ability of the coiled PEG

chains to sterically shield hydrophobic or charged groups and prevent non-covalent interactions. It has also been hypothesized that a cloud of water molecules around the PEG chains serves to repel hydrophobic groups on proteins [38].

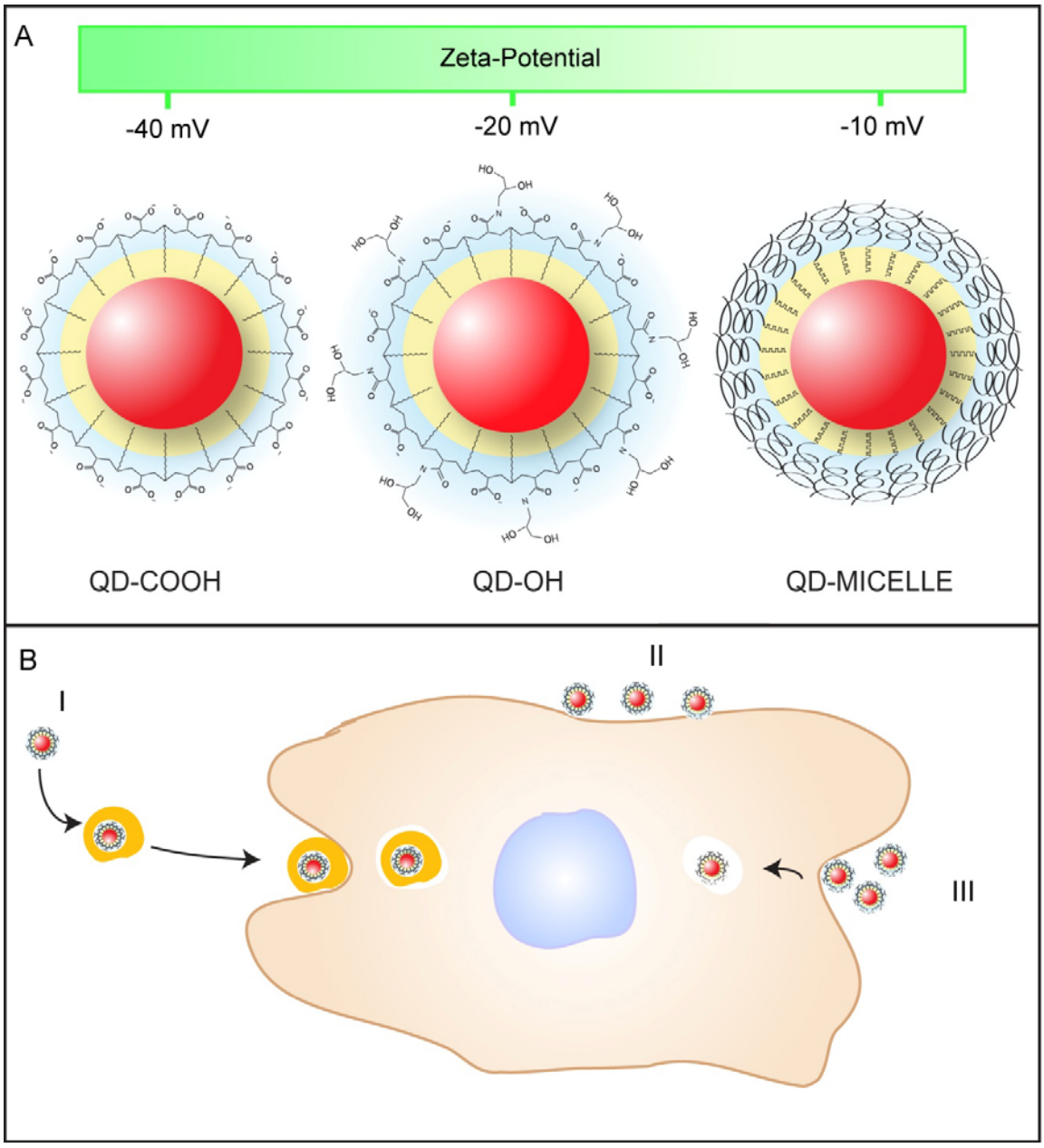

Figure 6.1: Schematic illustration showing different types of QD coatings and possible interactions with live human leukocytes. (A) Three different types of QD polymer coatings with varying degrees of net surface charge. (B) Possible scenarios for QD depletion in blood by

leukocytes include I. Nanoparticle opsonization and phagocytosis, II. Non-specific cell membrane interactions and III. Fluid-phase uptake (pinocytosis)

However, the method of PEGylation, surface heterogeneity and PEG surface density can drastically affect protein adsorption [16, 26, 39, 40]. Further, there is a significant increase in nanoparticle hydrodynamic diameter (see **Figure 6.2**), which can have an adverse effect on renal clearance of nanoparticles. Therefore, there is a need to engineer surface coatings that exhibit PEG-like properties but without the thick hydrophilic shell. There are few findings that examine how less-bulky hydroxyl group (-OH) modified nanoparticles interact with cells. Owing to the reduction in negative charge, we hypothesize that -OH modified QDs should prevent non-specific association with cells. For this purpose, we have prepared three types of nanoparticle surface coatings that have varying degrees of negative zeta-potentials, ranging from strongly anionic (QD-COOH) to near-neutral (QD-PEG-Micelle). The QD-OH nanoparticle coating was developed by partially modifying QD-COOH nanoparticles with an n-diol (**Figure 6.1A**).

The cellular components in blood play a significant role in determining the half-life of nanoparticle circulation in blood. Immune cells (leukocytes) are programmed to clear foreign bodies, antibody-coated particles, cell debris and other antigens in a rapid manner. Certain types of cells can ingest the nanoparticles or mediate or trigger an inflammatory response through cytokine secretion. These cells are diverse in origin, size, function and cellular structure and so the removal of nanoparticles by these cells can be described by three main mechanisms (**Figure 6.1B**). Phagocytosis is an actin-dependent highly regulated energy-dependent mechanism of particle internalization and antigen presentation only seen in specialized cells called phagocytes[41]. Foreign bodies such as large pathogens and nanoparticle clusters are cleared by phagocytes such as macrophages and neutrophilic granulocytes by recognition of opsonins on the

surface through a process called opsonization. Opsonins are small plasma proteins and fragments that are thought to encounter nanoparticles and pathogens by Brownian motion and bind to nanoparticles through non-covalent interactions. These tagged nanoparticles are detected by professional phagocytes and internalized. Second, nanoparticles, coated or un-coated by opsonins, can bind to the surface of the cell membrane, again through non-specific weak intermolecular electrostatic and Van der Waal forces, a process often termed as adsorptive endocytosis [19, 41, 42]. This membrane-association is typically dependent on nanoparticle charge and surface hydrophobicities [14, 19, 20]. Third, nanoparticles can enter a cell through a process called pinocytosis, which involves fluid-phase uptake of the extracellular milieu. The degree of uptake is therefore directly proportional to the concentration of nanoparticles outside the cell.

Nanoparticle characterization

The stability of QDs coated with –OH, -COOH and –PEG surfaces in isolated fresh human plasma was analyzed by measuring fluorescence signal in regular salt buffer (PBS) and plasma. Upon incubating QD samples in human plasma proteins for 24 hours fluorescence spectra were obtained (**Figure 6.3**). The slight decrease in the peak intensity together with a broad band present at shorter wavelengths can be attributed to scattering by larger proteins and presence of weakly fluorescent protein aggregates. Additional tests (data not shown) were performed to determine stability of QDs after incubation. These included fluorescence measurements after centrifugation to determine protein-induced aggregation. Among the three QD coatings, QD-PEG-Micelle was most stable and unaggregated whereas, QD-OH and QD-COOH showed ~50% decrease in fluorescence intensity after centrifugation due to aggregation.

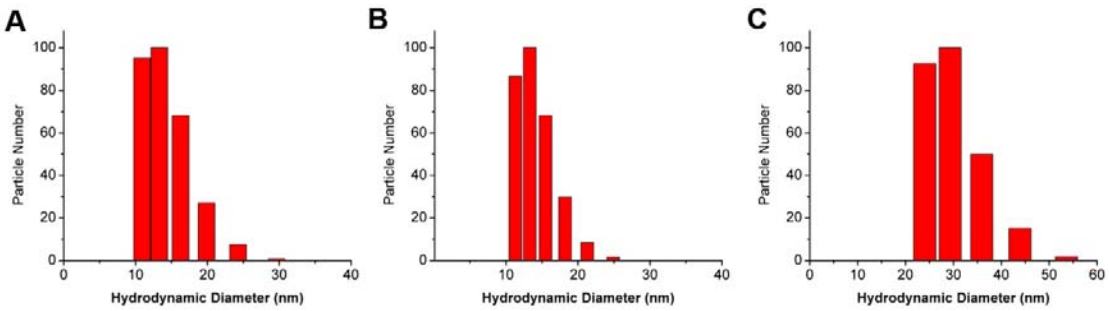

Figure 6.2: Hydrodynamic size of QDs with different surface coatings. (A) QD-COOH, (B) QD-OH and (C) QD-Micelle.

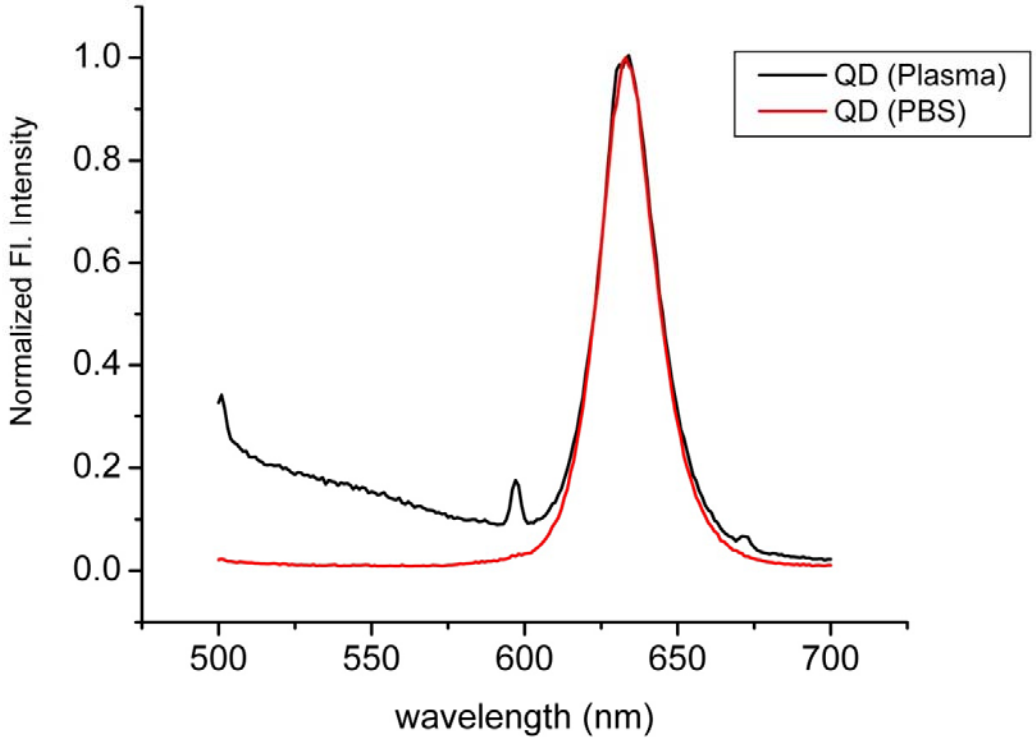

Figure 6.3: Fluorescence spectra of QDs in plasma. Scattering of light by plasma proteins and the excitation of weakly fluorescent proteins is evident by the broad band at shorter wavelengths. Excitation at 488 nm.

Based, on the apparent instability of QD-COOH and QD-OH in plasma, we investigated protein adsorption and nanoparticle clustering by running a gel mobility shift assay. QD-COOH and QD-OH were clearly unstable in plasma and exhibited reduced

mobility due to increase in size. The same batch of QDs were visibly aggregated and showed no blinking under excitation, a common test to confirm presence of single crystalline QDs. As expected, PEGylated QDs such as the QD-Micelle nanoparticles were still single, stable, and fluorescent after the plasma incubations, but migrated slightly towards the cathode, indicating protein adsorption.

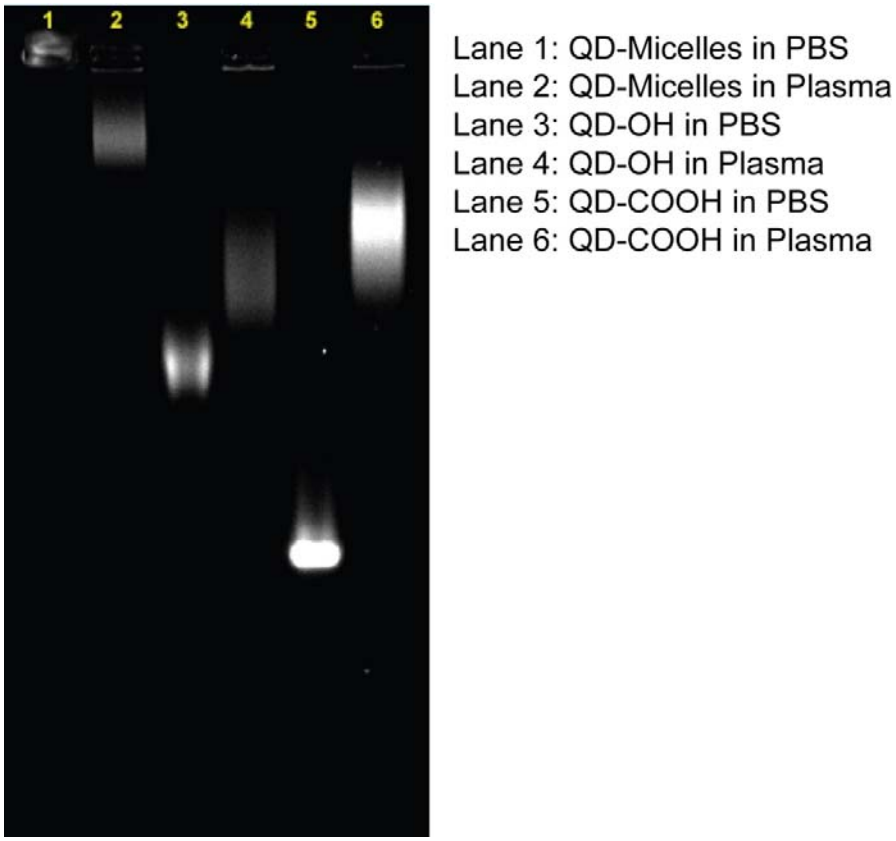

Figure 6.4: Gel mobility shift assay of coated QDs in the presence of human plasma proteins. QD-Micelles are stable but interact with the slightly negative charged proteins causing migration. Both QD-COOH and QD-OH are coated by plasma proteins and show decreased mobility towards the cathode due to increase in particle size.

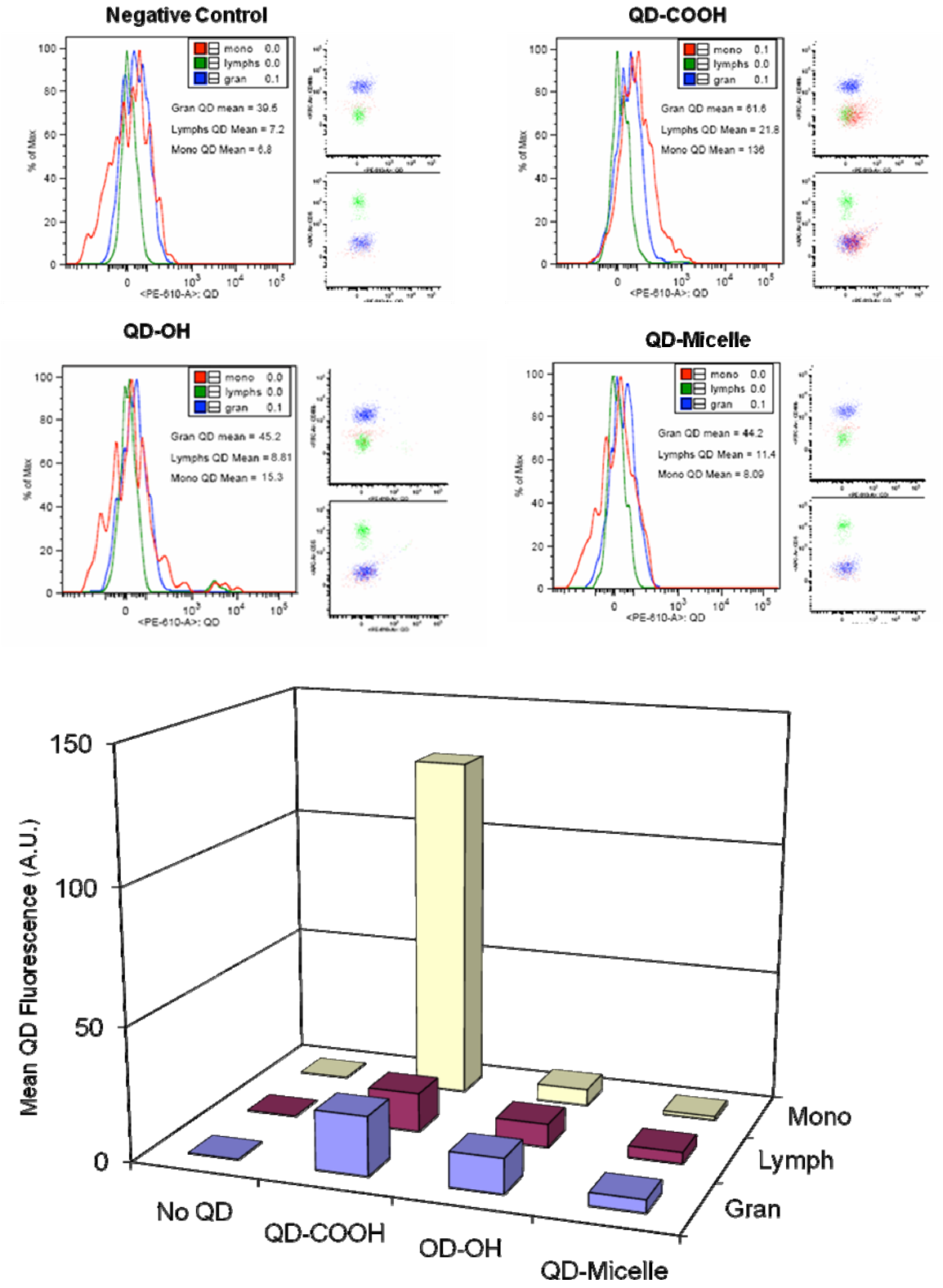

Figure 6.5: Quantitative analysis of QD uptake by leukocytes in presence of human plasma proteins using flow cytometry

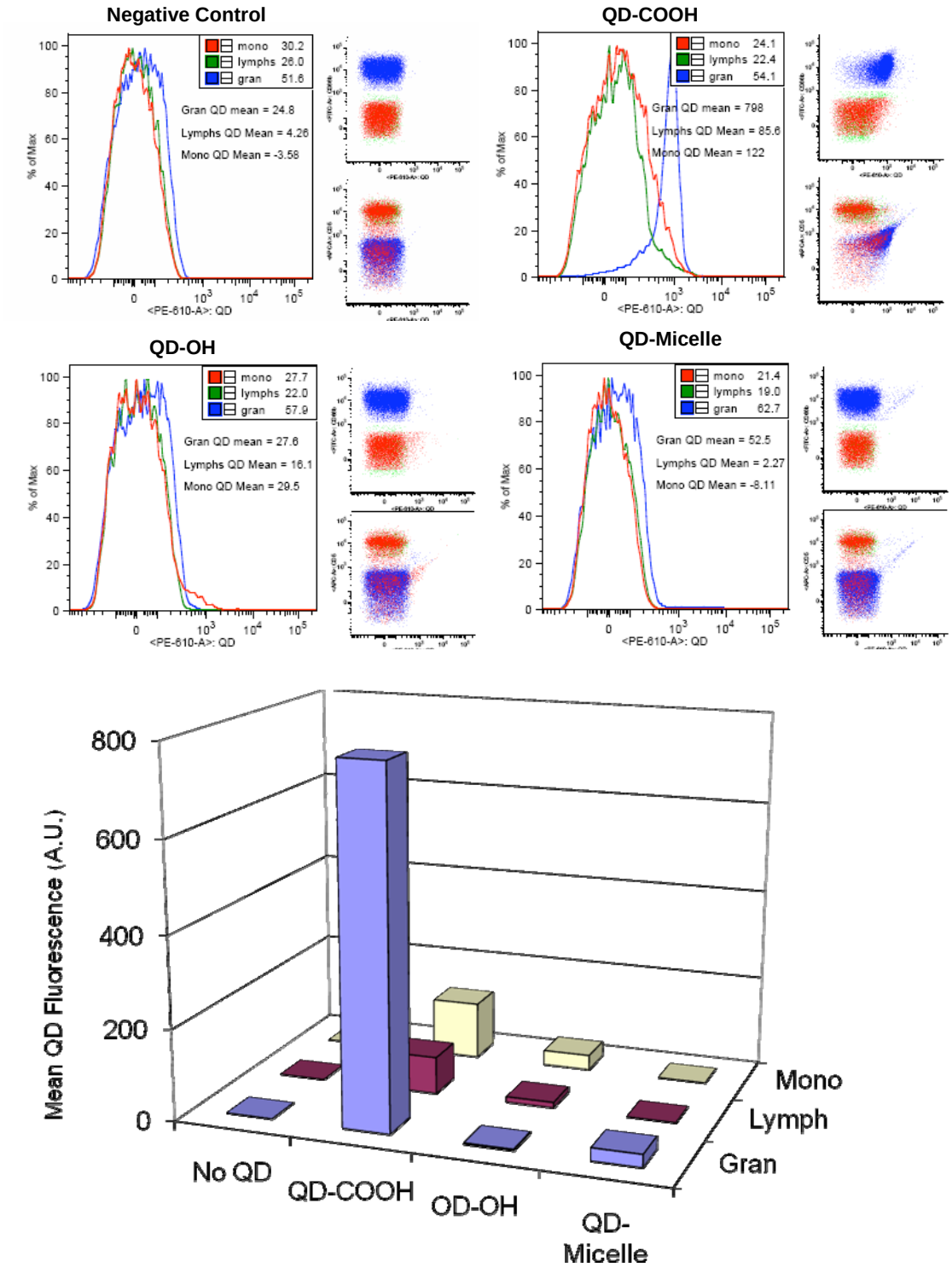

Figure 6.6: Quantitative analysis of QD uptake by leukocytes in absence of human plasma proteins using flow cytometry

It is possible that irregular coverage of PEG chains and exposed hydrophobic PMMA polymer chains could explain this observation. Literature suggests that no sterically protected nanoparticle is completely inert and can interact with proteins through collective weak associations of Coulombic, hydrophobic and Van der Waal forces[16]. Additionally, it is possible that the near-neutral zeta potential and the tight packing of PEG groups on these QDs may screen for small sized proteins to associate with the surface. Results from size exclusion chromatography on the same nanoparticle samples (data not shown) also support these observations.

Flow cytometry analysis

The three possible modes of QD-cell association have been described earlier. However, it must be noted that the mode of nanoparticle association or internalization in human blood is bound to be cell-dependent as leukocytes have different functions and may show dissimilar behavior with nanoparticles. Therefore, leukocyte interactions with QD nanoparticles were examined using flow cytometry. The extraordinarily bright fluorescence of QDs makes it easy to rapidly analyze and quantify nanoparticle-cell interactions as a function of surface coating in a high throughput manner.

As the three different types of leukocytes (granulocytes, monocytes, and lymphocytes) have varying roles in the immune system, this study also helps us understand cell-specific interactions and the role plasma proteins play in mediating the interactions. Initially, we studied interactions in the presence of plasma proteins by incubating QDs with whole blood containing plasma proteins. After 3 hours incubation at 37°C, the results revealed a very selective uptake of QD-COOH by monocytes and macrophages (mature monocytes) cell type (**Figure 5**). Monocytes and macrophages are phagocytes and are known to ingest particles coated with proteins in a very efficient manner. This opsonin-mediated uptake of nanoparticles by monocytes and

macrophages of the reticulo-endothelial system has been reported by others in the past [43]. QD-OH nanoparticles were surprisingly as inert as QD-Micelle and showed reduced leukocyte interaction. As majority of lymphocytes are non-phagocytic we see a reduced fluorescence signal from these cells. We observed that Granulocytes, which are predominantly composed of neutrophils (also professional phagocytes), did not interact with QD-COOH as strongly as monocytes. It may be argued that the greater protein adsorption and QD-COOH aggregation would expedite size-dependent uptake by monocytes. However, the same does not hold true for QD-OH which were also shown to aggregate in presence of plasma proteins. Interestingly, when QDs were incubated in leukocyte suspensions without plasma proteins, granulocytes showed a 5-fold increase in association with QD-COOH compared to monocytes (**Figure 6**). Clearly, the absence or presence of nanoparticle binding proteins modulates the behavior of both monocytes and granulocytes. All three QDs are single and non-aggregated in these conditions and therefore may prevent recognition and uptake by monocytes. Moreover, phagocytosis capability of monocytes is affected as opsonins are absent and cannot coat the nanoparticles. The spatial location and mode of internalization cannot be determined through flow cytometry. In order to further understand the apparent inertness of QD-OH cells were imaged using fluorescence microscope. Also, internalization patterns of QD-COOH in the presence and absence of plasma were studied.

Single cell microscopy

Leukocyte cell types were pre-sorted using fluorescence-activated cell sorting (FACS) and incubated with QD-OH, QD-COOH and QD-Micelle under differing conditions. Approximately, 1 million (1×10^6) QDs per cell were used for these studies, a number based on initial calculations and preliminary results.

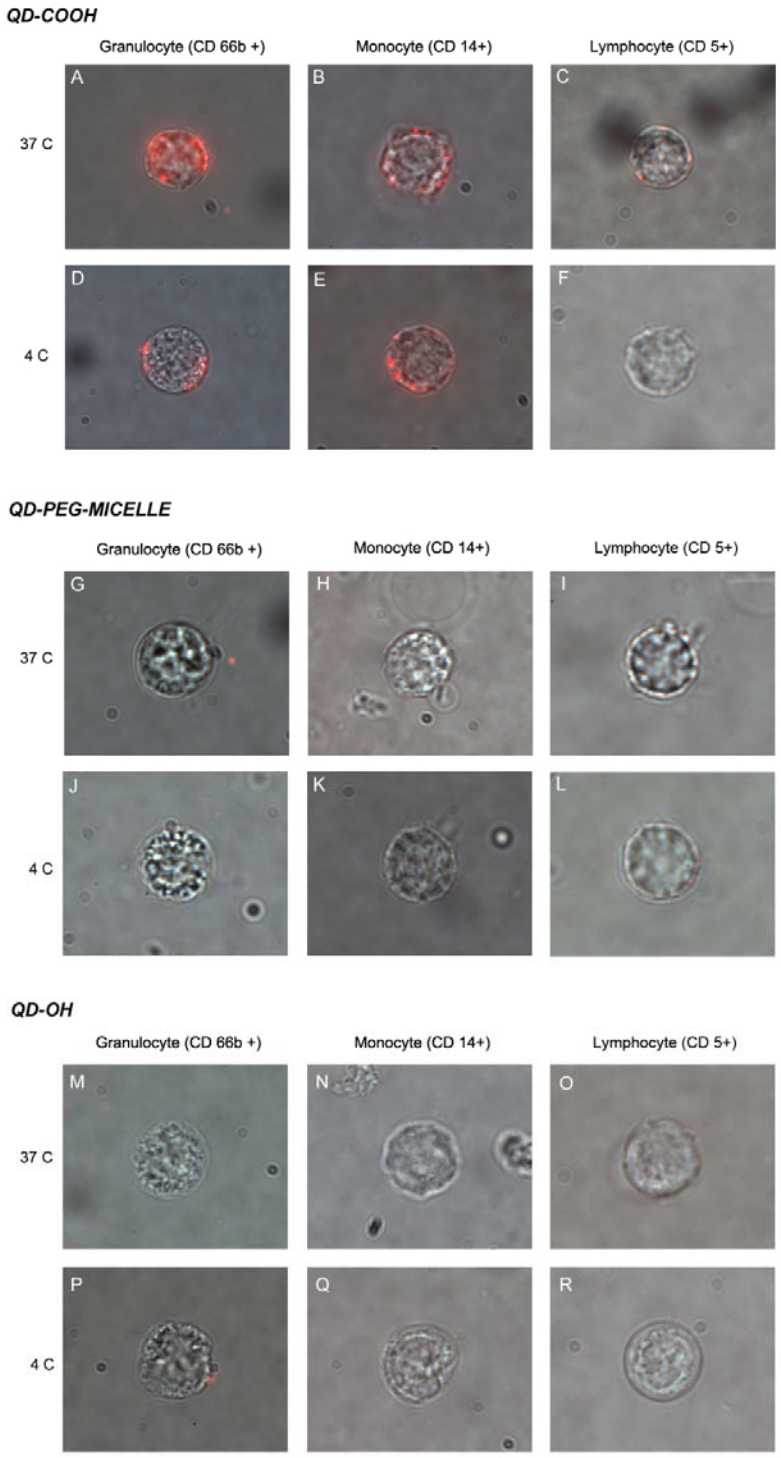

Figure 6.7: Single cell microscopy of QD uptake by leukocytes (presence of plasma) as a function of temperature and QD surface coating. QD samples are incubated with cells in presence of human plasma proteins for 24 hours.

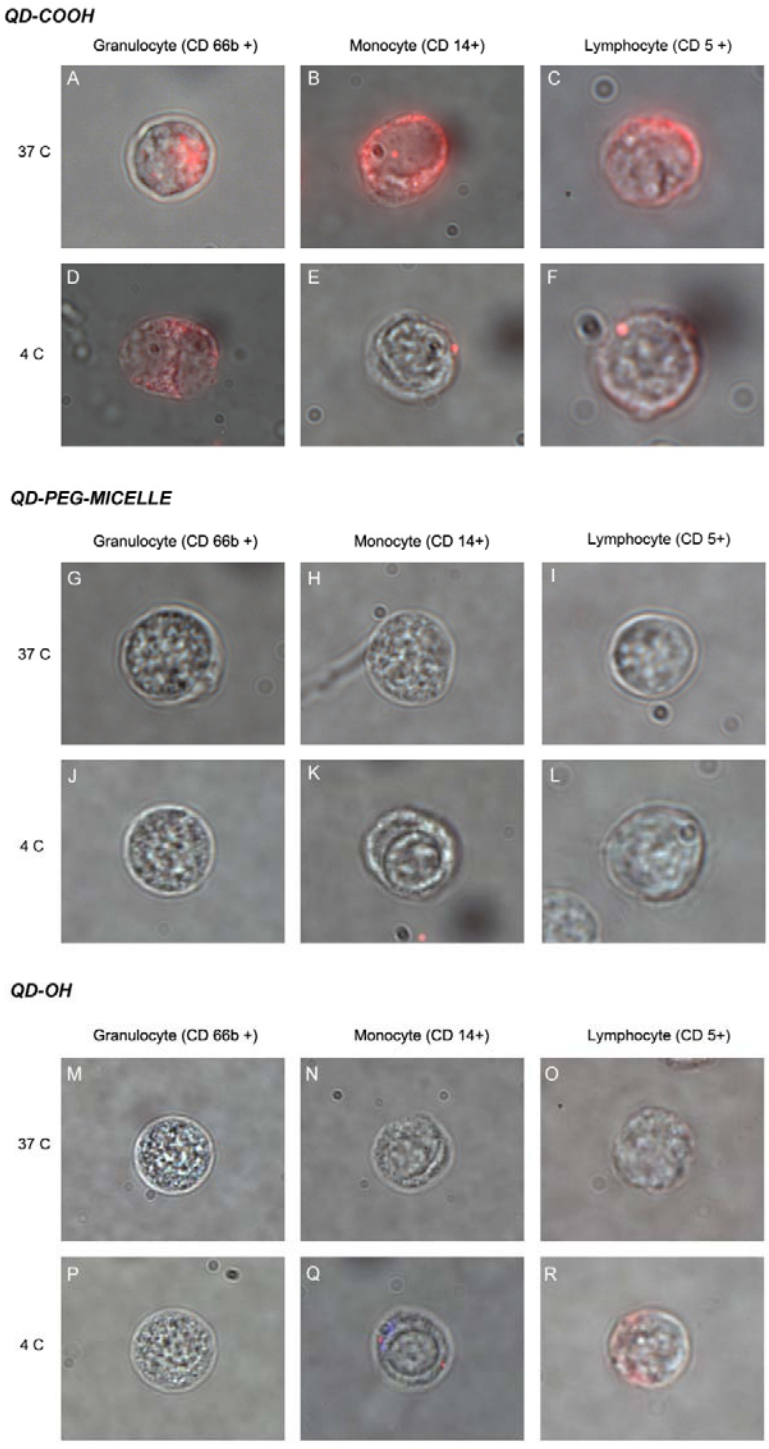

Figure 6.8: Single cell microscopy of QD uptake by leukocytes (absence of plasma) as a function of temperature and QD surface coating. QD samples are incubated with cells in absence of human plasma proteins for 24 hours.

As several endocytic mechanisms, such as phagocytosis, and certain forms of pinocytosis, are energy-dependent, we attempted to compare patterns of internalization at 37C to those at 4C. Further, leukocytes were incubated in the presence (**Figure 7**) or absence (**Figure 8**) of plasma proteins to examine difference in QD localization through protein interactions. As representative images of single cells are shown, the results offer a qualitative assessment of QD uptake or membrane association and cannot be used to quantify nanoparticle association. For cells incubated with plasma, QD-COOH nanoparticles were strongly associated with monocytes and granulocytes. Although, granulocytes appear to internalize more QDs than monocytes (**Figure 7**), it should be noted that there the duration of incubation in this study was 24 hours, compared to 3 hours in flow cytometry based studies. Therefore, cell images cannot be used to quantify QD uptake. More importantly, the results from these experiments confirm that –OH coated QDs behave as inert as PEGylated QD-Micelles and resist uptake or non-specific association with any type of leukocyte. This observation also reinforces the importance of surface coatings in nanoparticle binding with cells.

QD-COOH association with cells didn't change considerably at 4°C compared to 37°C, except in the case of granulocytes incubated without plasma.. Here, we clearly see QD compartmentalization in the peri-nuclear region of the cell. Recent observations in our group (Agrawal and Nie, unpublished) have observed expedited transport of negatively-charged nanoparticles to the MTOC (Microtubule Organizing Center), which is also located in the peri-nuclear region of the cell.

Time-dependence of QD-Cell Association

The association of QDs with three types of leukocytes was studied as a function of time for the three types of surface coatings.

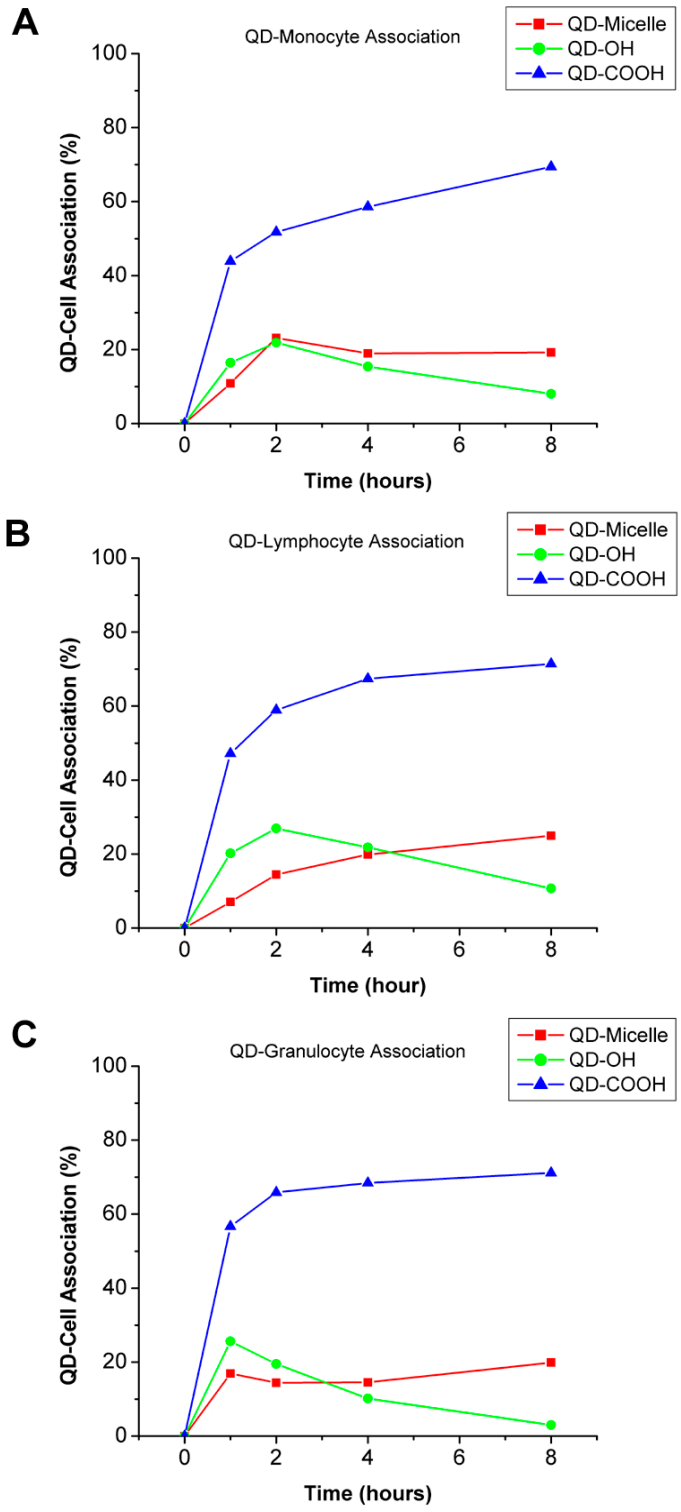

Figure 6.9: Time-dependent association of QDs with leukocytes as a function of QD surface coatings. Association kinetics shown for (A) Monocytes, (B) Lymphocytes and (C) Granulocytes.

Cells were incubated with a fixed concentration of QDs (10^6 QDs per cell) at room temperature in the absence of plasma proteins. The fluorescence intensity of the QD-cell suspension was immediately measured. After a fixed time interval, cells were centrifuged and supernatant's fluorescence was measured. The main assumption was that QDs that interacted with cells would be removed from solution after centrifugation and a drop in fluorescence would be proportional to association or uptake by cells. The percentage of nanoparticle-cell association was calculated and plotted as a function of time (**Figure 6.9**).

Consistent with other results, we see a strong association of QD-COOH with cells and a typical saturation curve that is normally expected in time-dependent uptake measurements. This association is irrespective of cell type but is stronger in granulocytes as seen by the steeper slope. QD-Micelle are moderately associated with the three cell types whereas QD-OH seem to temporarily associate and then surprisingly dissociate from the cells. So far, such a behavior has not been reported in literature, although one could speculate the possible causes. First, a photo-brightening of QDs over time may cause increase in fluorescence intensity leading to a negative association. This possibility can be ruled out because fluorescence intensity of the same batch of QDs in similar conditions remained constant up to 24 hours. Second, QD-OH is associating with the cells and then being exocytosed over time. Third, membrane blebbing of cells due to apoptosis may cause internalized QDs, or QDs bound to the membrane to be shed or released in solution after centrifugation. Although this may be possible, a similar trend should appear in the other samples, especially QD-Micelle.

In conclusion, we have systematically examined the interactions and behavior of nanoparticles with different types of leukocytes under various conditions and as a function of surface charge. QDs are ideal nanoparticles for understanding how nanoparticles interface with components of whole human blood because of their superior

fluorescent properties. We studied three types of QD surface-coatings, QD-COOH, QD-OH, and QD-Micelle and observed that hydroxyl modification of QDs (QD-OH) render inertness to a nanoparticle. This inertness is surprising considering the strong adsorption of proteins on the QDs, and the subsequent aggregation.

Subtle surface modifications and their effects on nanoparticle behavior will enable one to engineer non-immunogenic nanomaterials that are much smaller than bulky PEG-modified nanoparticles. As our understanding of protein-nanoparticle interactions expands, the role of proteins in determining in vivo fate will be important in developing a new class of nanoparticles for whole blood assays and targeted drug delivery. Further, it will be important to assess how *ex vivo* interactions as described in this chapter compare to interactions *in vivo*. In the future, the outcome of this study will allow for the design of magnetic nanoparticles for selectively capturing rare circulating tumor cells from whole blood without non-specific binding of leukocytes.

6.4 References

[1] M. Bruchez, Jr., M. Moronne, P. Gin, S. Weiss and A.P. Alivisatos, Semiconductor nanocrystals as fluorescent biological labels, *Science* **281**: 2013-2016. (1998)

[2] W.C. Chan and S. Nie, Quantum dot bioconjugates for ultrasensitive nonisotopic detection, *Science* **281**: 2016-2018. (1998)

[3] A. Agrawal, C. Zhang, T. Byassee, R.A. Tripp and S. Nie, Counting single native biomolecules and intact viruses with color-coded nanoparticles, *Anal Chem* **78**: 1061-1070. (2006)

[4] X. Gao, Y. Cui, R.M. Levenson, L.W. Chung and S. Nie, In vivo cancer targeting and imaging with semiconductor quantum dots, *Nat Biotechnol* **22**: 969-976. (2004)

[5] J.K. Jaiswal, E.R. Goldman, H. Mattoussi and S.M. Simon, Use of quantum dots for live cell imaging, *Nat Methods* **1**: 73-78. (2004)

[6] J.K. Jaiswal, H. Mattoussi, J.M. Mauro and S.M. Simon, Long-term multiple color imaging of live cells using quantum dot bioconjugates, *Nat Biotechnol* **21**: 47-51. (2003)

[7] Y. Xing, Q. Chaudry, C. Shen, K.Y. Kong, H.E. Zhau, L.W. Chung*, et al.*, Bioconjugated quantum dots for multiplexed and quantitative immunohistochemistry, *Nat Protoc* **2**: 1152-1165. (2007)

[8] A.P. Alivisatos, W. Gu and C. Larabell, Quantum dots as cellular probes, *Annu Rev Biomed Eng* **7**: 55-76. (2005)

[9] P. Alivisatos, The use of nanocrystals in biological detection, *Nat Biotechnol* **22**: 47-52. (2004)

[10] A. Smith and S. Nie, Chemical analysis and cellular imaging with quantum dots, *ANALYST* **129**: 672-677. (2004)

[11] A.M. Smith, X. Gao and S. Nie, Quantum dot nanocrystals for in vivo molecular and cellular imaging, *Photochem Photobiol* **80**: 377-385. (2004)

[12] D. Labarre, C. Vauthier, C. Chauvierre, B. Petri, R. Müller and M. Chehimi, Interactions of blood proteins with poly(isobutylcyanoacrylate) nanoparticles decorated with a polysaccharidic brush., *Biomaterials* **26**: 5075-5084. (2005)

[13] J. Klein, Probing the interactions of proteins and nanoparticles., *Proc Natl Acad Sci U S A* **104**: 2029-2030. (2007)

[14] Dobrovolskaia MA and S.E. McNeil, Immunological properties of engineered nanomaterials, *Nature Nanotechnology* **2**: 469-478. (2007)

[15] S. Kim, Y.T. Lim, E.G. Soltesz, A.M. De Grand, J. Lee, A. Nakayama*, et al.*, Near-infrared fluorescent type II quantum dots for sentinel lymph node mapping, *Nat Biotechnol* **22**: 93-97. (2004)

[16] S. Moghimi and J. Szebeni, Stealth liposomes and long circulating nanoparticles: critical issues in pharmacokinetics, opsonization and protein-binding properties., *Prog Lipid Res* **42**: 463-478. (2003)

[17] T. Cedervall, I. Lynch, S. Lindman, T. Berggård, E. Thulin, H. Nilsson, *et al.*, Understanding the nanoparticle-protein corona using methods to quantify exchange rates and affinities of proteins for nanoparticles., *Proc Natl Acad Sci U S A* **104**: 2050-2055. (2007)

[18] A. Gessner, A. Lieske, B. Paulke and R. Müller, Influence of surface charge density on protein adsorption on polymeric nanoparticles: analysis by two-dimensional electrophoresis., *Eur J Pharm Biopharm* **54**: 165-170. (2002)

[19] A. Vonarbourg, C. Passirani, P. Saulnier and J. Benoit, Parameters influencing the stealthiness of colloidal drug delivery systems., *Biomaterials* **27**: 4356-4373. (2006)

[20] M. Lück, B. Paulke, W. Schröder, T. Blunk and R. Müller, Analysis of plasma protein adsorption on polymeric nanoparticles with different surface characteristics., *J Biomed Mater Res* **39**: 478-485. (1998)

[21] R. Gref, M. Lück, P. Quellec, M. Marchand, E. Dellacherie, S. Harnisch, *et al.*, 'Stealth' corona-core nanoparticles surface modified by polyethylene glycol (PEG): influences of the corona (PEG chain length and surface density) and of the core composition on phagocytic uptake and plasma protein adsorption., *Colloids Surf B Biointerfaces* **18**: 301-313. (2000)

[22] A. Moore, R. Weissleder and A. Bogdanov, Jr., Uptake of dextran-coated monocrystalline iron oxides in tumor cells and macrophages, *J Magn Reson Imaging* **7**: 1140-1145. (1997)

[23] T. Cedervall, I. Lynch, M. Foy, T. Berggard, S.C. Donnelly, G. Cagney, *et al.*, Detailed identification of plasma proteins adsorbed on copolymer nanoparticles, *Angew Chem Int Ed Engl* **46**: 5754-5756. (2007)

[24] R. Langer and N.A. Peppas, Advances in biomaterials, drug delivery, and bionanotechnology, *Aiche J.* **49**: 2990-3006. (2003)

[25] Y. Ikada, SURFACE MODIFICATION OF POLYMERS FOR MEDICAL APPLICATIONS, *Biomaterials* **15**: 725-736. (1994)

[26] A. Zahr, C. Davis and M. Pishko, Macrophage uptake of core-shell nanoparticles surface modified with poly(ethylene glycol). *Langmuir* **22**: 8178-8185. (2006)

[27] A.M. Smith, H. Duan, M.N. Rhyner, G. Ruan and S. Nie, A systematic examination of surface coatings on the optical and chemical properties of

semiconductor quantum dots, *Physical Chemistry Chemical Physics* **8**: 3895-3903. (2006)

[28] G.T. Hermanson, Bioconjugate Techniques, Academic Press, San Diego (1996).

[29] G. Storm, S. Belliot, T. Daemen AND D. Lasic, Surface Modification Of Nanoparticles To Oppose Uptake By The Mononuclear Phagocyte System, *Advanced Drug Delivery Reviews* **17**: 31-48. (1995)

[30] V. Mosqueira, P. Legrand, A. Gulik, O. Bourdon, R. Gref, D. Labarre*, et al.*, Relationship between complement activation, cellular uptake and surface physicochemical aspects of novel PEG-modified nanocapsules., *Biomaterials* **22**: 2967-2979. (2001)

[31] A. Chonn, P.R. Cullis and D.V. Devine, The role of surface charge in the activation of the classical and alternative pathways of complement by liposomes, *J Immunol* **146**: 4234-4241. (1991)

[32] F. Roerdink, N.M. Wassef, E.C. Richardson and C.R. Alving, Effects of negatively charged lipids on phagocytosis of liposomes opsonized by complement, *Biochim Biophys Acta* **734**: 33-39. (1983)

[33] R.A. Schwendener, P.A. Lagocki and Y.E. Rahman, The effects of charge and size on the interaction of unilamellar liposomes with macrophages, *Biochim Biophys Acta* **772**: 93-101. (1984)

[34] A. Gabizon and D. Papahadjopoulos, The role of surface charge and hydrophilic groups on liposome clearance in vivo, *Biochim Biophys Acta* **1103**: 94-100. (1992)

[35] Y. Tabata and Y. Ikada, Effect of the size and surface charge of polymer microspheres on their phagocytosis by macrophage, *Biomaterials* **9**: 356-362. (1988)

[36] A. Hoshino, K. Fujioka, T. Oku, M. Suga, Y.F. Sasaki, T. Ohta*, et al.*, Physicochemical properties and cellular toxicity of nanocrystal quantum dots depend on their surface modification, *Nano Lett.* **4**: 2163-2169. (2004)

[37] P.R. Leroueil, S. Hong, A. Mecke, J.R. Baker, Jr., B.G. Orr and M.M. Banaszak Holl, Nanoparticle interaction with biological membranes: does nanotechnology present a Janus face?, *Acc Chem Res* **40**: 335-342. (2007)

[38] P. Vermette and L. Meagher, Interactions of phospholipid- and poly(ethylene glycol)-modified surfaces with biological systems: relation to physico-chemical properties and mechanisms, *Colloid Surf. B-Biointerfaces* **28**: 153-198. (2003)

[39] Z. Ademovic, B. Holst, R. Kahn, I. Jørring, T. Brevig, J. Wei*, et al.*, The method of surface PEGylation influences leukocyte adhesion and activation., *J Mater Sci Mater Med* **17**: 203-211. (2006)

[40] W. Yu, E. Chang, J. Falkner, J. Zhang, A. Al-Somali, C. Sayes*, et al.*, Forming biocompatible and nonaggregated nanocrystals in water using amphiphilic polymers., *J Am Chem Soc* **129**: 2871-2879. (2007)

[41] S. Conner and S. Schmid, Regulated portals of entry into the cell., *Nature* **422**: 37-44. (2003)

[42] M.G. Qaddoumi, H. Ueda, J. Yang, J. Davda, V. Labhasetwar and V.H.L. Lee, The characteristics and mechanisms of uptake of PLGA nanoparticles in rabbit conjunctival epithelial cell layers, *Pharm. Res.* **21**: 641-648. (2004)

[43] J.C. Leroux, F. Dejaeghere, B. Anner, E. Doelker and R. Gurny, An Investigation On The Role Of Plasma And Serum Opsonins On The Internalization Of Biodegradable Poly(D,L-Lactic Acid) Nanoparticles By Human Monocytes, *Life Sci.* **57**: 695-703. (1995)

CHAPTER 7

SUMMARY AND FUTURE DIRECTIONS

7.1 Summary

In this dissertation, we have described methods for the integration of optical and magnetic nanoparticles and demonstrated relevant applications for the detection and monitoring of cancer. Apart from preventive methods, early detection of cancer represents the best strategy to reduce mortality rates, which have not changed for the past several decades. In most cases, early detection will involve detecting a low number of molecules or cells associated with the disease, therefore, new technologies need to be developed that will allow standardized tests to be performed in a clinical setting with high detection sensitivity. For detection with high sensitivity, we need bright and stable fluorophores that can allow multiplexed assays through target encoding, spectrophotometric detection of captured molecules, and multicolored profiling of a panel of biomarkers on cells. Quantum dots and dye-doped nanobeads have been developed over the last decade and have been successfully used in a myriad of applications[1-8]. Also, we need a technology to permit capture and enrichment of target molecules and cells in a quick, efficient and reproducible manner. Magnetic nanoparticles have been used in the past for separation applications with great success, and can permit semi-automated assays for capturing target molecules or cells.

In the first few chapters of this dissertation, we describe the rationale behind our study, define the scope of the studies (Chapter 1) and offer a brief overview of each of these technologies, previous related studies, and a description of the issues being tackled (Chapter 2). In Chapter 3, we describe methods for developing a new class of dual-function beads that are optically encoded and magnetically separable. It was found that using mesoporous beads, we could precisely dope beads with magnetic

nanoparticles and semiconductor Quantum Dots (QD), but with increased amounts of magnetic iron oxide nanoparticles, a drastic reduction in fluorescence intensity of embedded QDs was seen. Through systematic studies, we revealed that the strong absorption of light by iron oxide was responsible for this attenuation[7]. Following this method development, we developed a bead-based sandwich immunoassay (Chapter 4) using magnetic beads (not optically encoded) and luminescent nanoparticles (QDs and dye-doped nanobeads). From this study, we were able to demonstrate femto-molar detection sensitivity of a protein TNF-alpha with a dynamic range of 2-3 logs[2].

In the next two chapters (Chapter 5 and 6) we discuss integration of magnetic and optical nanoparticles for potential cancer monitoring applications. In particular we have demonstrated multiplexed profiling for circulating tumor cells isolated from whole blood. These cells have been shown by several groups to be highly sensitive indicators of prognosis in metastatic cancer patients [9-12]. Therefore, by characterizing the captured cells for molecular biomarkers, there is potential for therapy monitoring and administration of tailored and personalized treatment. Specifically, we have made an attempt to demonstrate multicolor protein profiling of the magnetically captured cells from whole blood for the first time(Chapter 5). Using prostate cancer cell lines showing an epithelial to mesenchymal transition (EMT), we were able to isolate the spiked cells from phosphate buffer and blood, and label two biomarkers using QDs that allowed us to determine the phenotype and behavior of the cells. Further, breast cancer cell lines isolated from blood were profiled for three commonly used breast cancer markers that would determine treatment regimen. Through the course of this study, we also encountered that immunomagnetic nanoparticles were non-specifically isolating non-tumor leukocytes along with tumor cells. This issue was addressed by using brightly fluorescent QDs to probe the interactions between nanoparticles and components of peripheral blood as a function of surface properties (Chapter 6). The importance of this

study is not limited to non-specific capture of nanoparticles in whole blood assays, but also to assess immunological properties of nanoparticles and how they can be modulated for targeted *in vivo* applications. Interestingly, we observed a plasma-protein mediated cell specific uptake of negatively-charged QDs (QD-COOH) through flow cytometry. Carboxylated QDs were strongly associated with monocytes when incubated in whole blood containing proteins, whereas they were associated with granulocytes in the absence of the proteins. Surprisingly, hydroxyl-modified QDs (QD-OH) behaved as inert as PEGylated micellar QDs by not associating with granulocytes, monocytes or lymphocytes in the presence or absence of proteins. This finding may open avenues for a new class of polymer-coated nanoparticles that are biocompatible and can accumulate in target organs with minimum biodistribution in un-targeted organs.

7.2 Discussion and Future Directions

Near-IR QD encoded dual-function beads

From our studies, it is clear that the broad absorption spectrum of iron oxide attenuates fluorescence signal from embedded QDs. This observation can be detrimental for accurate decoding of beads after magnetic isolation. However, the iron oxide nanoparticle absorption spectrum (see Figure 3.6A) tapers at longer wavelengths, and the absorbance is almost negligible at wavelength of 750 nm and above. Therefore, hydrophobically capped near-IR QDs with emission peak greater than this value have the potential to permit optical bead encoding without concern of signal attenuation.

Mesoporous bead surface capping

We have demonstrated coating of dual-function beads, discussed in Chapter 3, with a combination of amphiphilic polymers and surfactants. This procedure has allowed the beads to remain stable for up to 45 days. However, we have not been able to

confirm the presence of the polymer on the surface. Further work needs to be done to characterize the polymer coating and determine availability and surface density of functional groups to permit attachment of targeting ligands. Apart from polymers, we also see the potential to grow a silica shell on the silica microbeads using alkylated silanes and orthosilicates. Currently, we are pursuing experiments to grow a silica shell with epoxy groups on the surface, so that they can be coupled to amine-rich IgG molecules. Preliminary results are encouraging, but more careful characterization needs to be done.

Simultaneous bead-based DNA and protein detection

Although we have demonstrated detection of protein with high sensitivity using magnetic bead enrichment and target labeling with luminescent nanoparticles, there is a need to develop beads and probes so that multiple target DNA molecules and proteins can be detected using the same assay and conditions. Such an assay would save time and would allow a clinician to monitor the levels of molecules implicated with the tumor or monitor molecules that can provide information on the side effects of a therapeutic agent.

Uniform magnetic nanoparticles for separation applications

We have briefly described the application of uniform magnetic nanoparticles for cell separation purposes. Compared to the gold standard of magnetic separation (150 nm magnetic nanoparticles produced by Immunicon Inc.), the nanoparticles generated by us are smaller uniform and have larger contact area to the increase in surface-area to volume ratio. Since the total magnetic mass present on the captured cell will determine its mobility towards a magnet, there is potential for smaller nanoparticles with uniform magnetization to improve separation efficiency. Further, when using multiple QDs for biomarker labeling, smaller magnetic nanoparticles on the cell will not pose steric

hindrance problems associated with larger magnetic nanoparticles. This is especially important for accurately determining the relative amounts of biomarkers in the cell.

Also, further work must be done to test whether a cocktail of antibodies attached to magnetic nanoparticles that are specific to epithelial cells will improve specificity. A major hurdle to this effort would be preventing non-specific binding to leukocytes, which has been discussed in Chapter 5. It should also be noted that even though non-specificity of nanoparticles to leukocytes can be obtained by engineering the nanoparticle surface, low level expression of EpCAM by a few leukocytes may still cause the unwanted interference by these cells. Therefore, negative depletion of leukocytes may be considered as long as tumor cells are not lost in the process. Typically, a test involving the least number of washing steps and sample transfer will reduce probability of cell loss. It is crucial in this respect that cells are not lost since enumeration of cells is closely linked to prognostic factors[13].

Understanding implications of QD protein interactions

An interesting observation from the studies described in Chapter 6 is that non-specific association of hydroxyl-modified QDs (QD-OH) is drastically reduced compared to carboxylated QDs (QD-COOH). However, both QD coatings tend to bind strongly to plasma proteins. This is clearly evident from gel shift assays and fluorescence microscope images where particles are clearly aggregated. It is thought that protein adsorption will ultimately decide the fate of the nanoparticle. Why QD-OH nanoparticles still inhibit association even after protein coating is an intriguing question and needs to be understood. The possibility of nanoparticle exocytosis is speculated but more in-depth studies to visualize this process using live cell imaging procedures need to be performed. Also, blood compositions varies substantially from person to person, therefore future studies must keep in mind these issues when studying protein-

nanoparticle interactions. Further studies to examine nanoparticle interactions with platelets were not included in this work and may provide a complete picture of the immunological properties of nanomaterials. Whether our observations will mimic the interactions in vivo cannot be concluded, but provide a basis for future studies.

7.3 References

[1] A. Agrawal, T. Sathe and S. Nie, Nanoparticle Probes for Ultrasensitive Biomolecular Detection and Imaging, Wiley Interscience (2006).

[2] A. Agrawal, T. Sathe and S. Nie, Single-bead immunoassays using magnetic microparticles and spectral-shifting quantum dots, *J Agric Food Chem* **55**: 3778-3782. (2007)

[3] P. Alivisatos, The use of nanocrystals in biological detection, *Nat Biotechnol* **22**: 47-52. (2004)

[4] W.C. Chan, D.J. Maxwell, X. Gao, R.E. Bailey, M. Han and S. Nie, Luminescent quantum dots for multiplexed biological detection and imaging, *Curr Opin Biotechnol* **13**: 40-46. (2002)

[5] X. Gao and S. Nie, Molecular profiling of single cells and tissue specimens with quantum dots, *Trends Biotechnol* **21**: 371-373. (2003)

[6] X. Gao, L. Yang, J.A. Petros, F.F. Marshall, J.W. Simons and S. Nie, In vivo molecular and cellular imaging with quantum dots, *Curr Opin Biotechnol* **16**: 63-72. (2005)

[7] T.R. Sathe, A. Agrawal and S. Nie, Mesoporous silica beads embedded with semiconductor quantum dots and iron oxide nanocrystals: dual-function microcarriers for optical encoding and magnetic separation, *Anal Chem* **78**: 5627-5632. (2006)

[8] A. Smith and S. Nie, Chemical analysis and cellular imaging with quantum dots, *ANALYST* **129**: 672-677. (2004)

[9] M. Cristofanilli, G.T. Budd, M.J. Ellis, A. Stopeck, J. Matera, M.C. Miller, *et al.*, Circulating tumor cells, disease progression, and survival in metastatic breast cancer, *N Engl J Med* **351**: 781-791. (2004)

[10] E. Racila, D. Euhus, A.J. Weiss, C. Rao, J. McConnell, L.W. Terstappen, *et al.*, Detection and characterization of carcinoma cells in the blood, *Proc Natl Acad Sci U S A* **95**: 4589-4594. (1998)

[11] T.E. Witzig, B. Bossy, T. Kimlinger, P.C. Roche, J.N. Ingle, C. Grant, *et al.*, Detection of circulating cytokeratin-positive cells in the blood of breast cancer patients using immunomagnetic enrichment and digital microscopy, *Clin Cancer Res* **8**: 1085-1091. (2002)

[12] B.K. Zehentner, Detection of disseminated tumor cells: strategies and diagnostic implications, *Expert Rev Mol Diagn* **2**: 41-48. (2002)

[13] M. Cristofanilli, D.F. Hayes, G.T. Budd, M.J. Ellis, A. Stopeck, J.M. Reuben, *et al.*, Circulating tumor cells: a novel prognostic factor for newly diagnosed metastatic breast cancer, *J Clin Oncol* **23**: 1420-1430. (2005)

VITA

TUSHAR R. SATHE

Tushar Sathe was born in a small mining township called Kalulushi in Zambia, a country located in South Central Africa. He attended primary school in Kalulushi, boarding school in Gwalior, India and secondary school Pune, India before receiving a B.S. in Chemical Engineering from The University of Oklahoma, Norman, Oklahoma in 2002. He immediately joined the Wallace H. Coulter Department of Biomedical Engineering at Georgia Tech in August 2002 to pursue a doctorate degree in the joint program. Apart from research, Tushar enjoys playing the guitar and recording music. He is a big fan of soccer and an ardent supporter of Liverpool Football Club.